University Review, Vol. 15, Issue 1, p.1-6, 2021.

UNIVERSITY REVIEW

USE OF STATISTICAL REGULATION IN MAINTENANCE PROCESSES

Alena Breznická[1*]

[1]Department of Design and Special Technology, Faculty of Special Technology, Alexander Dubček University of Trenčín, Ku kyselke 469, 911 06, Trenčín

ARTICLE INFO

***Article history*:**
Received: 15.3.2021
Received in revised form: 23.4.2021
Accepted: 3.5.2021

Keywords:
Maintenance
Analysis
Statistical process control

Abstract:

In a submitted paper we are going to deal with possibilities in using statistical instruments and methods of product quality management and with application of simulation modeling in production and maintenance introducing procedures on examples being solved in mechanical engineering companies in Slovakia.

1 Introduction

1.1 Manuscript preparation

The most widely used are in operative quality management. Seven basic Instruments enable solving problems of quality improvement in manufacturing areas from a condition determination through production sheets, through looking for ways and possibilities of their solution up to a statistical regulation of improved processes [1]. The basic Instruments include a check list, a histogram, causes and consequences diagram, Paret´s analysis, correlation diagram, flowchart and a regulation diagram. These Instruments have been used also in solving a defined aim of the work. Significance and importance of use of statistical Instruments and quality management methods in processes when welding a connector on a copper wire of glued carbon brushes in an unnamed company [2].

2 Basic classification of statistical methods

2.1 Basic Information

The concept of stability is derived from the systems theory. Several different definitions of the system stability can be found in the literature. Most of them refer to the concept of the point/state of balance and define the stability of a system as its ability to return to the state of balance after the disturbances that caused the instability have ceased. The stability of a production system will be understood as maintaining the steady state of the system for a certain assumed period.

The statistical methods and instruments used in an industrial practice can be divided in three categories:
1. simple (basic, elementary) statistical methods,
2. medium demanding statistical methods,
3. more demanding statistical methods [3].

Simple methods include seven instruments:
- check tables and recorders, histogram, flowchart, correlation diagram, Paret´s analysis, causes and consequences chart (Ishikawa´s diagram) and regulation diagrams.

Medium demanding and more demanding statistical methods include e.g.:
- Analysis of a measuring system, verification of a manufacturing equipment capability, verification of a process capability, statistical inspection, FMEA [4].

Quality control can be defined by STN EN ISO 9000:2005 as a part of quality management aiming to meet the quality requirements.
Statistical quality control is a part of a quality management, in which the procedures of mathematical statistics are used. There are three basic areas of a statistical quality control:
- statistical process regulation
- statistical (selective) inspection
- methods of experiment designing.

[*] Ing. Alena Breznická, PhD., Tel.: 0327400241
E-mail address: alena.breznicka@tnuni.sk

In the process the inputs are transformed to a product, on which the quality characteristics and quality indicators can be defined. Main problem of quality improvement is a reduction of variability of quality indicators values. Usually the variability of values of quality indicators can be reduced based on obtained results and to find such combination of levels of variables being controlled, that optimizes a process performance. After having indicated the most important variables, having effect on a process, often it is very useful to simulate relations between input variables and quality indicators of the product. When we know character of relations between variables, the techniques of a statistical regulation of the process can be applied in an effective way – one of an instrument of a so called on-line quality control, enabling monitoring of a process and maintaining it in a requested condition. A process of an implementation of methods of a statistical quality control in organizations usually starts by applying a statistical inspection (it relates a selective inspection, when a decision is taken, whether a batch is to be accepted or not based on results from selection or selections made from this batch), and goes on by implementation of a statistical regulation in a process and then often the methods of experiment designing start to be applied [5].

Based on these facts and after consultation in a company the following conceptual and simulation model has been proposed. The simulation model of a working place is composed of a set of three production machines, containers and conveyors for parts with random period intervals between failures, time period of a maintenance provided by repairmen. The machines process the parts with random intervals of manufacturing operations. To simplify a model the personnel servicing the machines is not depicted.

2.2 Statistical regulation of processes

Statistical regulation of a process is a set of instruments for maintaining a process stability and improvement of its capability through a reduction of variability. A fundamental question in an organization aimed at the quality is a question, to which extend is it capable to meet the expectations of the customers. When the expectations of the customers are defined, it is necessary that the supplier is able to quantify an extent he can satisfied such expectations. A product, which should be appropriate for a use, should be generally produced in a stable or a repeatable process. It means that a process should be able to produce products with an acceptable variability of defined indicators of quality in terms of their defined aims or values.

Statistical regulation of a process represents a preventive approach to a quality management, as it enables interventions into a process based on a timely detection of variations in a course of a process aiming to keep it for a long-time on a requested and stable level. Achieving and keeping a process on a requested and stable level is dependent on a comprehensive analysis of process variability, when it is needed to detect, how the process functions, what are its limitations and their reasons, whether they repeat and what kind of affect do they have on a process. So a statistical regulation of a process can be defined as an immediate and continuous control of a process, which is based on a mathematical-and-statistical assessment of product quality. It provides information for operative and timely interventions into a process [6].

Basic principle of an analysis and improvement of processes and systems, defined by W. Shewhart is based on a presumption, that variability of values of quality indicators are caused by two kinds of causes:

- Random causes; the causes being a permanent part of a process or a system and that influence all components of the process.
- Definable causes; the causes that are not a permanent part of a process or a system; however they come into being due to specific circumstances.

A process or a system, which is affected only by random a cause is called a stable process, it means, that it is in a statistically managed condition. Only natural variability is involved in a stable process or in its products. It means, that a variability of output values can be predicted in statistically defined limits. A process, whose outputs are influenced by random as well as definable causes is called a non-stable process, it means, that it is in a statistically non-mastered condition. It is called non-stable as variability on various time sections is non-predictable. When the definable causes are identifiable and they are removed, the process becomes stable [6].

3 Determination of a statistical stability of a manufacturing process

Statistical process control (SPC) is a method of quality control which employs statistical methods to monitor and control a process. This helps to ensure that the process operates efficiently, producing more specification-conforming products. In manufacturing, quality is defined as conformance to specification. However, no two products or characteristics are ever exactly the same, because any process contains many sources of variability. In mass-manufacturing, traditionally, the quality of a finished article is ensured by post-manufacturing inspection of the product. Stability of a manufacturing process means a capability to observe technical and technological regulations and specified limit values in a certain time period. Aiming to reveal the causes why the process is violated, therefore it is necessary to deal with such analysis enabling to reveal and eliminate them. SPC uses statistical tools to observe the performance of the production process in order to detect significant variations before they result in the production of a sub-standard article. There are many methods and techniques for system modeling, while a broad range of advanced IT packages for process modeling is available in the market. Statistical analysis and a process regulation are interlinked and at the same time they influence stabilization of a manufacturing process in three phases.

- Definition of an instability of a manufacturing process,
- Introducing a process from instable into a stable condition,
- Keeping a process in a stable condition [7].

A regulation diagram $(\bar{x}, R)$ for a diameter and a range was used to define an instability of a manufacturing process, which is one of the most widely used regulation diagrams due to its simplicity. An essence of this diagram is a superior sensibility to revealing of extreme values within a subgroup.

The diagram predicates about stability or instability of a monitoring process, i.e. whether the process has been mastered. Aiming to define a stability of a requisite amount of 125 products within 2 hours time intervals the subgroups consisting of 5 products were sampled being assigned for an analysis. Value from processing of a descriptive statistics for a mean value and a range is presented on the table (Table 1). The values of the measured quantity enter the assessment process, arranged in ascending order according to individual groups. Descriptive statistics offer us maximum, minimum and mean values.

Table 1 Table of a descriptive statistics for a mean value and a range

Variable	Descriptive statistics			
	Mean	Minimum	Maximum	Range
Subgroup 1	43,26	43,12	43,36	0,24
Subgroup 2	43,24	43,18	43,31	0,13
Subgroup 3	43,17	42,99	43,32	0,33
Subgroup 4	43,19	43,11	43,38	0,27
Subgroup 5	43,26	43,16	43,37	0,21
Subgroup 6	43,15	43,03	43,28	0,25
Subgroup 7	43,25	43,16	43,33	0,17
Subgroup 8	43,21	43,11	43,31	0,20
Subgroup 9	43,19	43,04	43,29	0,25
Subgroup 10	43,23	43,11	43,35	0,24
Subgroup 11	43,14	43,04	43,25	0,21
Subgroup 12	43,17	43,07	43,24	0,17
Subgroup 13	43,22	43,01	43,39	0,38
Subgroup 14	43,15	42,99	43,27	0,28
Subgroup 15	43,23	43,14	43,36	0,22
Subgroup 16	43,17	43,05	43,36	0,31
Subgroup 17	43,27	43,20	43,34	0,14
Subgroup 18	43,09	42,98	43,18	0,20
Subgroup 19	43,21	43,11	43,37	0,26
Subgroup 20	43,18	43,05	43,23	0,18
Subgroup 21	43,18	43,08	43,30	0,22
Subgroup 22	43,21	43,17	43,26	0,09
Subgroup 23	43,17	42,97	43,32	0,35
Subgroup 24	43,14	43,00	43,19	0,19
Subgroup 25	43,20	43,09	43,30	0,21

Analysis of stability of a manufacturing process:

The data measured were analyzed using the Palstat software. Its main task is a computer aided support to a statistical regulation of a process, monitoring and taking measures of processes, verification of processes and machines capabilities. It facilitates a definition, which remedies are to be implemented in a process in order to achieve its stability and so cost reduction as well due to defectiveness. Value from processing of using the Palstat software are preseted in the figure 1.

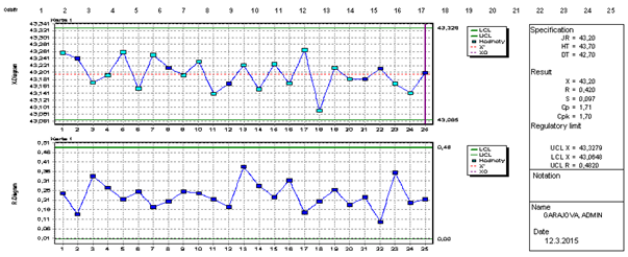

Fig. 1 Histogram and critical value of a testing statistics at exponential distribution [own resource]

It stems from a regulation diagram for a mean and a range that a process is statistically mastered. Regulation limits were exceeded in neither case, so the process appears as a stable one. We can say that a regulation diagram for this particular process had been properly chosen [7]. Information about a fact, whether the values of an attribute sufficiently approach a normal distribution was obtained through an analysis of values plotted into a probability grid.

Result of normal distribution test is shown in the figure 2.

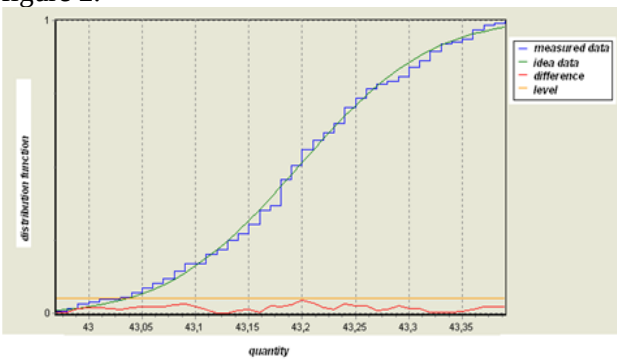

Fig. 2 Normal distribution test

A green line suggests ideal values and a blue line points at real measured values. A red line shows a difference in terms of significance of measured values. Resulting values are presented in the figure 3.

Parametr	Value
X'	43,196
R	0,42
S	0,097
Minimum	42,97
Maximum	43,39
Cp	1,71
Cpk	1,70
Cp	stable process
Cp	1,78
Cpk	1,77
UCL X	43,328
LCL X	43,065
PE	0,000 %
Nad HT	0
Pod DT	0
out of tolerance	0,00 %

Fig. 3 Assessment of SPC analysis

SPC is method of measuring and controlling quality by monitoring the manufacturing process. Quality data is collected in the form of product or process measurements or readings from various machines or instrumentation. The data is collected and used to evaluate, monitor and control a process. SPC is an effective method to drive continuous improvement. Statistical Process Control is based on the analysis of data, so the first step is to decide what data to collect. There are two categories of control chart distinguished by the type of data used: Variable or Attribute. It stems from resulting analyses that a particular process of welding a connector onto a copper line of a carbon brush is stable, so the customer´s requirement was met; it means that series production can be started. Then we acted upon a check plan. In the next part we were focused on a saw production line, where the dimensions of pieces cut away are collected with a slide gauge with a digital display, which is considered as an objectionable in terms of number of faulty pieces.

In addition to an improved manufacturing process through an implementation of a SPC method, we planned to adopt a new measuring method on a given line. As we can see in the table thereinafter, we analyzed measurements in three operators, who had taken measures of a cutting angle in ten products with three repetitions. Resulting values are presented in the table 2.

Table 2 Analysis of measurements operators

	operator A			operator B			operator C		
	1st series	2nd series	3rd series	1st series	2nd series	3rd series	1st series	2nd series	3rd series
1	89,341	89,016	89,825	90,033	90,175	91,133	91,100	89,791	90,525
2	89,692	88,908	89,333	89,691	90,400	89,566	90,300	91,041	90,691
3	88,691	88,891	89,175	89,566	90,358	89,366	89,883	90,441	90,066
4	89,716	90,441	89,066	89,491	90,400	89,858	89,283	89,975	89,991
5	89,491	90,258	89,091	89,375	90,200	90,973	89,033	89,941	89,750
6	89,550	90,083	89,300	90,116	89,725	88,866	90,366	90,025	90,583
7	89,558	89,966	88,883	90,350	89,116	89,750	89,983	90,775	90,558
8	89,575	89,975	89,708	88,800	90,383	89,066	91,008	90,208	90,583
9	88,858	88,608	90,100	90,008	90,073	89,325	90,841	90,200	90,075
10	88,891	89,850	89,916	90,316	90,666	90,483	90,033	90,600	89,966

We used a measuring system analysis (MSA), to define a capability of that particular measuring gauge, namely through indicators of repeatability and reproducibility. MSA is defined as an experimental and mathematical method of determining the amount of variation that exists within a measurement process. Variation in the measurement process can directly contribute to our overall process variability. A measurement systems analysis (MSA) is a thorough assessment of a measurement process, and typically includes a specially designed experiment that seeks to identify the components of variation in that measurement process. The analysis of this measuring method is based on tolerance. Acceptable tolerance range of a cutting angle is 91,5 up to 88,5 degrees and a mean required value has got 90 degrees. In the under mentioned table there are situated the measured values expressed as a variance, or a discrepancy from a mean value and characteristics for computation of required indicators

Resulting values are presented in the table 3. The data are from the monitored production process

where:
R – range of values in particular operators
R – a mean of value ranges
X – a mean of measured values

Table 3 Table of a descriptive statistics

	operator A									
	1	2	3	4	5	6	7	8	9	10
1 series	-0,659	-0,308	-1,309	-0,284	-0,509	-0,450	-0,442	-0,425	-1,142	-1,109
2 series	-0,984	-1,092	-1,109	0,441	0,258	0,083	-0,034	-0,025	-1,392	-0,150
3 series	-0,175	-0,667	-0,825	-0,934	-0,909	-0,700	-1,117	-0,292	0,100	-0,084
R_A	0,809	0,784	0,484	1,375	1,167	0,783	1,083	0,400	1,492	1,025
$\overline{R}_A$	0,940	$\overline{X}_A$	-0,541							

	operator B									
	1	2	3	4	5	6	7	8	9	10
1 series	0,033	-0,309	-0,434	-0,509	-0,625	0,116	0,350	-1,200	0,008	0,316
2 series	0,175	0,400	0,358	0,400	0,200	-0,275	-0,884	0,383	0,073	0,666
3 series	1,133	-0,434	-0,634	-0,142	0,973	-1,134	-0,250	-0,934	-0,675	0,483
R_B	1,100	0,834	0,992	0,909	1,598	1,250	1,234	1,583	0,748	0,350
$\overline{R}_B$	1,060	$\overline{X}_B$	-0,079							

	operator C									
	1	2	3	4	5	6	7	8	9	10
1 series	1,100	0,300	-0,117	-0,717	-0,967	0,366	-0,017	1,008	0,841	0,033
2. series	-0,209	1,041	0,441	-0,025	-0,059	0,025	0,775	0,208	0,200	0,600
3series	0,525	0,691	0,066	-0,009	-0,250	0,583	0,558	0,583	0,075	-0,034
R_C	1,309	0,741	0,558	0,708	0,908	0,558	0,792	0,800	0,766	0,634
$\overline{R}_C$	0,777	$\overline{X}_C$	0,254							

Analysis of the process capability was performed based on data obtained from regulation cards filled in with a sufficient ranges of values. Statistical Process Control is based on the analysis of data, so the first step is to decide what data to collect. There are two categories of control chart distinguished by the type of data used: Variable or Attribute. Statistical process control was developed as a feedback system that aids in preventing defects rather than allowing defects to occur. One element of a process control system is control charts.

Variable data comes from measurements on a continuous scale, such as: temperature, time, distance, weight. Attribute data is based on upon discrete distinctions such as good/bad, percentage defective, or number defective per hundred. We drew the above mentioned regulation diagram for a median and a range so that we can analyze a particular process. We can see from diagrams, that in the process there are no definable causes and it is statistically mastered. So additional requirement for analyzing of the process capability was met. Analysis through SPC regulation diagrams is shown in the figure 4.

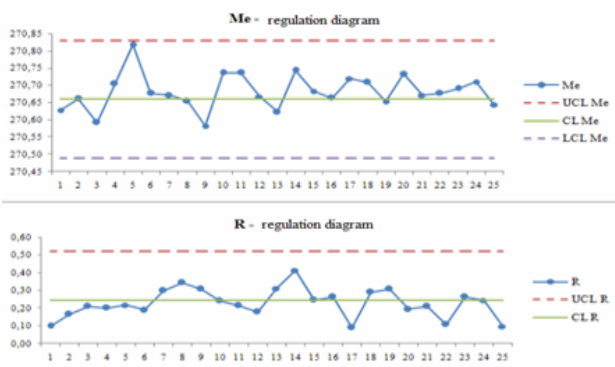

Fig. 4 Analysis through SPC regulation diagrams.

Computation of the indexes of process capability
Based on the same data as we had drawn regulation diagrams, we compute a capability index Cp, which expresses what we are able to achieve and Cpk, showing us a fact – what we had achieved and therefore a fact about the process condition. We analyzed a capability of this particular process using Minitab 12 software for Windows results of which are stated hereinafter in the figure 5.

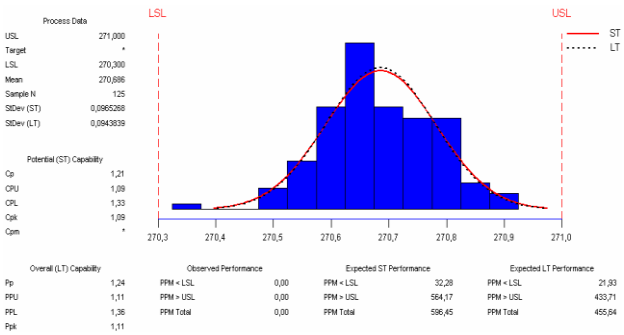

Fig. 5 Assessment of an analysis through a histogram

Another suitable approach that is appropriate to assess the processes in the company by means of mathematical analysis is a tool Histogram and critical value of a testing statistics at exponential distribution. Histograms are graphs that display the distribution of your continuous data. They are fantastic exploratory tools because they reveal properties about your sample data in ways that summary statistics cannot. The histogram shows sample data. On the other hand, the customized distribution line will try to find a probability distribution function for monitored quantity that has the maximum probability of creating a distribution that exists in monitored sample. It is well known that, the exponential distribution is one of the fundamental lifetime models and is widely used for describing a failure mecha-

nism of a system. Applications of this distribution in survival analysis and reliability theory are presented in statistical literature. Therefore, there is a clear need to check whether the exponential distribution is a reasonable model for the observations.

Testing statistics χ^2 = 8,54. A critical value of χ^2 distribution in such case has a value of $\chi^2 < \chi^2$<0,95,4=13,124. So $\chi^2 < \chi^2_{0,95,4}$. As a testing statistics is smaller than a critical value of χ^2 distribution, H_0 on a significance level α=0,05 is not refused and therefore we can note with credibility 0,95 that a time period between failures is a random variable, which has an exponential distribution. The elements is presented in the figure 6.

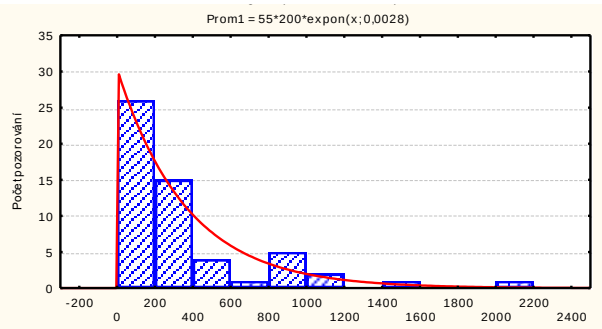

Fig. 6 Histogram and critical value of a testing statistics at exponential distribution

4 Results and discussion

The above mentioned methods were developed in real conditions of a company, which its manufacturing area concentrated into production of carbon materials, semi-finished products and finished pieces. It has been acting in electrical engineering, mechanical engineering, transport, automotive industry, chemical and metallurgical industry etc.

5 Conclusion

When performing an analysis in presented outputs we can note, that the processes are statistically mastered, but a prediction tool is missing for a maintenance crew intervention that should in an appropriate way to influence a next development. Statistical processing of data provides us with a basic for an analysis of a present condition, which is a base for predicative measures. In practice, it is very advantageous to use modeling and simulations based on the obtained statistical data using SPC. Simulation and evaluation predict the process and we do not have to spend money on failures or adverse events that would actually occur. Operations performed on a model instead of the actual production system do not disturb the stability of production processes. Treating a model as a duplicate of the actual system enables, inter alia, the transfer of the conclusions from the studies performed on the computer model to the actual production system. The use of statistical analysis methods allows us to predict in which direction the monitored processes will go. The article presents several possibilities of using SPC analyzes, which were performed in the past in various companies in order to improve maintenance processes.

[1] Papoulis, A., Pillai, U.: *Probability, Random Variables and Stochastic Processes*, ISBN-13: 978-0071226615, Edition: 4th, 2002

[2] Oakland, J.: *Statistical Process Control*, Science direct 2012,ISBN:978-0-7506-6962-7

[3] Rausand, M., Royland, A.: *System Reliability Theory: Models, Statistical Methods, and Applications*, 2nd Edition (Wiley Series in Probability and Statistics), ISBN-13: 978-0471471332 | Edition: 2nd, 2003

[4] Mikuš, P., Krbaťa,M.: *Termografia v pre ventívnej údržbe*, 2018.In: Vedecké práce a štúdie - 14. - Trenčín : TnUAD, 2018. - ISBN 978-80-8075-845-5.-s.104-107 ,

[5] Krbaťa, M., Mikušová,I.: *Teoretické rozdelenie kompozitných vlákien*, 2017, In: Transfer 2017 : Využívanie nových poznatkov v strojárskej praxi. - Trenčianske Teplice : Trenčianska univerzita Alexandra Dubčeka v Trenčíne, Fakulta špeciálnej techniky, 2017. - CD-ROM. - ISBN 978-80-8075-787-8. - CD ROM, [7 s.].

[6] Rykov, V., Balakrishnan, N., Nikulin, S.: *Mathematical and Statistical Models and Methods in Reliability*, Birkhauser Boston Inc, Pages 457, 2010, ISBN 0817649700

[7] Krbaťa, M., Eckert, M.: *Základy modelovania v programe Catia V5R20tiky*, - 1. vyd. - Trenčín : TnUAD, 2019. - 152 s. - ISBN 978-80-8075-89

3niversity Review, Vol. 15, Issue 1, p. 7-13, 2021.

UNIVERSITY REVIEW

DETERMINATION OF AUSTENITIZATION AND MARTENSITIC TRANSFORMATION TEMPERATURES OF M398 STEEL

Róbert Cíger[1] – Igor Barényi[2] – Michal Krbaťa[3]

[1] Department of Engineering Technologies and Materials, Faculty of Special Technology, Alexander Dubček University of Trenčín, Ku kyselke 469, 911 06 Trenčín
[2] Department of Engineering Technologies and Materials, Faculty of Special Technology, Alexander Dubček University of Trenčín, Ku kyselke 469, 911 06 Trenčín
[3] Department of Engineering Technologies and Materials, Faculty of Special Technology, Alexander Dubček University of Trenčín, Ku kyselke 469, 911 06 Trenčín

ARTICLE INFO

***Article history*:**
Received: 15.3.2021
Received in revised form: 23.4.2021
Accepted: 3.5.2021

Keywords:

Carbide
Dilatation curve
Tool steel
Microstructure
M398

Abstract:

The article deals with dilatometric analysis of M398 steel. It is a chromium steel, produced by Böhler using MICROCLEAN powder metallurgy process. The investigated steel is high-alloy chromium and vanadium with a high carbon content. The steel is characterized by high strength, resistance to abrasive wear and corrosion. The result of the dilatometric analysis will be dilatation curves for selected cooling modes in order to determine the initial austenitization temperatures Ac_1 and Ac_3 and the beginning of the matrensitic transformation Ms. Since the steel is highly alloyed with Cr and V, its microstructure is formed by a very high content of carbides of the M_7C_3 and MC type. These carbides affect the resulting mechanical properties of the material M398 and predetermine its use for screws in injection molding machines in the plastics industry, where this steel has the highest use so far.

1 Introduction

1.1 Dilatometric analysis

Dilatometric analysis is an experimental method used to study the phase transformations of metals and their alloys. The method uses volume changes associated with phase changes and is based on recording the change in the length of the experimental sample due to the temperature during its heating and cooling [1].
By dilatometric analysis, we can also determine, in addition to the phase transformations of the material also the thermal expansion, the rate of course of the phase transformations, and the values of critical temperatures. The volume changes during the phase transformation arise due to the difference between the grid parameter of the original and the newly formed phase. In the case of steels, it is mainly the transformation of the α phase (ferrite, K8) to the γ phase (austenite, K12) during heating associated with austenitization and subsequent transformation of austenite γ to martensite, bainite or perlite during cooling. The lattice parameter γ - iron is approximately 3.65×10^{-10} m. The value of the grid parameter - iron depends on the temperature and increases up to the value of 2.9×10^{-10} m [2].
Another variation of dilatometric measurement can be the measurement of deformation processes under heat, in which we monitor the dependence of defor-

* Corresponding author. Tel.: 00421-32-7400 265
E-mail address: robert.ciger@tnuni.sk

mation and temperature of the examined sample. The authors of Krbaťa, Barényi, Eckert, Mikušová, deal with this topic in an article entitled: Hot Deformation Process Analysis and Modelling of X153CrMoV12 Steel.[3]

For the required measurement accuracy, it is necessary to use a suitable dilatometric device. Experimental measurements will be performed on a dilatometric device DIL 805. The output of the measurement will be a dilatation curve, representing the dependence of the change in length during heating and cooling of the examined sample. In the case of a phase change, the length does not change in proportion to the temperature change. The volume change of the sample will subsequently be reflected on the dilatation curve Fig.1, which will allow us to evaluate it.

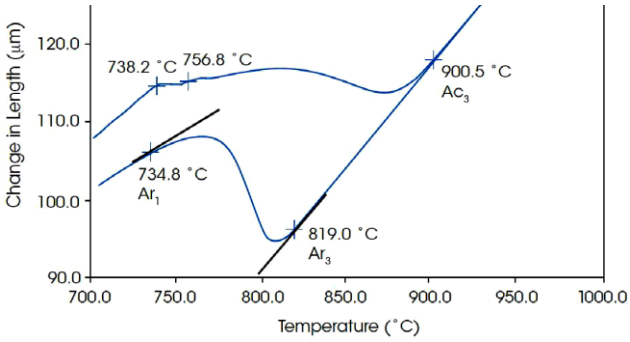

Fig. 1 Dilatation curve for medium alloy steel - high temperature range [4]

In the case of steels, these are mainly the limit temperatures in the ARA and IRA diagrams, which are important in the design and optimization of heat treatment processes [3, 4]. The main parameter influencing the shape of the resulting ARA diagram is the proportion of individual alloying elements. The secondary parameter influencing the shape of the ARA diagram is the height of the austenitization temperature. In Fig. 2 we can see how the individual alloys affect the final shape of the diagram.

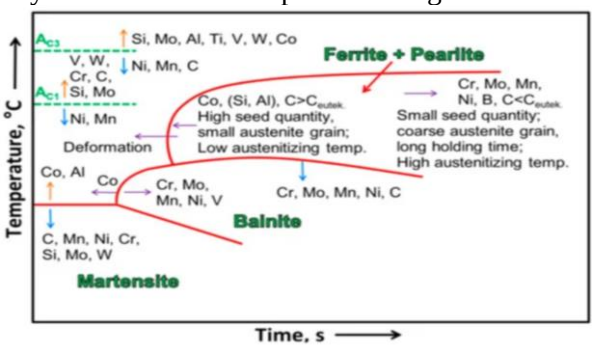

Fig. 2 Influence of alloying elements on the shape of the ARA diagram

2 Experimental details

2.1 Chromium tool steel M398

In industrial practice, a variety of tool steels are used in the manufacture of various components, which are subject to high stress and wear during processes of friction that have a large impact during their operating life.[5]

The investigated material M398 developed by BÖHLER focuses on the high requirements in the field of plastics processing. It is a high-carbon, martensitic steel, made of powder metallurgy. Thanks to the production method and chemical composition, the steel provides extremely high resistance to mechanical wear as well as corrosion resistance.

The prerequisite for the use of steel is the replacement of the currently used material M390 in the production of injection molding screws. Thanks to the high wear resistance of M398 steel, it would be possible to create screws enabling the processing of plastics with an increased content of glass fibers or to prolong the life of the screws. Other properties of M398 steel include high dimensional stability during heat treatment, good corrosion resistance, the possibility of polishing to a high gloss.

Table 1 shows the chemical composition provided by BÖHLER as well as the results of the spectral analysis provided by SPECTROLAB Jr. CCD device of the investigated M398 steel.

Table 1 Chemical composition of the M398 steel (wt. %)

	BÖHLER M398	Spectral analysis M398
C	2.70	2.65
Si	0.50	0.55
Mn	0.50	0.51
Cr	20.00	20.09
Mo	1.00	1.00
V	7.20	7.1
W	0.70	0.43

Figures Using the THERMOCALC software, a phase diagram of Fig. 3 and a diagram of the phase fractions of Fig. 4 of the examined steel with a carbon content of up to 3% were created. The created pair of diagrams is a useful tool in the analysis of expansion curves, as we can assume the formation of individual phases at given temperatures.

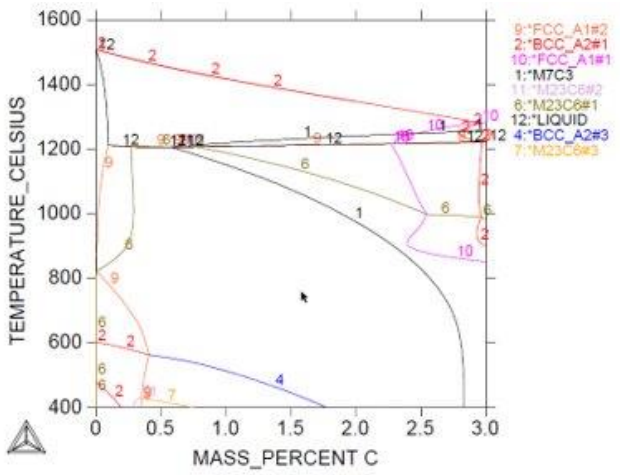

Fig. 3 Phase diagram of M389 steel with carbon content < 3%

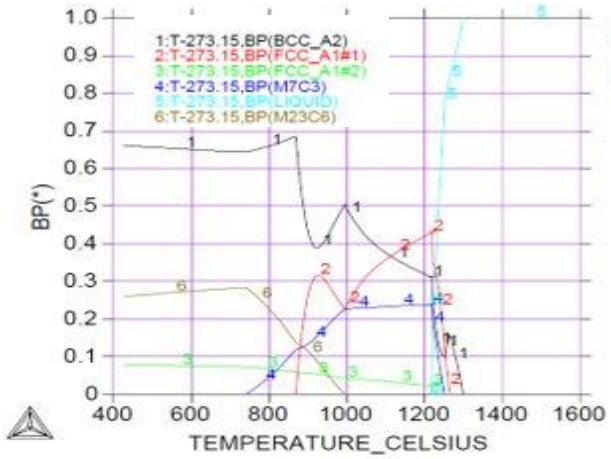

Fig. 4 Phase fractions

The main concept for increasing the macro-hardness is the high content of MC and M_7C_3 carbides, which can be observed in the microstructure itself provided by BÖHLER in Fig.5.

On the Fig. 6 we can observe the effect of tempering temperatures on the resulting hardness of the material M398. As the figure shows, the highest hardness is reached after cooling the material to negative temperatures. With this material, the cooling temperature following hardening is set at -70 °C, with a residual austenite value of less than 1% (Fig. 7). Tempering temperatures in the range of (200 - 300) °C are suitable when the material is designed for high corrosion resistance. For materials that have not been cooled to sub-zero temperatures, there is an area in the tempering temperature range of (540 - 560) °C where the material is most resistant to wear. For materials that are frozen, this area is shifted between (510 - 530) °C.

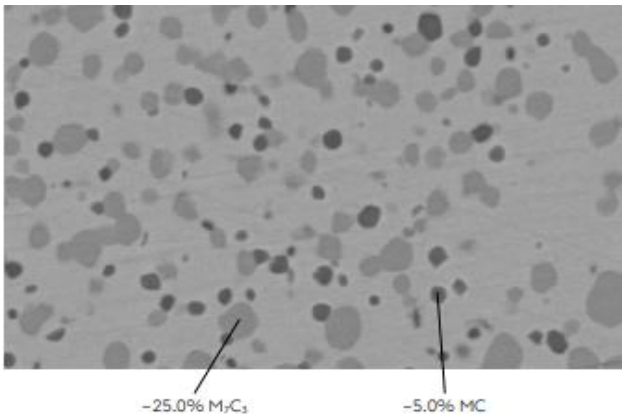

Fig. 5 Microstructure of M398 steel [6]

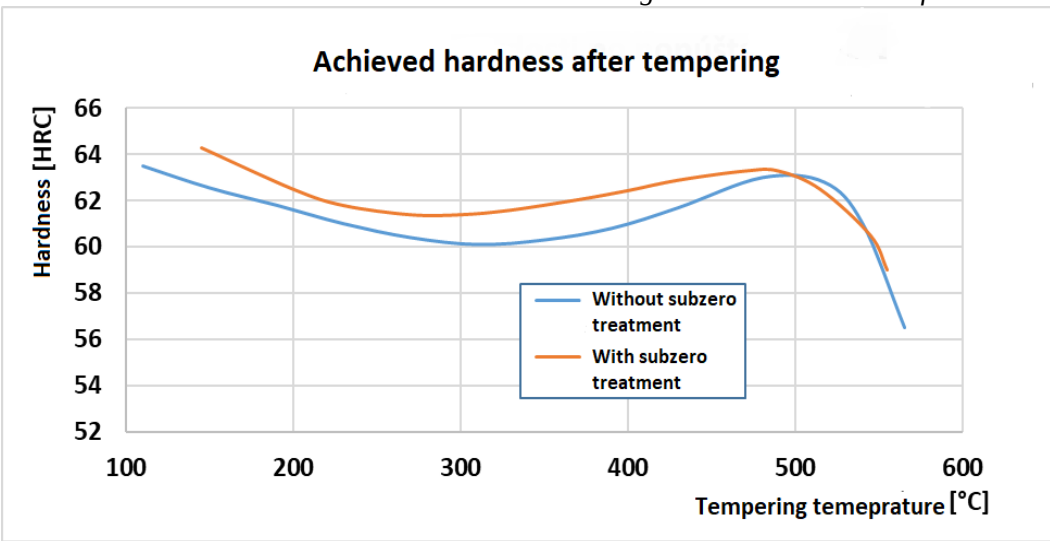

Fig. 6 Graph of achieved hardness after tempering of M398

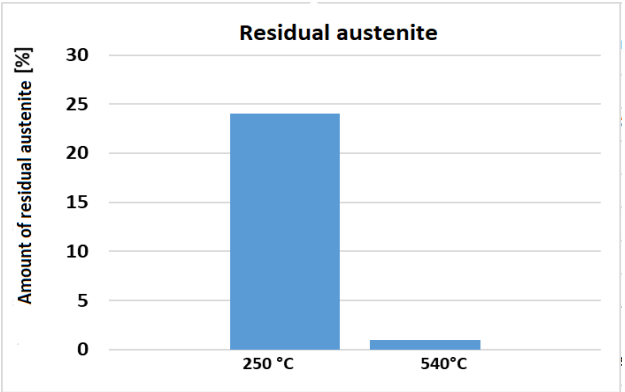

Fig. 7 amount of residual austenite after heat treatment

2.2 Methodology of dilatometric analysis using dilatometer DIL 805A

The DIL805A / D dilatometer is a laboratory device that is used either to measure and record expansion curves or to measure hot deformation resistances. It is intended for physical modeling of heat treatment processes (805A) or hot metal forming processes (805D) [5,6]. An experimental sample of the prescribed shape and dimensions is placed in a working chamber (Fig. 8a) between the Al_2O_3 tips. The tips are connected to a precision extensometer, which thus records changes in length during the execution of the set temperature cycle. [7]

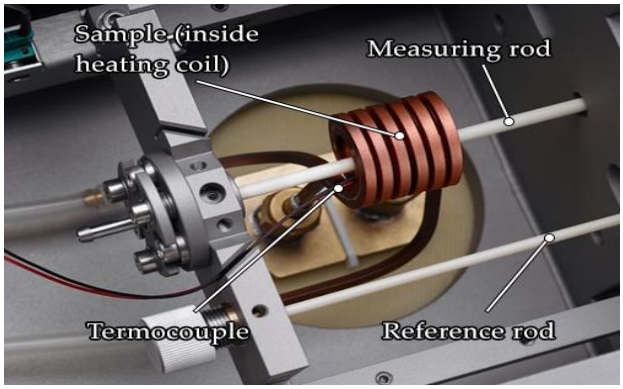

a)

b)

Fig. 8 a) Working chamber of dilatometric device DIL805A, b) parameters of experimental sample for DIL805A

Welded to the sample are high temperature resistant conductors based on high fusible metals (Pt, Pt + Rh), connected to a thermocouple for recording and regulating the temperature inside the chamber. [7]

The first step of dilatometric measurement is to set the temperature mode and its parameters using the device software. The system makes it possible to carry out one or more successive temperature cycles, consisting of heating, possible holding at temperature and cooling. After inserting the sample and connecting the thermocouple to the system, the chamber is closed and evacuated. The phases of heating the sample and holding at temperature take place in a vacuum (5×10^{-3} mbar). The sample inserted inside the coil is heated by induction heating. At the beginning of the cooling phase, the heating is switched off and a cooling gas is pressurized into the chamber - most often H_2, N_2 or Ar. During the whole process, the temperature of the sample and its change in length due to temperature with a resolution of 0.05 µm / 0.05 °C are recorded very accurately. The graphical representation of this record is the dilatation curve. The step changes in the dimension on the curve represent phase changes (PF → A, A → B, A → M, etc.). The dilatometer software has tools for reading the temperatures of the beginning and end of these phase changes, most often in the form of a tangent at the point of beginning of change (first derivative dl / dT) or second derivative dl / dT. [7]

An experimental samples with dimensions according to Fig. 8b. were prepared for dilatometric analysis of M398 steel. Subsequently, 3 dilatometric measurements representing rapid cooling were performed on a DIL805A dilatometer. The measurement itself has three phases, heating, endurance, cooling. The heating rate of the sample was constant in all modes. Heating was performed at a rate of 1 °C/s followed by holding at 1150 °C for 30 min with cooling modes according to the parameters specified in Tab.2. The initial and final cooling temperatures were constant for all modes (T_{max} = 1150 °C, T_{min} = 50 °C). Cooling was performed using H_2 gas with ambient temperature (approx. 23 °C).

Table 2 Input cooling parameters for selected temperature modes of dilatometric analysis of M398 steel

Cooling mode	Cooling time T_{max} to T_{min}			Cooling rate	T_{max} [°C]	T_{min} [°C]
	t [s]	*t* [min]	*t* [hr.]	*v* [°C/s]		
1	11	0.18	0	100	1150	50
2	110	1.83	0	10	1150	50
3	220	3.67	0	5	1150	50

3 Results and discussion

The method for determining the limit temperatures Ac_1 and Ac_3 is shown in Fig. 9. The phase transformation is reflected in the expansion curve as a step change in the length of the experimental sample as a function of temperature. The initial temperature Ac_1 corresponds to the temperature at which the expansion curve begins to deviate from the linear expansion during heating due to the onset of austenite formation. Subsequently, the temperature Ac_3 is defined as the temperature at which the expansion curve begins to regain a linear character during heating. The average value obtained from all three dilatometric measurements for M398 steel is Ac_1 = 955 °C and Ac_3 = 1085 °C. The figure shows the derivation of the heating curve, which is used to determine the beginning and end of the austenitization temperatures Ac_1 and Ac_3. Also, in the figure we can observe a step change of the derivative curve at 710 °C and a return to its linear direction at 735 °C. This short deviation records the dissolution of M_7C_3 type carbides, which is also shown in Fig. 4.

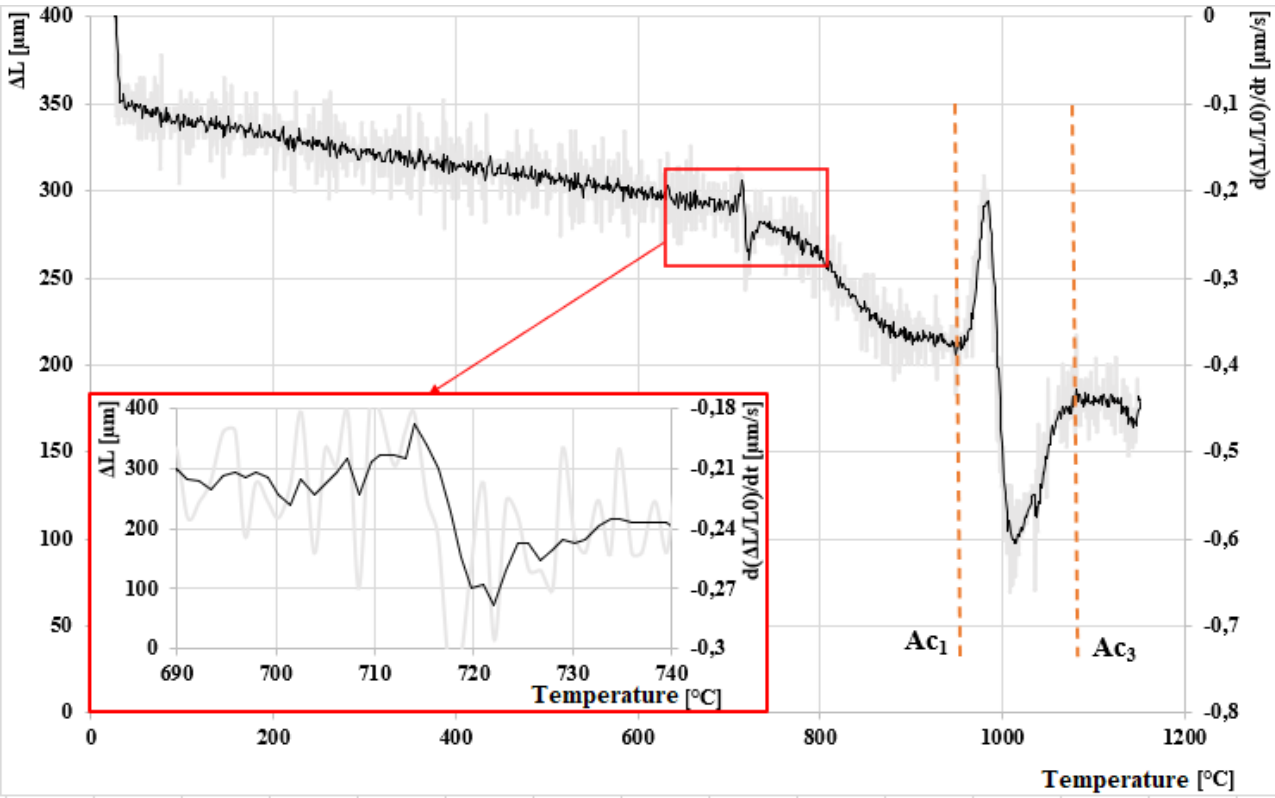

Fig. 9 Derivation of the dilatation heating curve

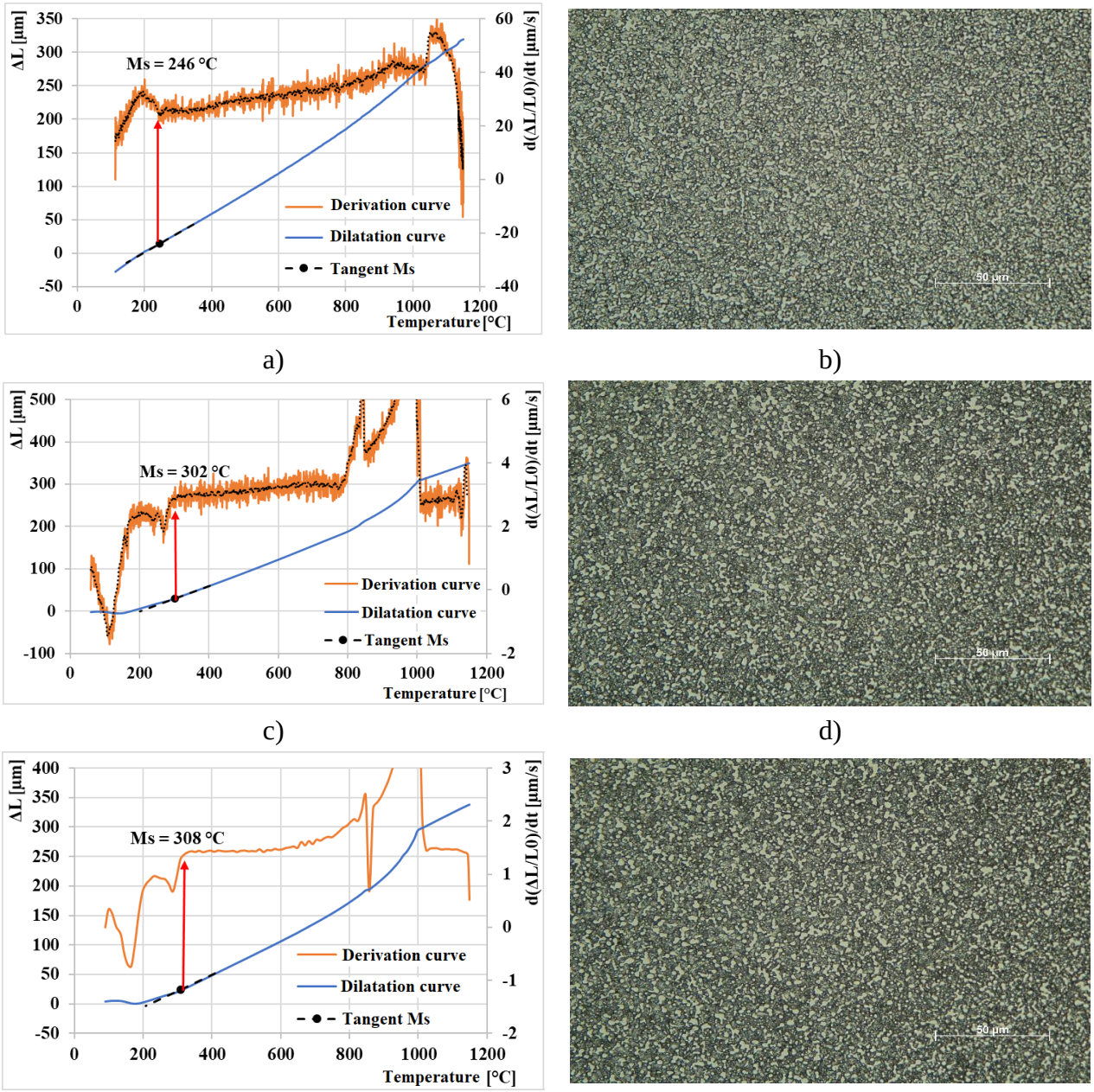

Fig. 10 Dilatation curves for selected cooling modes

The expansion curve from the austenitization temperature of 1150 °C is shown in Fig. 10a. An expansion curve cooled at 100 °C/s and its derivatives were used to determine the initial temperature of martensite formation and its value is Ms = 246 °C. The dashed line in the figure is a tangent copying the linear part of the expansion curve. The point of deviation between the tangent and the curve is considered to be the initial temperature Ms. This point also corresponds to the Ms temperature determined from the derivation curve. The final microstructure obtained is shown in Fig. 10b and is fully formed by a carbide-containing martensitic matrix.

Another expansion curve at a cooling rate of 10 °C/s is shown in Fig. 10c. Given the dilatation curve, two types of martensite probably formed in the structure of the material. Since the initial temperature Ms reached 302 °C, this shows an increase in the initial temperature Ms by 55 °C compared to the previous expansion curve. Due to the decreasing cooling rate, the temperature Ms cannot have an increasing character [10]. Likewise, this deflection cannot represent the beginning of the formation of a bainitic trans-

formation because the investigated M398 steel is highly alloyed with chromium and vanadium, and these two elements according to Fig. 2 move the entire ARA diagram to the right. The microstructure of the sample tax is shown in Fig. 10d. it is also formed by a martensitic matrix with a high carbide content.

The same paradox occurred in the last sample examined, which was cooled at a rate of 5 °C/s (Fig. 10e). Here, the initial temperature of Ms reached 308 °C. At a temperature of about 860 °C, a step change in the derivative curve can also be seen. This change is probably related to the transformation of the FCC austenitic lattice to a BCC lattice as shown in Fig. 4. The resulting microstructure is shown in Fig. 10f.

However, it must be stated that metallographic analysis using an optical microscope is insufficient. For a qualitative evaluation of the resulting expansion curves it is necessary to use an electron microscope, which will be equipped and a chemical analysis of EDS.

4 Conclusion

The paper describes dilatometric analysis of tool steel M398. The theoretical part of the article is supplemented by several thermo-mechanical-chemical properties of the investigated material M398. The study of the expansion behavior of the steel was performed at three different cooling rates of 100, 10 and 5 °C/s from an authentication temperature of 1150 °C. Dilatation results are supplemented by metallographic analysis of experimental samples using an optical microscope.

The following conclusions can be drawn from this work:

1) The temperature value Ac_1 = 955 °C and Ac_3 = 1085 °C were determined from all three measurements and their average value was determined. These temperatures reach higher values than conventional tool steels due to the high content of Cr and V-based alloying elements.

2) At a cooling rate of 100 °C/s, a martensitic matrix with a high carbide content is formed in the resulting structure. Carbides are formed on the basis of M_7C_3 and MC, which must be proved using an electron microscope and chemical analysis of EDS elements.

3) At cooling rates of 10 and 5 °C/s, two types of high carbide martensite were likely to form in the resulting structure. These carbides probably bound carbon and other alloying elements, while a different type of martensite began to form in their immediate area, which must be proved using an electron microscope and chemical analysis of EDS elements.

5 Acknowledgement

Authors are grateful for the support of experimental works by project APVV 15-0710.

References

[1] Zhong Zhan, Y., Du, Y., Hong Zhuang, Y.: *Chapter four - determination of phase diagrams using equilibrated alloys, In: Methods for Phase Diagram Determination*, Elsevier Science Ltd, (2007), p. 108-150.

[2] Morales-Rivas, L.: *Nanomechanical characterization of nanostructured bainitic steel: Peak Force Microscopy and Nanoindentation with AFM*, Scientific Reports volume 5, Article number: 17164 (2015).

[3] Krbaťa, M., Eckert, M., Križan, D., Barényi, I., Mikušová, I.: *Hot deformation process analysis and modelling of X153CrMoV12 steel*, Volume 9, Issue 10, October 2019, Article number 1125.

[4] Pernis, R., Ličková, M.: *Rozšírené použitie dilatometra DIL 805*, Transfer, TnUAD, Trenčín, (2016), p. 1-5.

[5] Krbaťa, M., Eckert, M., Majerík, J., D., Barényi, I.: *Wear Behaviour of High Strength Tool Steel 90MnCrV8 in Contact with Si3N4*, metals 2020 , p. 16.

[6] BOHLER, prezentačný materiál ocele M398 dostupné https://www.bohler-edelstahl.com/app/uploads/sites/92/2019/09/M398En.pdf

[7] Barényi, I.: *Dilatometrická analýza ocele OCHN3MFA*, 2018. p. 7.

[8] Dilatometry, TA Instruments, Hüllhorst, Germany, 2013

[9] DIL 805: User manual. TA Instruments, Hüllhorst, Germany, 2013.

[10] Krbata, M.; Majerik, J.; Barenyi, I. Eckert, M.: *Experimental determination of continuous cooling transformation diagram for high strength steel OCHN3MFA*, IOP Conference Series Materials Science and Engineering, 2020, p. 776

University Review, Vol. 15, Issue 1, p. 14-19, 2021.

UNIVERSITY REVIEW

INVESTIGATION OF NANOMECHANICAL PROPERTIES OF MICRO-STRUCTURAL COMPONENTS OF SELECTED ALLOY TOOL STEEL

Jana Escherová[1*] – Jozef Majerík[1] – Michal Krbaťa[1]

[1]Department of Engineering Technologies and Materials, Faculty of Special Technology, Alexander Dubcek University of Trencin, Ku kyselke 469, 911 06 Trencin, Slovakia

ARTICLE INFO

***Article history*:**
Received: 15.3.2021
Received in revised form: 23.4.2021
Accepted:3.5.2021

Keywords:
Quasistatic nanoindentation
Berkovich test tip
Nanohardness
Reduced Young's modulus
Tool steels

Abstract:

The aim of this study is to measure and evaluate of mechanical properties of microstructural components of alloyed tool steel C120U according to STN Standard. The measurement was performed on an experimental device Hysitron TI 950 Triboindeneter, which is a part of CEDITEK Laboratories at FST TnUAD. The testing of alloyed tool steel C120U was performed due to the high demands on tool steels in industrial practice, such as high strength, toughness, fatigue and abrasive wear resistance, corrosion resistance, temperature stability and others. The Berkovich test tip type was used in the research process. Chapter 1 describes the research of foreign authors who focused on the mechanical properties of high-strength steels. Chapter 2 shows the results of own experiments such as chemical composition, mechanical properties, evaluation and description of microanalysis of alloy tool steel C120U by using light microscopy. The calculation of the Young's modulus of elasticity and the experimental method are also found in Chapter 2. Chapter 3 presents the measured mechanical properties of the components of the structure of the tested steel, the distribution of individual indent positions on SPM (Scanning Probe Microscopy) scans, the nanoindentation curve obtained from indents on SPM scans and a comparison of Young's modulus of elasticity Er and calculated Young's modulus of elasticity phase Es. The conclusion and evaluation of the measured data is given in Chapter 4.

1 Introduction

Quasi-static nanoindentation is a contact method which consists in mechanical contact of the test tip of the investigated material, where the output measured quantities are reduced Young's modulus of elasticity E_r [GPa] and nanohardness H [GPa]. Their use is in areas where these quantities cannot be measured by conventional methods of measuring mechanical properties. Quasi-static nanoindentation differs from basic methods in that nanometers (10^{-9} m), are used as a measure of penetration depth, in contrast to conventional methods where the units are micrometers (10^{-6} m) or millimeters (10^{-3} m) [1,7]. In conventional tests for measuring the hardness of materials, the contact area is calculated from direct

[*] Corresponding author. Tel.: +421327400265;
E-mail address: jana.escherova@tnuni.sk.

measurements of the dimensions of the residual impression which remained on the sample surface after removal of the load [1,5]. When tested method by the quasi-static nanoindentation is the size of the residual impression in micrometers is too small to be measured directly. Therefore, it is common to determine the contact area by measuring the penetration depth of the test tip into the surface of the test specimen [1]. Nanoindentation techniques can also be used to calculate elastic modulus, deformation curing exponent, fracture toughness (for example for brittle materials) and viscoelastic properties. Data are obtained when the test tip is brought into contact with the flat surface of the sample with increasing load. Load and indentation depth are recorded with each load increment, which ultimately provides a measure of modulus and hardness as a function of depth below the surface [1]. Nanoindentation tests are commonly used to measure the hardness of materials, but diamond test tips such as Vickers, Berkovich and Knoop can also be used to investigate other mechanical properties of solids, such as strength, fracture toughness and tensile / compressive residual stresses [1]. The authors [4] in his work performed nanoindentation tests of samples at room temperature on a NanoTest nanoindent supplied by company Micro Materials Ltd., Wrexham, UK, with using a three-sided Berkovich diamond tip with a nominal angle of 120 ° and a radius r = 100 nm [4]. Nanoindentation tests were performed at the same maximum load (F = 500 mN), with load speed of 50, 25, 16.67, 12.5, 10, 5 and 1 mN.s^{-1} The test tip was then left to endurance at maximum load for t = 5 s. Then it followed by unloading with speed of 50 mN.s^{-1} and for all tests. At least 10 indentation points were performed and for each load separately. The measurements results were subsequently averaged [4]. All hardness values measured during the nanoindentation process in the authors' study [4] are higher than the hardness values of the tested steel H13 [6,8]. The steel H13 was produced in the basic state, but without the use respectively participation SLM (Selective Laser Melting) obtained from the results of the Mencin process [3,4]. The results of this study are in agreement with the results of previous experimental reports on nanoindentation tests of H13 material [6,8]. The authors of the study [2] performed nanoindentation tests with samples at room temperature in order to evaluate the mechanical properties of SLM H13 steel. A three-sided diamond Berkovich test tip was used from company Micro Materials Ltd., Wrexham, UK. The maximum load was chosen with sufficient size to ensure the presence of indents at all stages of sample testing. Nanoindentation tests were performed at the same maximum load (500 mN) with the achieved load speed heights of 50, 25, 16.67, 12.5, 10.5 and 1mN.s^{-1}. The test tip was then left to endurance at maximum load for t = 5 s behind which followed by unloading at a speed of 50 mN.s^{-1} and for all tests. For each load there were at least ten indents and the results are then averaged [2]. The load stress (r), a representative load from the nanoindentation test, is defined as the instantaneous load (P) divided by the projected contact surface (Ac), which is also the definition of the indentation hardness (H) measured during [2]. In addition, during nanoindentation tests at a constant load speed, the degree of deformation is a non-linear function of time, which can be estimated from the depth and time data obtained for a given range of indentation depths [2].

2 Materials and methods

2.1 Experimental method

Nanoindentation analysis was performed on a measuring device of the Hysitron Triboindenter TI 950 type (Fig. 1) and its evaluation software Triboscan (Fig. 2). Testing was performed at room temperature with the application of Berkovich's internal geometry in the laboratory of mechanical testing CEDITEK at the FST in Trenčín. Quasi-static nanoindentation measurement was realized on a metallographic sample (Fig. 3).

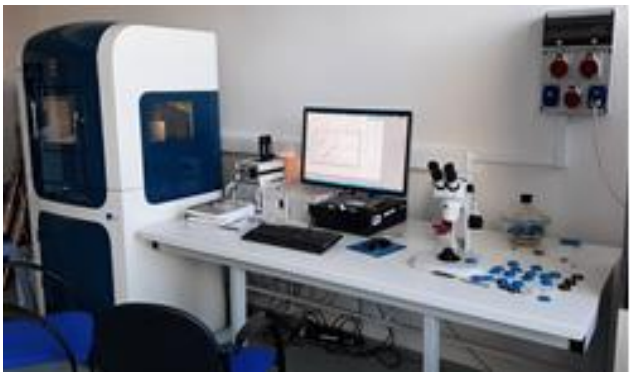

Fig. 1 Work equipment Hysitron TI 950 Triboindenter with accessories

During the nanoindentation measurement was recorded the load together with the displacement, when the Berkovich tip was pressed into the surface of the

measured sample using standard *P-h* profiles. The quasi-static nanoindentation method was used at designated locations of the base material of the microstructure of the test sample (Fig. 3).

Fig. 2. Selection from the basic menu - selection of an appropriate measurement methodology.

The individual areas of research were determined with the help of an optical microscope as an built-in part of the device (Fig. 3).

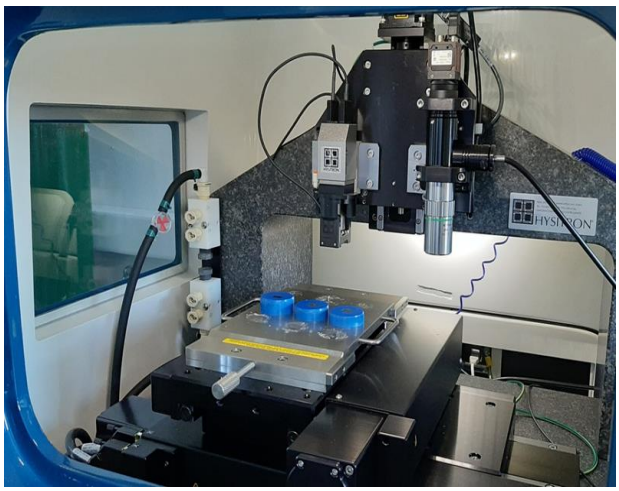

Fig. 3. Display of a metallographic sample

Subsequently, an SPM scan of a selected area with dimensions of 50x50 µm was performed (see Fig. 5). The selection of individual places for the implementation of indents for the selected material were defined by a mechanical form with a selected number of indents on the examined area. As a loading curve was used in the process experiment a standard trapezoid with a maximum at 8000 µN and with the total indentation time t = 2 s. The designations of the positions for the individual indents for the base material of the tested tool steel C120U are shown in Fig. 5. This way measured the values of nanoindentation hardness H [GPa] and reduced Young's modulus Er [GPa] in their individual positions were using of Triboscan software subsequently evaluated. At the end of the measurement process, *P-h* curves are generated for the individual indents shown in Fig. 6.

2.2 Calculation of Young's modulus of elasticity of the phase

The calculation of the Young's modulus of elasticity of the phase E_s for the investigated alloyed tool steel C120U was realized according to the relation (1):

$$E_s = (1-\upsilon_s^2)/(\frac{1}{E_r} - \frac{1-\upsilon_i^2}{E_i}) \qquad (1)$$

where E_i is the modulus of the test tip and υ_s a υ_i are the Poisson constants for the sample and the Berkovich type test tip. The values E_i = 1141 GPa, υ_i = 0,07 a υ_s = 0,29 are used in all calculations.
The value E_s for the cementite phase:
The calculation of the Young's modulus of elasticity of the phase E_s for the cementite phase for alloy tool steel type C120U it is calculated below. Where the calculated average value of the reduced Young's modulus of elasticity is E_r =212,06 GPa. After substituting the given values into the relation (1), the Young's modulus of elasticity of the phase is E_s = 238,30 GPa. The values of the reduced Young's modulus of elasticity E_r and the Young's modulus of elasticity of the phase E_s are given in Table 1.

Table 1 The Reduced modulus of elasticity and Young's modulus of elasticity of the phase

Steel	Phase			
	Cementite		Perlite (cementite component)	
	Es [GPa]	*Er* [GPa]	*Es* [GPa]	*Er* [GPa]
19221	238,30	212,06	201,84	184,85

The value E_s is for the perlite phase (cementite component):
The average value of the reduced Young's modulus of elasticity in this phase is E_r = 184,5 GPa. Other

values such as test tip modulus and Poisson constants for sample and test tip are the same as in the previous phase. The Young's modulus of elasticity of the phase for the perlite phase (cementite component) is E_s = 201,84 GPa.

2.3 Mechanical properties and chemical composition

The steel C120U is an alloyed tool steel with a higher carbon content of 1.1%. This steel was chosen from due to achievement a high hardness after hardening (min. 64 HRC) and which is tempered to 60 ± 2 HRC. This type of alloyed tool steel is used for cutting, shearing and forming tools, hand tools and gauges. The steel C120U has good toughness in core, insensitivity to hardening cracks, more difficult hot formability and good machinability in the annealed state. The chemical composition and mechanical properties of the tested alloyed tool steel C120U are shown in Table 2.

2.4 Microstructural analysis

The steel C120U is a supereutectoid steel with a cementitic-pearlitic structure (Fig. 4). The steel is in the state after normalization annealing. The dark places represent perlite, what is a eutectoid mixture of ferrite and cementite. The white areas represent secondary cementite.

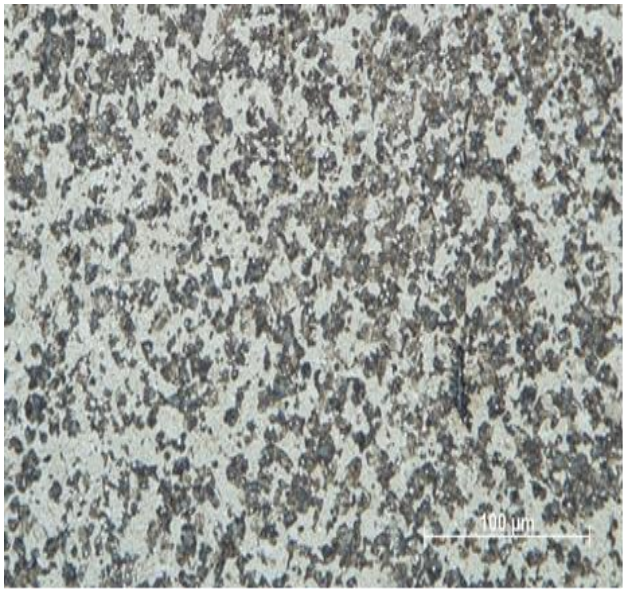

Fig. 4. Microstructure of alloyed tool steel C120U

Table 2 Chemical composition and basic mechanical properties of alloyed tool steel C120U

Chemical composition and mechanical properties of the tested steel C120U							
Chemical composition of steel C120U according to ISO Standard [wt. %]							
Element.	*C*	*Mn*	*Si*	*P*	*S*	*Cr*	*Ni*
wt. %	1,10-1,24	0,20-0,35	0,15 - 0,30	max 0,025	max 0,30	max 0,15	max 0,20
Chemical composition of steel C120U measured by spectral analysis [wt. %]							
Element	*C*	*Mn*	*Si*	*P*	*S*	*Cr*	*Ni*
wt. %	1,15-1,25	0,10-0,40	0,10 - 0,30	max 0,03	max 0,03	max 0,15	max 0,20
Mechanical properties of steel C120U							
Hardness HRC	59 - 66 (H. t. 770 °C / water; T. t. 250 – 100 °C / 2h)						
Flexural strength R_{mo} [MPa]	⊔ 3 750 (at HRC 60)						
Yield strength in pressure R_{et} [MPa]	⊔ 2 600 (at HRC 60)						

3 Results and discussion

As part of the nanoindentation test, measurements were performed consisting of six to seven indents at the selected place of the microstructure of the test area (Boundary). In the process experiment was measured area bounded by dimensions of 50x50 µm. As the loading curve was for realized measurement used standard trapezoid with a maximum at 8000 µN and an indentation time t = 2 s. The experimental device nanoindentor type Hysitron Triboindenter TI 950 was used as a test device. The measured positions of the individual indents are shown on the SPM (Scanning Probe Microscopy) scan of the evaluated area of the tested sample from C120U steel (Fig. 5). The measured values of nanoindentation hardness H [GPa] and reduced Young's modulus of elasticity E_r [GPa] in individual positions are given in Table 3. On Fig. 6 are shows the resulting shapes of the individual nanoindentation curves obtained from the indents on the SPM

scan of the evaluated area of the test sample. The designation of the curves is identical with the designation of the measuring positions in Fig. 5 and in Table 3.

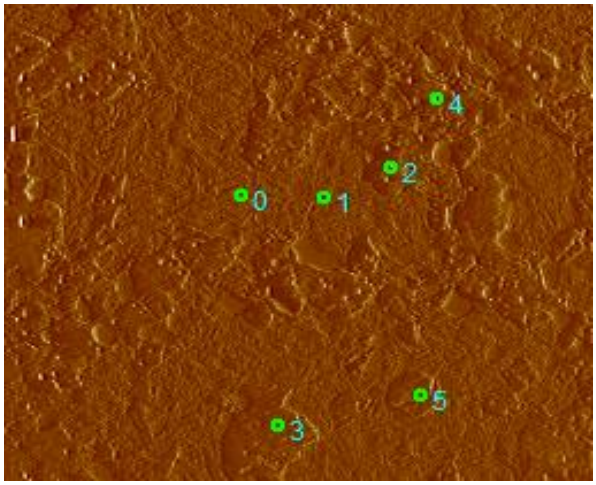

Fig. 5. Deployment of individual positions indents on SPM scan in the tested sample of alloyed tool steel C120U

Table 3 Measured mechanical properties of components structure alloyed tool steel C120U

Position	Nanohardness H [GPa]	Reduced modulus of elasticity E_r [GPa]	Phase (estimated)
0	10,88	207,69	Cementite
1	11,38	216,43	Cementite
2	5,98	178,60	Perlite (cem. c.)
3	6,03	170,65	Perlite (cem. c.)
4	6,14	189,91	Perlite (cem. c.)
5	6,53	200,23	Perlite (cem. c.)

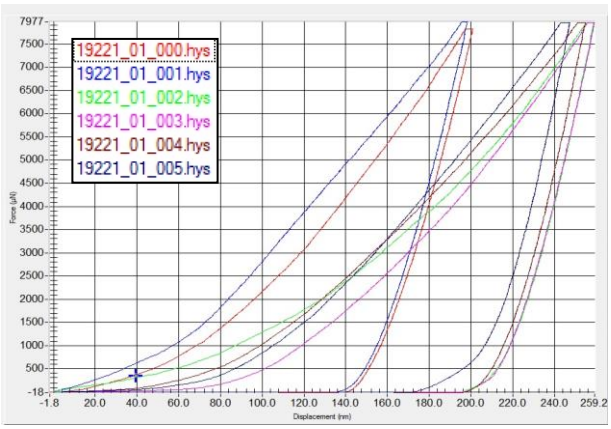

Fig. 6. Nanoindentation curves obtained from indents on SPM scans steel C120U

Load part of the indentation curve is used to evaluate nanohardness, where the unloading part is used to calculate reduced Young moduluas (see Fig. 6). Overall overview of the individual tested phases for the alloyed tool steel C120U and its nanohardness H and the reduced Young's modulus of elasticity E_r are shown in Table 3. A mutual comparison of the reduced Young's modulus of elasticity E_r and by relationship (1) the calculated Young's modulus of elasticity of phase E_s for the tested alloy tool steel C120U is shown on Fig. 7.

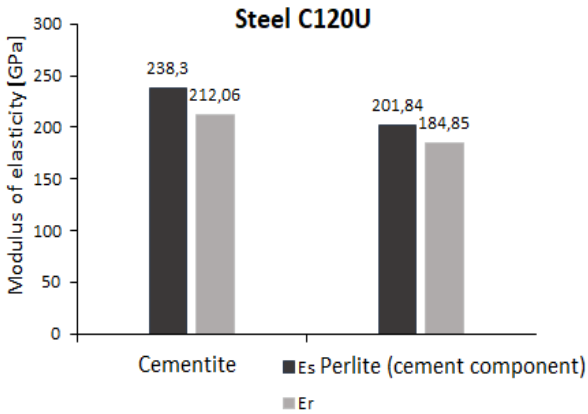

Fig. 7. Comparison of measured modulus Er and calculated modulus Es for alloyed tool steel C120U

Using the Hysitron TI 950 Triboindenter, the nanohardness values of the individual structural phase components were determined, as well as the reduced modulus of elasticity. The Berkovich type was used as a test tip. The reduced modulus of elasticity was used to calculate the modulus of elasticity of specific structural phase components. The results of the calculation are clearly marked in the graph on the Fig 7. It can be seen from the comparison that the values of the tensile modulus of elasticity of the individual phases are higher by 3% to 14% than their reduced modulus, assuming the above-mentioned values of the Berkovich indenter.

4 Conclusion

The aim of the performed experiment was to test the nanohardness of the basic structural components of the selected alloyed tool steel C120U with using the experimental method of quasi-static nanoindentation. The reason for the chosen alloy tool steel C120U was the fact that on this steel higher demands are placed in practice, such as high strength, wear resistance, toughness and other mechanical

properties that can be review and evaluated on the basis of hardness. Using the test device Hysitron TI 950 Triboindenter, which is equipped with the evaluation software Triboscan were detected the nanohardness values through experiment by of the specific structural phase components as well as the reduced Young's modulus of elasticity. During testing was used indentation tip type Berkovich. The determined reduced Young's modulus of elasticity obtained by nanoindentation was used to calculate the Young's modulus of elasticity of the phase. The result of the calculation is clearly shown in Fig. 7. It is clear from the comparison that the values of the tensile modulus of elasticity of the individual phases are higher than their reduced modulus of elasticity, assuming the stated values of the Berkovich indenter.

5 Acknowledgement

This publication was created within the implementation of the project "Development and support of research - development activities of the Center for Quality Testing and Diagnostics of Materials in the field of specialization RIS3 SK", ITMS2014 +: 313011W442, supported by the Operational Program Integrated Infrastructure and European Regional Development Fund.

References

[1] Fischer – Cripps, A. C.: Nanoindentation Springer Science (3rd edition), New York, ISBN – 13: 9781461429609, 2013.

[2] Nguyen, V. L., Kim, E. A., Yun, J., Choe, J. Yang, D. Y., Lee, Ch, W., Yu, J., H.: N*ano-mechanical behavior of H13 tool steel fabricated by selective laser melting method,* Metallurgical and material transactions A: Physical metallurgy and material science Vol. 50 (2019), Issue 2, p. 523-528.

[3] Mencin, P., Tyne, C. J. V., Levy, B. S.: *A method for measuring the hardness of the surface layer on hot forging dies using a nanoindenter,* Journal of Material Engineering Performance, Vol. 18 (2009), p. 1067-1072.

[4] Nguyen, V. L., Kim, E. A., Lee, S. R., Yun, J. C., Choe, J. H., Yang, D. Y., Lee, H. S., Lee, C. W., Yu, J., H.: *Evaluation of strain rate sensitivy of selective laser melted H13 tool steel using nanoindentation tests,* Metallurgical and material transactions A: Metals, Vol. 8 (2018), p. 589.

[5] Oliver, W., Pharr, G. M: *An improved technique for determining hardness and elastic modulus using load and displacement sensing indentation experiments,* Journal of Material Response, Vol. 7 (1992), Issue 6, p. 1564-1583.

[6] Marashi, J., Yukushina, E., Xirouchakis, P., Zante, R., Foster, J.: *An evaluation of H13 tool steel deformation in hot forging conditions,* Journal of Material Processing Technology, Vol. 246 (2017), p. 276-284.

[7] Fischer-Cripps, A. C.: *Critical review of analysis and interpretation of nanoindentation test data,* Surface and Coating Technology, Vol. 200 (2006), p. 4153-4165.

[8] Luong Nguyen, V., Kim, E., Yun, J., et al.: *Evaluation of strain-rate sensitivity of selective laser melted H13 tool steel using nanoindentation tests,* Metals MDPI, Vol. 8 (2018), p. 589-599.

University Review, Vol. 15, Issue 1, p. 20-25, 2021.

UNIVERSITY REVIEW

PERFORMANCE CHARACTERISTICS OF STEEL 1.2842 AFTER NITRIDATION

Michal KRBAŤA[1*]

[1] Department of Engineering Technologies and Materials, Faculty of Special Technology, Alexander Dubček University of Trenčín, Ku kyselke 469, 911 06 Trenčín

ARTICLE INFO

***Article history*:**
Received: 15.3.2021
Received in revised form: 23.4.2021
Accepted: 3.5.2021

Keywords:
plasma nitriding
microhardness
coefficient of friction
pin on disc

Abstract:

The paper deals with the change in mechanical properties and wear of 1.2842 universal tool steel after plasma nitriding, which is widely used to produce cutting tools with good durability and low operating costs. Plasma nitriding was performed at a temperature of 500 °C for 10 hour period in a standard N2 /H2 atmosphere with 1:3 gases ratio. Microstructure, phase structure, thickness of a nitriding layer and surface roughness of samples were measured with optical microscopes and a profilemeter. Verification of a chemical composition was carried out on the BAS TASMAN Q4 device. Wear resistance was measured on a universal TRIBOLAB UTM 3 tribometer, through a, "pin on disc" method. The results of experiments have shown that plasma nitriding process, significantly improves the mechanical and tribological properties of selected materials.

1 Introduction

The 1.2842 tool steel is suitable for the plasma nitriding process due to its chemical composition. This steel has a wide range of applications for the production of universal cutting tools. Authors Studený et al. [1] solved importance of diffusion process on the fatigue life of this type of steel in their scientific research. Investigations with the same workpiece material were also realized by the authors [9, 10,12]. Authors Pilch at al. [2] solved the corrosion resistance of turbocharger stator after plasma nitriding process. The authors [4, 5] also studied and dealt with the same problem of plasma nitriding. Tribology of these parts plays an important role in their functionality and lifetime. Tribological problems can often be solved with a surface finish. Authors Doan et al. [3] have dealt with their research with the improvement of wear resistance for C45 steel using plasma nitriding, nitrocarburizing and nitriding. Also the authors Dubovská and Majerík [7] conducted the research analysis of surface finish and wear on the special tribological device. The effect of nitrogen on surface morphology of layers was solved by the authors Pokorný et al. [6]. Plasma nitriding, with regard to many advantages unlike common kinds of nitriding found an increasing industrial application [5, 11]. The main problem of nitridations in salt bathes is connected with a toxicity of cyanide salts. Traditional gaseous nitriding requires a longer time for treatment to obtain a needed nitridation depth. Direct current of plasma nitriding (DCPN) has been recently one of conventional treatment of a surface finish being used in industry aiming to improve mechanical features and wear resistance of mechanical engineering materials. Various layers may rise on

[*] Corresponding author. Tel.: 00421-32-7400 225
E-mail address: michal.krbata@tnuni.sk

a surface due to a plasma nitriding. These layers are classified by composition of particular phases. With respect to a steel composition, its layer is mainly composed of ferrous nitrides (γ'-Fe_4N or ε-$Fe_2$3N) and nitrides of alloying elements. Research studies showed that a microstructure of a nitriding layer can be affected with a change of parameters of a nitriding process, as temperature, time and plasma composition of the gas. Changes in a microstructure of nitriding layer effect mechanical and tribological features of the material, as surface hardness, wear resistance and endurance strength [2, 4, 8]. For a diffusion controlled growth, a thickness of a nitriding layer increases with temperature and nitridation time [6]. However a maximum surface hardness is achieved only at a certain nitridation time and temperature. Previous studies showed that a chemical potential of nitrogen is important a plasma nitriding of steels.

2 Experimental materials

The samples were annealed. Process of a plasma nitriding was carried out on the Rubig 60/60 device. The parameters of a plasma nitriding were chosen so that a nitriding layer is reached as thick and as hard as possible, Table 1.

Thermally treated and surface finished steel samples were numerically marked. Chemical composition of given steel was verified through a BAS TASMAN Q4 device and subsequently it was compared with the DIN 1.2842 technical standard Table 2.

Measurements of micro hardness and thickness of a nitriding diffusion layer were taken on each sample through a Vickers method. Impressing of a diamond pyramid under vertex angle of 136º is essence of the method. The LECO M400H microhardness meter will be used to verify and to compare achieved results before and after plasma nitriding. The load force will be 0, 5 N and force action time in accordance with DIN 50190 standard will be 10 sec. The measurements of micro hardness will be taken on a crosssection of a nitrided sample, upright from a surface to the material core. The achieved values on hardness will be displayed as a function of a distance from a surface. Thickness of a nitride layer will be taken on 18 imprints and 5 imprints in the material core. Limit value in terms of this standard is a hardness value, designated as limit hardness GH) and it is indicated as the Vickers hardness and it applies:

GH = average measured value in a core + 50 HV (rounded to 10HV)

Metallographic analysis is based on a polishing of samples and a subsequent etching with Nital. Etching of samples brings up their microstructures. We make out matallographical pictures of all samples with the Olympus GX51 optical matallographical microscope. With the microscope we can monitor a size of a white layer as well as an approximated size of a diffusion layer. Then we can assess a resulting structure of a diffusion layer as well as a basic material.

Roughness of surface was measured on the Talysurf CCI Lite 3D device. All samples had been grinded on a magnetic grinder with 0,001mm precision before plasma nitriding and marking. Surface roughness was measured before and after plasma nitriding aiming to define changes of roughness.

Measurement of wear was executed on the BRUKER UTM 3 device using „pin of disc“ method. This method is based on imprinting a firmly gripped body in a ball shape into a testing material in a disc shape, being rotated with constant revolutions. The testing ball was made of the 440C stainless steel with a 6,35 mm diameter and 746 HV hardness. The measurements were taken from 6 samples at 3 loads and three measurement radiuses. The Measurement radiuses for each sample are shown in Table 3.

Table 1 The parameters of plasma nitriding

Pressure [mbar]	2.8
Voltage [V]	700
Atmosphere PN	N_2 / H_2 1/3
Temperature PN [°C]	500
Time PN [hour]	10

Table 2 Chemical composition 1.2842 steel [in wt. %]

Element	DIN standard	BAS Tasman Q4
C	0.27 - 0.34	0.34
Mn	0.40 - 0.70	0.69
Si	Max 0.40	0.39
Cr	2.30 - 2.70	2.38
Mo	0.15 - 0.25	0.21
V	0.10-0.20	0.20

Table 3 Measurement parameters for tribology

Sample	Heat treatment	Turning radius	Load [N]	Rotation speed [rpm]
1	Annealed	19	50	250
		21	50	
		23	50	
2	Annealed	19	100	250
		21	100	
		23	100	
3	Annealed	19	150	250
		21	150	
		23	150	
4	Plasma nitriding	19	50	250
		21	50	
		23	50	
5	Plasma nitriding	19	100	250
		21	100	
		23	100	
6	Plasma nitriding	19	150	250
		21	150	
		23	150	

3 Metallographic structure

There is a microstructure of the 1.2842 steel, which can be seen in the Fig. 1, in a treated condition and after having etched 2% Nital and it was assessed as perlite, small with primary carbides and large secondary carbides. Perlite occurs both in lamellar and globular form. An average micro hardness had a value of 270 HV. After plasma nitriding on a metallographic section there were expressly visible and measurable only thicknesses of white layers. There is a coherent and relatively even white layer of nitrides on the samples surface. Under a white layer there is a diffusion layer.

The white layer with an average thickness 6.3 µm was created at the plasma nitriding temperature of the 500 °C and nitriding period of 10 hours (can be seen in Fig. 2). Optically is recognizable on the sample surface. In this case, the diffusion layer is not optically distinct from the core of the material.

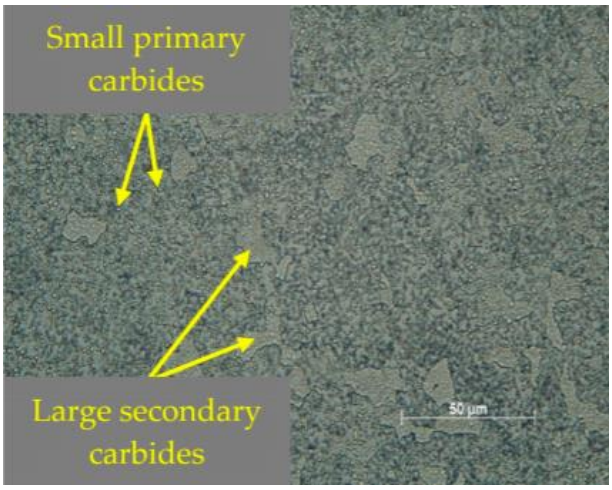

Fig. 1 Cross-sectional microstructure

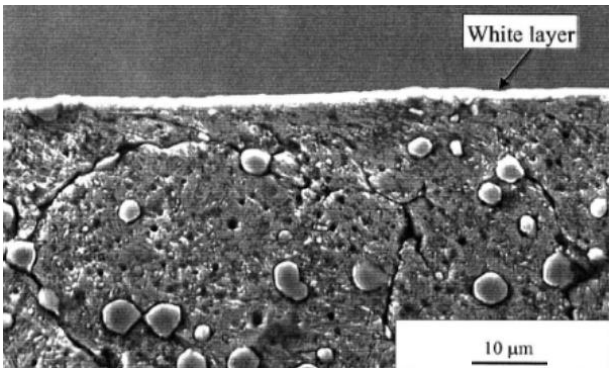

Fig. 2 Cross-sectional microstructure with white layer

3.1 Profiles of micro hardness and a depth of steel nitriding layers.

The Table 4 was developed from the measurement results, where thicknesses of particular diffusion layers of steels are documented. In the Tab. 4 there are also displayed the values of thicknesses of white layers on particular samples. From the table it is obvious that the results are the same for thickness of nitriding layer as well as for the white layer. At the sample 5 a minimum increase of a diffusion layer is visible, which shows no significant change in subsequent measurements. We can note that all samples had passed through plasma nitriding process at the same conditions and a risen diffusion layer is the same on all samples.

Table 4 The results of thickness diffusion and white layers

Sample	Thickness of diffusion layer[µm]	Thickness of white layer [µm]
4	0.38	6.3
5	0.37	6.1
6	0.38	6.5

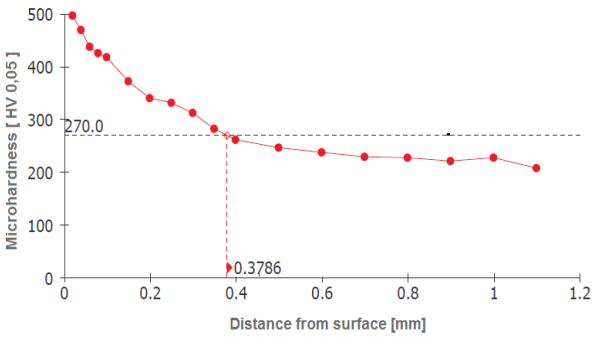

Fig. 3 Micro hardness depth profile sample No. 4

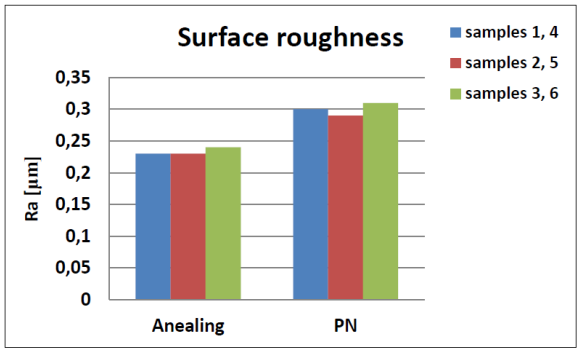

Fig. 4 Surface roughness 1.2842 before and after plasma nitriding

3.2 Surface roughness

Qualitative data on roughness are shown in the Fig. 4. Surface roughness on all samples, that have passed through the plasma nitriding process, are deteriorated in average by 30 % comparing with samples without plasma nitriding. This deterioration was caused by a dedusting process and due to a rise of a new nitride surface layer.

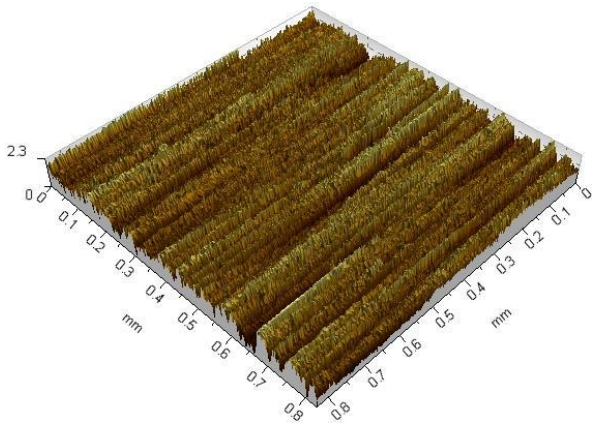

Fig. 5 3D profile steel 1.2842 without application of plasma nitriding; Sa 0.23µm

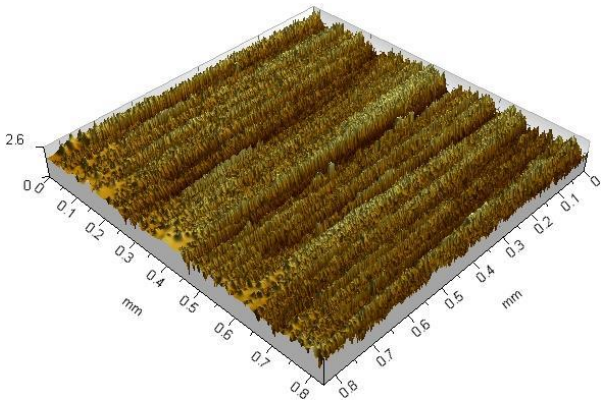

Fig. 6 3D profile of the steel 1.2842 nitrided at 500 °C and time of 10 hours; Sa 0.30 µm

3.3 Surface wear

The results on wear before and after plasma nitriding are shown in the Fig. 5. In the picture we can distinctly see different traces after wearing. The wear shown in the picture 7a), points at a high rate of wear, as this sample had passed only through a basic type of a thermal treatment. For the next samples 7b), 8c), 8d), a significant improvement of a surface profile occurred and these samples were plasma nitrided and they featured with much higher quality of surface. It can make a comparison, which can be seen in the Graph.2 (Fig. 9), between all the measurements of wear at different load parameters and different radiuses of rotation. The depth of wear was measured with profile meter and the results are displayed on a plot in the Graph.3 (Fig. 10). Each measurement of a depth was taken on

four different places and subsequently an average depth of an imprint was defined. The results expressly point at excellent mechanical features of plasma nitrided samples, as their depth of the imprint was ranging only in several micrometers comparing with tempered samples.

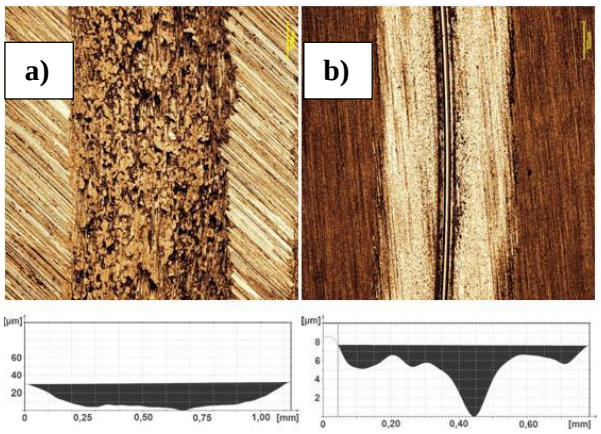

Fig. 7 Surface profiles of wear and depth tracks a) before PN, COF 0.59, h 31 µm, b) after PN, COF 0.42, h 7.2 µm,

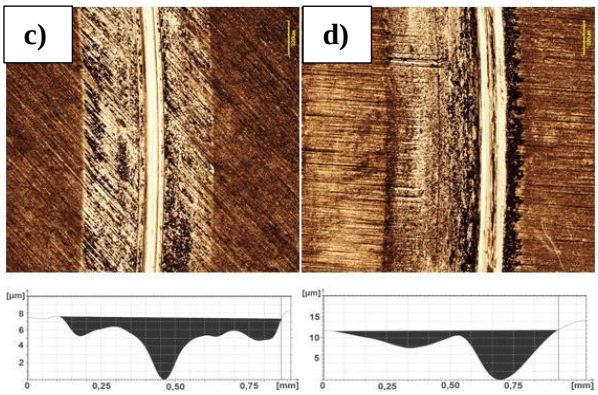

Fig. 8 Surface profiles of wear and depth tracks after PN c) COF 0,40, h 7.6 µm, d) COF 0.39, h 10.1 µm

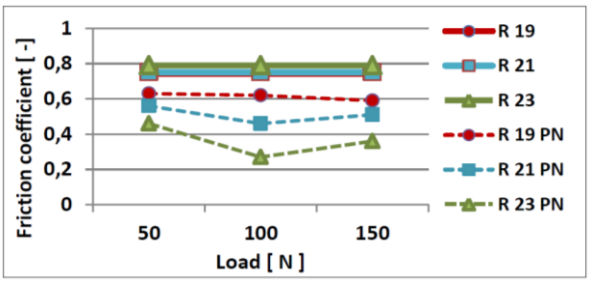

Fig. 9 Comparison of friction coefficient for all samples

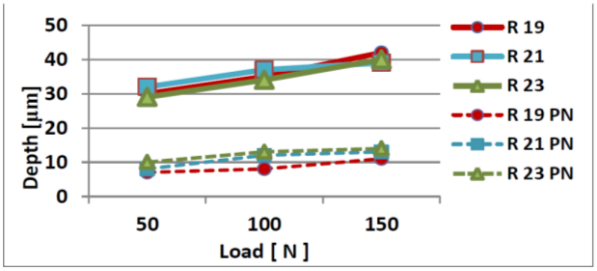

Fig. 10 Comparison indention depth in all samples

4 Conclusion

All measurements were focused on a study of the 1.2842 structural nitride steel. Plasma nitriding was carried out at standard conditions and parameters were chosen in such a way to achieve the best possible diffusion layer. The research brought us some valuable information about mechanical features of the 1.2842 steel. From a study of a microstructure and based on results the following conclusions can be made:

- The 1.2842 tool steel is suitable for a plasma nitriding process due to is chemical composition and the results of micro structure point at a rise of a diffusion layer of 0,38 µm thickness, mainly composed of ε-phase ($Fe_2$3N).
- A surface hardness of tempered samples had a value of 270 HV, it increased after plasma nitriding in average to a value of 500 HV, i.e. we can note, that plasma nitriding significantly increases a surface hardness and so the lifetime as well, as the majority of degradation processes start spreading from the surface into the material core.
- Material roughness before nitriding process was ranging on the level of 0,23 µm, after plasma nitriding the surface quality got worse by 30 % to the value of 0,30 µm. Such deterioration is caused by a dedusting process, when the nitride cations bombard a material surface and subsequently atoms of various elements, being on a material surface are shot out.
- Resistance to wear plays one of the most important roles in a material lifecycle.

Plasma nitriding process significantly decreases a friction coefficient. The friction coefficient decreased at plasma nitrided samples comparing with samples that had passed only a basic thermal treatment at all three loads. The same results are obtained from an imprint depth, left by a measuring ball. These findings are connected with a rise of a hard diffusion layer on a surface after a plasma nitriding process.

From the results of the experiment, we can state that a plasma nitriding improves a quality of mechanical features of the 1.2842 steel except of material roughness. It brings a great benefit in area of improvement of tribological features of materials as well as their application in various sectors of mechanical engineering industry and cutting tools.

References

[1] Studený, Z., Dobrocký, D., Pokorný, Z.: *Importance of diffusion process on the fatigue life of steel*, Manufacturing Technology, 2017, p. 94–99.

[2] Pilch, O., Faltejsek, P., Hrubý, V., Krbaťa, M.: *The corrosion resistance of turbocharger stator after plasma nitriding process*, Manufacturing Technology, Vol. 17, (2017), Issue 3, p. 360–364.

[3] Doan, T. V., Kusmič, D., Pospíchal, M., Dobrocký, D.: *Improvement of wear resistance for C45 steel using plasma nitriding, nitrocarburizing and nitriding/ manganese phosphating duplex treatment*, IOP Conference Series: Materials Science and Engineering, Vol. 179, (2017), p.1-7.

[4] Kusmič, D., Doan, T.V., Pilch, O., Krbaťa, M.: *Corrosion resistance and tribological properties of plasma nitrided and tenifered 42CrMo4 steel*, METAL 2016 - 25th Anniversary International Conference on Metallurgy and Materials, Conference Proceedings, (2016), p. 1103-1108.

[5] Ulutan, M., Kılıçay, K., Kaya, E., Bayar, I.: *Plasma transferred arc surface modification of atmospheric plasma sprayed ceramic coatings*, Journal of Mechanical Science and Technology, Vol. 30, (2016), Issue 8, p. 3813–3818.

[6] Pokorný, Z., Hrubý, V., Studený, Z.: *Effect of nitrogen on surface morphology of layers*, Kovové Materiály, Vol. 54, (2016), No. 2.???

[7] Dubovská, R., Majerík, J.: *The research analysis of surface finish and wear on the special tribological device*, Procedia Engineering, Vol. 100, (2015), p. 730–736.

[8] Mikuš, P, Chovanec, A. Breznicá. A Barényi, I.: D.: *Impact of hardness of rubber compounds on tire wear*, University review, Vol. 13, 2019, p. 30-34.

[9] Ekinovič, S., Dolinšek, S., Begovič, E.: *Machinability of 90MnCrV8 steel during high-speed machining*, Journal of Materials Processing Technology, Vol. 162-163, (2005), No. 1-3, p. 603–608.

[10] Axén, N., Zum Gahr, K H.: *Abrasive wear of TiC-steel composite clad layers on tool steel*, Wear, Vol. 157, (1992), Issue 1, p. 189–201.

[11] Taylan, F., Çolak, O., Kayacan, M. C.: *Investigation of TiN Coated CBN and CBN cutting tool performance in hard milling application*, Strojniski Vestnik/Journal of Mechanical Engineering, Vol. 57, (2011), Issue 5, p. 417–424.

[12] Barrena, M. J., Gómez, J. M., de Salazar, Matesanz, L.: *Interfacial microstructure and mechanical strength of WCCo/90MnCrV8cold work tool steel diffusion bonded joint with Cu/Ni electroplated interlayer*, Materials and Design, Vol. 31, (2010), Issue 7, p. 3389–3394.

University Review, Vol. 15, Issue 1, p. 26-32, 2021.

UNIVERSITY REVIEW

Experimental research of flank wear process of carbide cutting inserts during hard milling of Armox 500 steel

Mária Kubasáková[1]*, Jozef Majerík[1]

[1] Alexander Dubcek Univesrsity of Trencin, Faculty of special technology, Department of engineering technologies and materials, Ku Kyselke 469, 911 06, Trencin, Slovakia, maria.kubasakova@tnuni.sk
[1] Alexander Dubcek Univesrsity of Trencin, Faculty of special technology, Department of engineering technologies and materials, Ku Kyselke 469, 911 06, Trencin, Slovakia, jozef.majerik@tnuni.sk

ARTICLE INFO

***Article history*:**
Received: 15.3.2021
Received in revised form: 23.4.2021
Accepted:3.5.2021

Keywords:
Armox 500 steel, long term testing, flank wear VB, hard milling, cutting parameter

Abstract:

The authors' article deals with the research or implementation of long-term testing of the process of wear of the flank surface of indexable carbide cutting inserts with PVD coating. The mentioned wear process is realized through the technological process of milling high-strength steel Armox 500. The material Armox 500 is used in practice in the special engineering industry and in the production of external ballistic protection of combat vehicles. In practice, there is a demand for ever higher parameters, such as increased mechanical properties of such steels. This increases the ballistic resistance of Armox armor sheets, which in practice presents new problems associated with mechanical processing to the desired state. Therefore, the authors' research for this reason is focused on monitoring the technological milling process of Armox 500 steel in terms of the wear process, which is important for the achieved dimensional accuracy and quality of machined surfaces. The face milling experiment was performed on a FA3V vertical milling machine with SNHF 1204EN-SR-M1 geometry cutting inserts with tool material type 8230 (P30) from DormerPramet. The cutting inserts were clamped in a 50 mm diameter Narex face milling cutter. The experiment consisted of monitoring the process of wear of the flank surface VB with the set criterion of flank wear VB = 0.2 mm.

1 Introduction

Steel armor is used for its ability to withstand more impacts in a small area. Hardness of 400 to 450 HBW are mainly used for vehicle chassis that are prone to explosions from mines and improvised explosive devices. Armor with a hardness of around 400 HBW is hard and tough at the same time and can therefore withstand an immediate explosion. Armor with a hardness of over 500 HBW is used as a base material for construction because it has high hardness and ballistic resistance and can be processed relatively well. Armor with a hardness of over 600 HBW has the best ballistic properties, but due to their high hardness they cannot be bent. They are used for additional cladding of places prone to impact.

[1] Corresponding author. Tel.: +421 32 7400 108
E-mail address: maria.kubasakova@tnuni.sk

Armox type armor steels are characterized by high density in combination with excellent mechanical properties, e. g. ultra-high strength and high hardness thus the ability to resist penetration against fired projectiles [1]. Under these circumstances, said high-strength steels experience large plastic deformations of the order of 10^2 to 10^3 s^{-1} and the deformation process is affected by the effects of strain hardening and thermal softening. [2].

The authors [3, 4, 11] used a wide range of machined and cutting materials to investigate the face milling process. In this paper, the mathematical least squares method was used as an experimental method, as well as the use of SEM (Scanning Electron Microscopy). Direct heat generation at the tool-machined material interface has a significant effect on dimensional changes due to thermal deformation in the machining process or a surface defect caused by oxidation, as reported in the literature [5]. During the performed experiments, several machining parameters were entered. It can be said that Armox was machined using cemented carbide cutting inserts and PVD coated. The research was performed to analyze the performance in terms of cutting conditions, wear on the flank surface and tool life in order to evaluate the efficiency of used cemented carbide cutting inserts. This was recorded and documented using a Tescan Vega TS 5135 SEM microscope. The same observation, which was made by Pokorný et al. [6], An et al. [7] and Li et al. [8], reported experimental studies and researches of the technological process of hard milling of high-strength steels using cemented carbide cutting inserts. All the following articles were devoted to the investigated surface integrity factor including all investigated characteristics [7, 8]. Gopalsamy et al. [9] reported an investigation into the hard machining of hard tool steels. Experiments were performed to analyze the performance of cutting conditions existing in hard milling technology with respect to material removal rate (MRR), wear, tool life and surface quality to determine the effectiveness of the sintered carbide cutting inserts used for the milling used cutters. The results were confirmed by SEM microscopy. Cui et al. [10] published research on the mechanisms of the flank wear process in particular and confirming that with increased cutting speed, the effect of oxidative wear on the side becomes more pronounced, while the effect of adhesive wear is subsequently reduced. All these studies investigate the possibility of machinability and the achieved results visibly improve the face milling process.

2 Experimental details

2.1 Basic Information

The chemical composition and mechanical properties of tested Armox steel, which is determined by the supplier Winfa Ltd., was realized in the CEDITEK (Center of diagnostics and testing of materials) Laboratories.

2.2 Additional Information

The authors of the article used Armox 500 armor plate as a test material in the process of experiments. It is an armor made in Sweden and is used in practice as a ballistic protection of the outer parts of combat vehicles and weapon systems. The authors of the article also performed their own measurement of chemical composition by the method of spectral analysis of chemical elements on the Spectrolab JrCCD device in the laboratory of spectral analysis at the Faculty of Special Technology TnUAD in Trencin. The measured percentage results of the content of chemical elements in Armox 500 steel can be seen in Table 1. Results of chemical composition was obtained by spectral analysis method measured in the Spectrolab JrCCD measuring device. The hardness of the experimental material was also measured in the laboratory of mechanical tests at the Faculty of Special Technology by the Rockwell method. The resulting hardness of the base material reached the value HRC = 48 ÷ 52. The summary results of the chemical composition and measured mechanical properties of the tested steel Armox 500 can be seen in Table 1 as was mentioned above.

Table 1 Chemical composition and mechanical properties of high-strength steel Armox 500 where: Mn, Cr, Ni, Mo, B - alloying elements C, Si, P, S - admixtures (accompanying elements)

Chemical composition [wt. %]	C	Si	Mn	P	S	Cr	Ni	Mo	B
	0.27	0.23	1.10	0.014	0.009	0,81	1,58	0.7	0.004

Mechanical properties	Tensile strength R_m [MPa]	Limit of proportionality $R_{p0.2}$ [MPa]	Toughness KU [J]	Hardness [HBW]	Elongation A_5 [%]
	1638	1422	25	516	9

From a microstructural point of view, Armox 500 is a structural medium-alloyed high-strength steel

(with a higher Ni content), which has a fine-grained martensitic structure obtained by low-temperature tempering. In Fig. 1, a hard, low-tempered martensitic structure is observable with some small amount of retained austenite expected. From the microstructure it is also possible to observe the occurrence of carbides (small white polygonal-shaped particles) as a product of the transformation of tetragonal martensite (dark color) to cubic tempered martensite (dark color) during tempering.

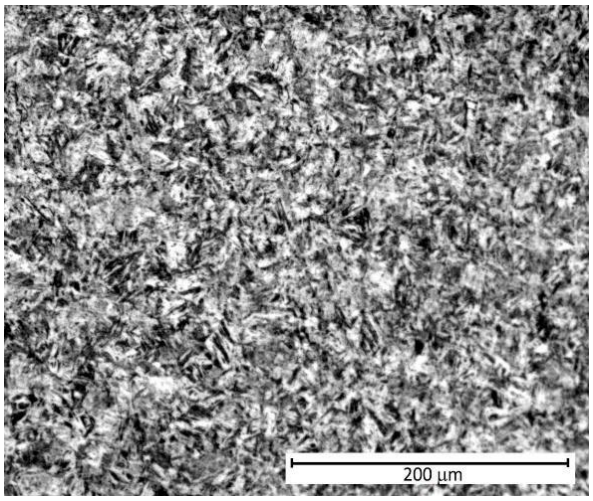

Fig. 1 Microstructure of Armox 500 steel base material obtained by light microscopy

2.3 Experimental methods

The authors of the article in their experiment focused on the so-called long-term testing of carbide interchangeable cutting inserts of SNHF 1204EN-SR-M1 geometry (see in Fig. 2) with cemented carbide type 8230 from DORMERPRAMET Ltd. (type P30 according to ISO standard) with PVD coating TiAlCN + TiN. Changeable cutting inserts were mechanically clamped in a NAREX type face milling cutter (see in Fig. 4) with a diameter of Ø50 mm with the designation PN222460.12 according to the ISO standard and with the number of teeth z = 4. The inserts were supplied with the following cutting edge geometry: cutting edge setting angle χ_r = 75º; orthogonal rake angle γ_o = -7º; cutting edge inclination angle λ_S = - 4º; and with clearance angle α = 7º. The experiment was carried out on a machine tool of the FA3V type using two pieces of machine vices for clamping 2 pieces of Armox 500 armor sheets with thicknesses of 2x 20 mm and a height of 160 mm, as can be seen in Fig. 3. To determine the dependence of tool life as a function of cutting speed T = f (v_c) in face milling process of Armox 500 armor sheet, the authors followed the principles valid for long-term tool life test depending on cutting speed according to ISO 3685. The prepared material has dimensions 20 x 160 x 500 mm. The face milling method was proposed by the authors using the face milling method, which satisfies the condition that the milling width $a_e = B$ is (0.6 to 0.8). D. The dependence T = f (v_c) was monitored at the following constant cutting parameters: depth of cut a_p = 2 mm; width of cut $a_e = B$ = 40 mm; feed per tooth f_z = 0.056 mm; at the specified wear criterion valid for high-strength materials VB_K = 0.2 mm. The face milling process was carried out without the use of cutting or cooling medium.

Fig. 2 Geometry of tested cutting inserts used in the face milling process

Fig. 3 A look at the method of clamping 2 pieces of ARMOX 500 sheets, using two machine vices on a FA 3V machine tool

To determine the graphical dependence of tool life T = f (v_c), the authors will monitor the impact of cutting speeds in the process of research, as follows:

v_{c1} = 55.7 m.min^{-1} at n_1 = 355 min^{-1}
v_{f1} = 80 mm.min-1
v_{c2} = 78.5 m.min-1 at n_2 = 500 min^{-1}
v_{f2} = 112 mm.min^{-1}
v_{c3} = 111 m.min-1 at n_3 = 710 min^{-1}

v_{f3} = 160 mm.min^{-1}

Ensures a constant feed rate per tooth is f_z = 0.056 mm, feed per revolution f_o = 0.224 mm at number of teeth of the milling cutter is z = 4. Each experiment was performed twice by the authors of the article at the same cutting parameters and after rotating the cutting inserts in the milling cutter, which meets the recommendations of the literature [3].

The results of flank wear and achieved tool life were recorded by the authors in the table and in graphical form (see in Fig. 8) *VB* = f (time). It was clean at the stated cutting parameters machine time of face milling as follows:

$$t_{AS1} = \frac{1+1_v}{f_z.zn} = \frac{505}{0{,}0563.4.355} = 6.31\text{min}$$

$$t_{AS2} = \frac{1+1_v}{f_z.zn} = \frac{505}{0{,}0563.4.500} = 4.48\text{min}$$

$$t_{AS2} = \frac{1+1_v}{f_z.zn} = \frac{505}{0{,}0563.4.710} = 3.15\text{min}$$

Fig. 4 View of the face milling process at a cutting speed v_c = 111 m.min^{-1} (machine spindle speed n = 710 min^{-1}), depth of cut a_p = 2 mm, and feed rate per tooth f_z = 0.056 mm

The circumferential throw of the clamped cutting inserts in the face milling cutter was measured by the authors indicator watch and the maximum throw was 0.02 to 0.03 mm. Measurement wear of the cutting inserts was continuously ensured with a Brinel magnifying glass with magnification 10x, after removing the milling cutter from the machine tool and inserting it into the rotary clamp. Subsequently, the flank wear of the most extended cutting insert, which was marked for this reason. The cutting insert that was extended by 0.02 to 0.03 mm at circuit to other cutting inserts also had maximum wear VB_{max} and after exceeding VB_K = 0.2 mm, this carbide cutting insert was also cut at the spindle speed of the machine n = 710 min^{-1}, as evidenced by the departure of glowing chips (as can be seen in Fig. 4). The resulting wear of the flank surface of the tested cutting inserts was observed by means of a scanning electron microscope (see in Fig. 5) of the Tescan VEGA 5135 type with X-Ray microanalyzer Noran Six / 300.

Fig. 5 View of a scanning electron microscope type Tescan VEGA 5135 with X-Ray microanalyzer Noran Six / 300, which was used in the experimental process to monitor the final wear of tested cutting plates type SNHF1204ENSR-M during face milling process of Armox 500 steel

3 Results and discussion

Long-term tool life testing of cemented carbide cutting inserts during machining with a defined cutting edge geometry is defined by the international standard ISO3685-E-77-05-15. Tool life values are derived from the characteristic wear curves of the tested cutting inserts for a given wear criterion on the flank surface *VB*, or for the rake face of the cutting insert according to the *KT* criterion (groove depth on the face). It is recommended to perform the long-term testing process from three to five times. The long-term test is repeated using one variable two to four times. Then the credibility of the achieved results is statistically guaranteed and correctly determined. The tool wear criterion VB_k = 0.6 mm is for roughing operations or VB_k = 0.3 mm for finishing the machining method. When machining high-strength materials, it is necessary to determine the VB_k criterion for at least half values. The results of the tool wear of the flank surface of the tested carbide cutting inserts and the achieved tool life of the cut-

ting tool are given in Tab. 2 and in the resulting graph (shown in Fig. 8), according to a predetermined criterion *VB* = f (time).

Table 2 Measured values to determine the durability of the tested cutting tool T (min) with the values of the logarithm v_{ci} (m • min $^{-1}$) and Ti (min)

N	v_{ci}	T_i	log T_i	log v_i	log T_i. log v_i	$\log^2 v_i$
1	55,7	166	2,22011	1,74586	3,87600	3,04803
2	78,5	93	1,96848	1,89487	3,73001	3,59053
3	111	29	1,46240	2,04532	2,99678	4,1993
1	55,7	185	2,26717	1,74586	3,95816	3,04803
2	78,5	113	2,05308	1,89487	3,89032	3,59053
3	111	30,5	1,48430	2,04532	3,04165	4,1993
Σ	-	-	11,455	11,3721	21,4930	21,6757

Note: where N is the number of measurements (individual selected cutting speeds)

$\sum \log^2 v_{ci} = 21.6757$

$(\sum \log v_{ci})^2 = (11.3721)^2 = 129.325$

Substituting the appropriate values from Tab. 2 into the equation for (*m*) we get the following form:

$$m = \frac{N.(\sum \log T_i.\log v_i) - \sum \log T_i.\sum \log v_i}{N.\sum \log^2 v_{ci} - (\sum \log v_{ci})^2}$$

$$= \frac{6.(11{,}455.11{,}3721) - 11{,}455.11{,}3721}{6.21{,}6757 - (11{,}3721)^2} = -1{,}7956 = -b$$

Determine the constant C_T by substituting the calculated value for the exponent m into equation (26) and obtain the following form:

$$\log C_T = \frac{\sum \log T_i + m.\sum \log v_i}{N}$$

$$= \frac{11{,}455 + 1{,}7956.11{,}3721}{6} = 5{,}3126$$

Then

$$C_T = 10^{\log C_T} = 10^{5{,}3126} = 205400 = 2{,}05.10^5$$

The resulting dependence $T = f(v_c)$, obtained from the graphs and processed by the least squares method, is in Fig. 9, in a logarithmic coordinate system. Final shape for calculating cutting life edges depending on the cutting speed for face milling of high-strength Armox material 500 has the following final shape:

$m = 1.7956 = \text{tg}\ \alpha$

$\alpha = \text{arctg}\ 1.7956 = 60.88\ ^{o} = 60\ ^{o}\ 53'$

$$T = \frac{C_T}{v_c^m} = \frac{2{,}05.10^5}{v_c^{1{,}7956}}$$

After performing long-term tests on Armox 500 face milling, the appearance of the back surface of the worn cutting inserts is shown in Fig. 6a, b and in Fig. 7a.b obtained by observation on an SEM microscope of Tescan Vega.

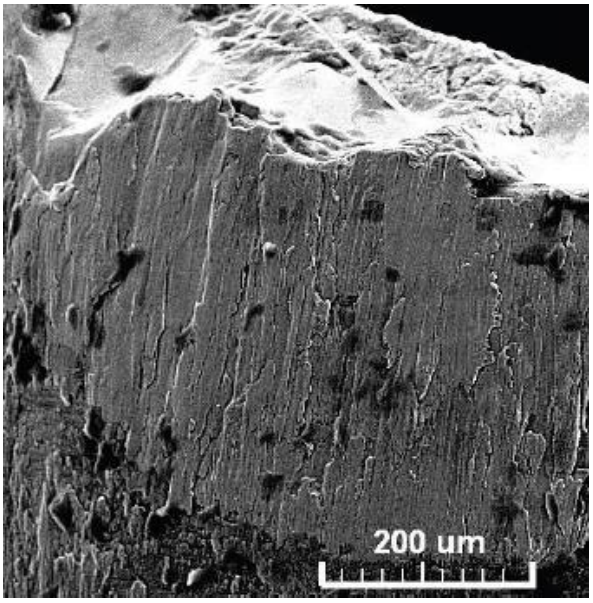

Fig. 6a SEM display of VB wear (250 ×), cutting speed v_c = 55.7 m • min $^{-1}$

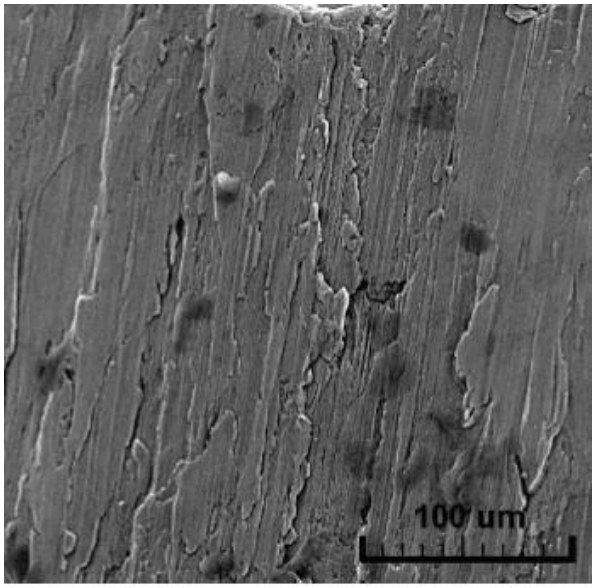

Fig. 6b SEM display of VB wear (500 ×), cutting speed v_c = 55.7 m • min $^{-1}$

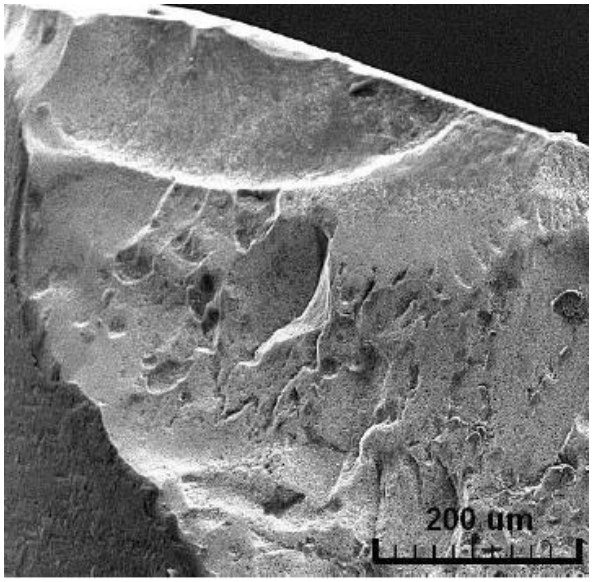

Fig. 7a SEM display of VB wear (250 ×), cutting speed v_c = 78.5 m • min $^{-1}$

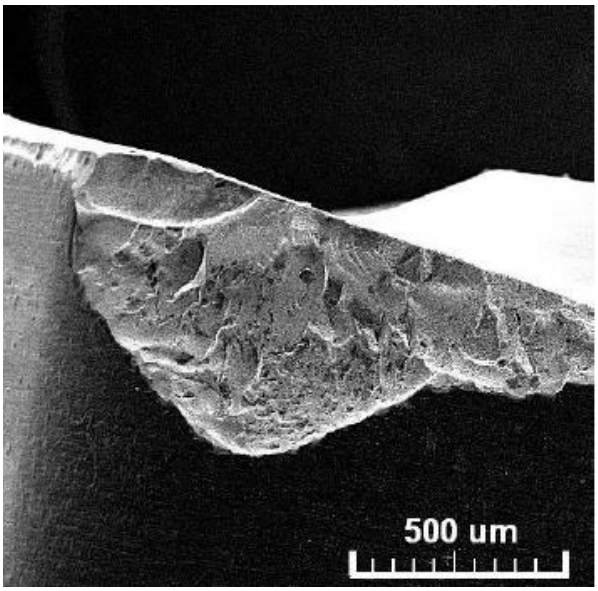

Fig. 7b SEM display of VB wear (100 ×), cutting speed v_c = 78.5 m • min $^{-1}$

4 Conclusion

Implemented long-term tests of face milling of high-strength steel ARMOX 500 with milling cutter of type NAREX Ø50 mm PN222460.12; with number of teeth z = 4; χ_r = 75º; γ_o = -7º; λ_S = - 4º; α = 7º; MK -50 and using carbide cutting inserts type 8230 (P30) and geometry SNHF 1204EN-SR-M1 at depth of cut a_p = 2 mm, and milling width of cut a_e = 40 mm showed that hard face milling can be realized even with increased cutting parameters in the range of cutting speeds v_c = 55.7; 78.5 to 111 m.min^{-1} with the specified wear criterion VB_K = 0.2 mm. Experimental tests of hard face milling of high-strength steel Armox 500 showed lower values of achieved tool life at the value of reported values of cutting speeds in the range v_c = 55.7 to 111 m.min^{-1}. Throwing of face milling teeth was ensured in both cases in the range 0.015 ÷ 0.02 mm. A throw value of 0.05 mm is no longer permitted. Experimental tests of hard face milling of Armox 500 armor plates with a milling cutter with interchangeable inserts have also shown that the use of emulsion cooling is not necessary. Due to the higher hardness of Armox 500 high-strength steel, for example, compared to the abrasion-resistant Hardox 500 material with the same DORMERPRAMET type 8230 cutting material, tool life at the same cutting speeds was 18 to 38% lower, on average 28%.

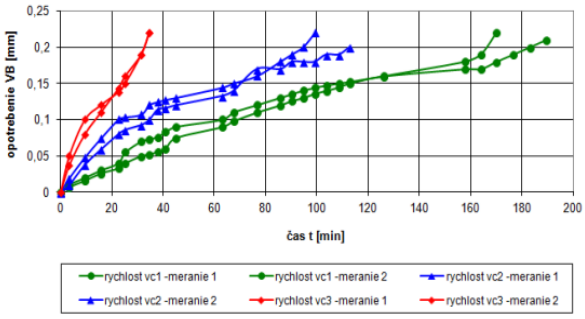

Fig. 8 Graphical dependence of the wear course on time for milling high-strength steel ARMOX 500 with interchangeable inserts type SNHF 1204ENSR-M1: 8230 from DORMERPRAMET to determine the dependence T = f (vc)

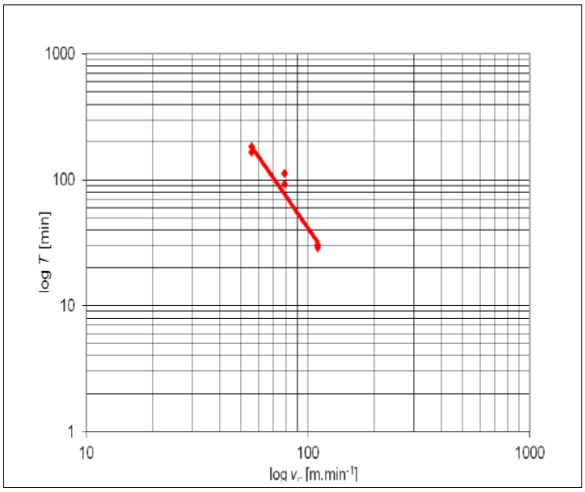

Fig. 9 Dependence T = f (vc) obtained during milling of ARMOX 500 high-strength steel

5 References

1 Zejian Xu, Huang Fenglei (2012) Plastic behavior and constitutive modeling of armor steel over wide temperature and strain rate ranges. Acta Mech Solida Sin 25:598–608

2 Ambuj Saxena, A. Kumaraswamy, Mahdu Vemuri. Investigation of S-D effect on plastic behavior of Armox 500T steel. Journal of the Brazilian Society of Mechanical Sciences and Engineering (2018) 40:463

3 Čep, R., Janásek, A., Čepová, L., Petrů, J., Hlavatý, I., Car, Z., & Hatala, M. (2013). Experimental testing of changeable cutting inserts cutting ability. *Tehnički vjesnik, 20*(1), 21-26.

4 Nath, C., Brooks, Z., & Kurfess, T. R. (2015). Machinability study and process optimization in face milling of some super alloys with indexable copy face mill inserts. *Journal of Manufacturing Processes*, 20, 88-97. https://doi.org/10.1016/j.jmapro.2015.09.006

5 Prakash, M., Shekhar, S., Moon, A. P., & Mondal, K. (2015). Effect on machining configuration on the corrosion of mild steel. *Journal of Materials Processing Technology*, 219, 70-83.https://doi.org/10.1016/j.jmatprotec.2014.11.044

6 Pokorný, Z., Hrubý, V., & Studený, Z. (2016). Effect of nitrogen on surface morphology of layers. *Kovové Materiály, 54*(2), 119-124. https://doi.org/10.4149/km _2016_2_119

7 An, Q., Wang, C., Xu, J., Liu, P., & Chen, M. (2014). Experimental investigation on hard milling of high strength steel using PVD-AlTiN coated cemented carbide tool. *International Journal of Refractory Metals and Hard Materials*, 43, 94-101. https://doi.org/10.1016/j.ijrmhm.2013.11.007

8. Li, W., Guo, Y., & Guo, C. (2013). Superior surface integrity by sustainable dry hard milling and impact on fatigue. *CIRP Annals - Manufacturing Technology, 62*(1), 567-570. https://doi.org/10.1016/j.cirp .2013.03.024

9 Gopalsamy, B. M., Mondal, B., Ghosh, S., Arntz, K., & Klocke, F. (2009). Investigations on hard machining of Impax Hi Hardtoolsteel. *International Journal of Material Forming, 2*(3), 145-165. https://doi.org/10.1007/s12289-009-0400-5

10 Cui, X., Zhao, J., & Tian, X. (1990). Tool wear in high-speed face milling of AISI H13 steel. *Journal of Engineering Manufacture, 226*(2), 5-21.

11 Jozef Majerík, Rozmarína Dubovská, Jaroslav Jambor, Robert Čep, Jiří Kratochvíl, Karel Kouřil: Experimental investigation into tool wear and tool life of milling cutter PVD coated carbide inserts while Armox 500 steel hard milling. Tehniški Vjesnik, Vol. 25, No, 6., 2018, p. 1603-1610. https://doi.org/ 10.17559 /TV-20161128094553

University Review, Vol. 15, Issue 1, p. 33-38, 2021

UNIVERSITY REVIEW

USE OF TRIBODIAGNOSTICS IN PRACTICE

Pavol Mikuš[1] –Maroš Eckert[1*]

[1]Department of Design and Special Technology, Faculty of Special Technology, Alexander Dubcek University of Trencin, Ku kyselke 469, 911 06 Trenčín

ARTICLE INFO

***Article history*:**
Received: 15.3.2021
Received in revised form:23.4.2021
Accepted: 3.5.2021

Keywords:
Tribodiagnostics
Lubrication fluid
Wear
Friction
Oil

Abstract:

Tribodiagnostics deals with the problems of lubrication, friction and analysis of oils in technical fluids. Based on the results of parameter monitoring and chemical analysis of the oil, it is possible to determine the impending failure of the entire system very accurately. Today, this relatively young field of technical diagnostics is gradually becoming very viable and its results are fully in line with classical vibroacoustic diagnostics or thermodiagnostics. It is used in all mechanical systems containing oil systems. This is one of the methods of non-disassembly technical diagnostics, which is based on the knowledge that the lubricant after a certain period of use in the lubrication system reflects the condition of the equipment and the conditions in which this equipment was operated.

1 Introduction

The growing demand for vehicles forces us to think about ensuring a high level of operational reliability, which should be close to the inherent reliability, which is ensured by optimal use, maintenance, repairs, etc. For the maintenance to be technically and economically optimal, it is also necessary to optimize the technical diagnostics, resp. also a significant part of it - tribodiagnostics. The term tribology (from the Greek TRIBOS - friction and logos - science) is historically very old and has probably existed since the beginnings of written history. Examples of the development of wheels, bearings, friction surfaces, etc. are documented. Already in the early civilizations (Archimedes) and also the targeted scientific development of tribology has a relatively long history (15th century), when the foundations of the law come from Leonardo da Vinci. Important scientists who dealt with tribology were e.g. Lavoisier, Leibnitz, Tower, Reynolds, Stribeck and others [2].

1.1 Tribotechnical systems

From a narrower point of view, tribology is a science and practice that deals with the behavior of contacting surfaces in motion, or in an attempt to move relative to each other (sliding, rolling, rotating, impact, oscillating, flow of gases, liquids, etc.). When the surfaces interact with each other, there is resistance to movement and friction. At the same time, the engineering observation of friction has a predominantly phenomenological character, since it uses in particular its external manifestations, effects in the field of contact and effects on the environment. Generally speaking, there are generally two basic areas of research and application of tribology:

- the field of man-made artificial technical tribological systems,
- the area of natural tribological systems (e.g. human locomotor system - joints, plant roots, etc.),

An approximation of the sizes and dimensions in which tri-diagnostics is performed in the area of vehicle groups is shown in Fig. 1 and Fig. 2.

Both artificial and natural tribological systems include at least two, but usually four, system elements, namely a basic friction body, a counteracting friction body, an Interfacial Medium and an Ambient Medium.

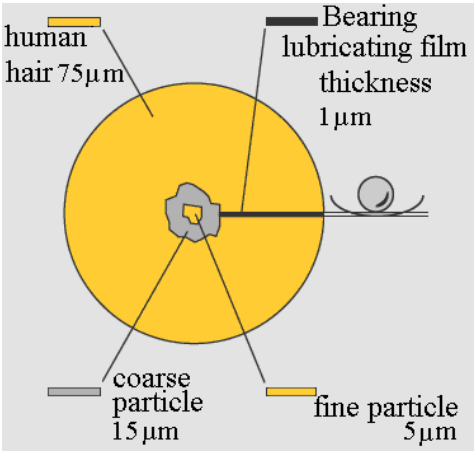

Fig. 1 An example of the size of the lubricating film and wear particles in the field of tribodiagnostics

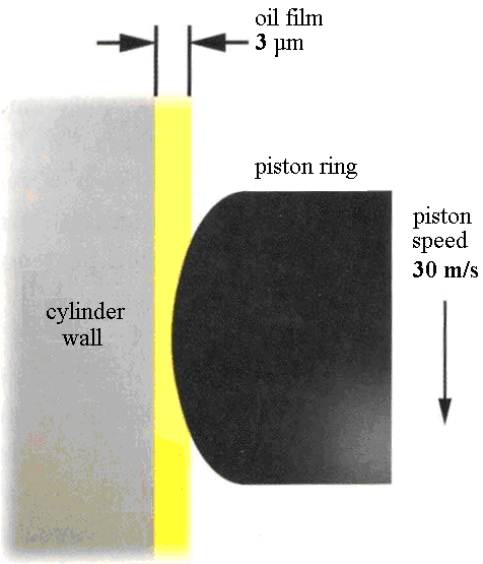

Fig. 2 Example of an oil film size for an internal combustion engine

The Tribotechnical System (TTS) generally includes relationships between the following variables:

- Input Variables:
  - desirable,
  - undesirable (disturbing).
- Output Variables:
- useful variables,
- loss variables.

Undesirable - interfering input variables negatively affect the values of usable and lossy output variables. The role of TTS in practice is the conversion of input variables such as input torque, input speed, type of input movement, resp. in the case of several different movements, their sequence also includes, for technically usable output variables e.g. output torque, output speed and output movement. While the two contacting surfaces are part of each TTS, the interfacial medium and the surrounding medium may be absent from the system if it is a process taking place e.g. in a vacuum. Open systems are those where the base body is in contact in time with a different type of contact body or with several different bodies, e.g. when transporting materials or machining. Closed TTSs are those where the contacting bodies meet repeatedly. In addition to the other features of the tribological process mentioned above, when comparing open and closed systems, the ability of the system to function properly depends on:

- in the case of open TTS only for wear of the base body,
- in the case of closed TTS for wear of the base and opposing body [4].

1.2 Tribological load and interaction

The tribological load in tribotechnical systems is caused by the already mentioned input and disturbing variables, more precisely by their influence on the structure of the tribotechnical system. Tribological loading includes contact, kinematic, dynamic and thermal processes. A tribological load is a contact load of a base surface in the solid phase by another surface, which may be in the solid, liquid or gaseous phase, with relative relative movement of the two surfaces. This is done with the help of real contact surfaces. Plastic deformation and wear can cause a change in the size of individual real contact surfaces during the tribological process. Mechanical energy dissipates by friction, i.e. they dissipate and are converted into thermal energy, which affects the rate of wear. The nominal or apparent surface is decisive for lubrication when the two contact surfaces are not in direct contact and there is a sufficient amount of lubricant between them. With mixed lubrication, the lubrication parameter Λ is equal:

$$\Lambda = \frac{h_{\min}}{\left(R_{q1}^2 + R_{q2}^2\right)^{1/2}} \quad (1)$$

where h_{min} is minimum thickness of lubricating layer (μm), R_{q1} root mean square deviation of the base body surface profile (μm), R_{q2} mean square deviation of the surface profile of the opposing body (μm).

In the range $1 \leq \Lambda < 5$, in the case of limit friction (lubrication) $\Lambda < 1$ and in the case of dry friction, when both bodies are in direct contact, whether partial or complete, the boundary or real contact surfaces have a decisive influence. If there is direct contact between the friction surfaces, there will also be interactions between atoms / molecules and mechanical interactions at the locations of the real contact surfaces and in the affected area close below the surface of both bodies. This gradually leads to elastic and finally to plastic contact deformations and the creation of real contact surfaces. The type of interaction that occurs depends mainly on the state of lubrication. If it is a sufficiently lubricated contact, then atomic / molecular interactions are insignificant compared to mechanical interactions.

1.3 Wear

Wear can be characterized as an increasing loss of material from the surface of the solid phase upon interaction and relative motion with the solid phase body, liquid or gas. Wear of two rigid bodies occurs in direct contact, ie. in case of insufficient thickness of lubricating film, or in case of absence of lubricant. Wear is manifested by the release of particles from the surface of the material of one or both bodies in frictional contact. Wear can be caused by several mechanisms, the following four being the most important of them:

- surface fatigue,
- abrasion,
- adhesion,
- tribochemical reaction or erosion [1].

2 Tribotechnical diagnostics

Tribotechnical diagnostics is a set of methods and means of checking the technical condition (diagnosis, localization, prognosis, or genesis) of usually complex, closed friction moving joints of mechanical systems using lubricating media (oils, greases, greases, etc.) hydrau -lic liquids and. i. It organically combines the measurement, evaluation and forecasting of parameters and characteristics of processes taking place in a given facility. The results of the analyzes are used to perform the following tasks:

1. Monitoring the condition, trend and mode of wear of machinery based on, e.g. determination of the content of abrasions, resp. abrasion metals in the lubricant, while the decisive factor is mainly the trend of measured values.

2. Determination of the service life of the lubricant by determining the degree of its degradation by chemical reactions, products of thermal-oxidation processes, internal contamination, external impurities, etc. Increased number of impurities, e.g. in oil it not only means greater wear of the lubricated parts, but the contained deposits can clog the lubrication holes and grooves. The service life of the lubricant is expressed by a set of relatively objectively determined indicators.

3. Determination of optimal times for changing individual lubricants. The importance of this task is currently increasing with the rising price of lubricants and cost-saving measures.

By fulfilling the above tasks, we can get an overview of the technical condition of the relevant mechanical system, the aging and deterioration of the lubricant, wear of functional parts of the machine, or. about the location of excessive wear, which is usually the cause of failures and sometimes system crashes. Analytical data on the lubricant provide, in addition to diagnostic information, also prognostic information and make it possible to predict and also prevent accident situations. Lubricant analysis makes it possible to very sensitively determine the wear rate of the system as a function of time, resp. in real time, provides additional control options, e.g. filtration systems, tightness of cooling systems, etc. In addition to the requirement of complexity, tribotechnical diagnostics must meet the condition of correct selection of the necessary tribodiagnostic methods, their simplicity, speed and unambiguous responses to the state (mode) of system wear and further usability of the lubricant. In terms of use, depending on the complexity of the technique, the organizational level, the traffic intensity, the instrumentation and the personnel possibilities, the meth-

ods of tribotechnical diagnostics can be divided as follows:

- Simple methods and tests - express methods (speed methods).
- Standard methods and tests - according to STN EN.
- Special methods and tests - tribodiagnostic methods.

From the point of view of the essence and physico-chemical principles, the methods of tribodiagnostics can be divided into:

- Methods for determining the concentration of abrasive metals.
- Methods for evaluating the morphology and distribution of abrasive particles.
- Methods for determining the physico - chemical properties of a lubricant [5,6].

2.1 Ferrography

The detection of wear of oil-lubricated mechanical systems is based on the knowledge that the oil after a certain period of operation reflects the technical condition of the mechanical system and the operating conditions. This multidimensional information is carried by metal abrasion, which is dispersed in the oil and which, after quantification by a suitable method, allows indirect monitoring of the wear regime and mechanical changes in the system in which the oil is used. From the detected amount of metal abrasion, the intensity of the increase in the number of particles, the shape, morphology, size and material composition of particles and wear fragments, certain conclusions can be drawn - if the increase in abrasion and other parameters are systematic and compared with the nominal values determined for a given mechanical system (determined by calculation, long-term monitoring, etc.), it can be relatively reliably judged to be a normal course of wear without an increased risk of system failure. A sudden increase in the number of metal particles and the finding of particles of shapes characteristic of abnormal wear mechanisms signal an extraordinary event. From the size and shape of the particles, the growth rate, their number, morphology and other parameters, the severity of the disorder and the urgency of corrective action can be inferred. An important diagnostic circumstance is the ability to locate the site of increased abrasion and incipient disorders. According to the material composition of the metal abrasion, it is possible to determine the friction pair in which there is a sharp increase in wear. For these purposes, a suitable method is ferrography, based on the separation of solid metallic and non-metallic particles contained in the oil filling of lubrication systems of machines and equipment from the actual oil. Describes trapped particles (especially ferromagnetic) and assigns them to individual wear mechanisms; allows you to detect an impending machine failure. Abrasive particles can be divided according to their composition, size and other characteristics using this method. The separation takes place in a ferrograph, Fig. 3 - a sample of the examined lubricant flows down an inclined pad, which is placed in a magnetic field. The largest ferromagnetic particles settle at the beginning of the substrate and then the particles settle according to their magnetic properties, composition, size and shape. With this method it is possible to distinguish the shape of particles, their origin, place of origin (location of wear), morphology, etc. Ferrography is focused on the analysis of ferromagnetic abrasives in a lubricant using a magnetic field. It is a technique for separating metallic (and non-metallic) substances from used oil. In the ferrographic analysis, a diluted sample of oil is drained over an inclined transparent substrate (foil), under which a strong magnet is placed. The inclination of the substrate causes a particle size distribution along the transparent substrate due to the gradient (variable force) of the magnetic field. At the beginning, larger particles are captured (>15 micrometers) and the closer the film is to the magnet, the smaller particles are captured (<5 micrometers, or at the end up to 1-2 micrometers). After passing the oil sample, the oil is washed away with a suitable solvent (technical gasoline) and the particles are fixed on a transparent support with a transparent varnish, thus obtaining the so-called Ferrogram. Ferrogram allows to assess particle size, ratio of large particles (10-100 micrometers) to small particles, morphological (shape) characteristics of particles, etc. Based on the observation of particles on a special bichromatic microscope (combination of metallographic and biological microscopes - reflected as well as transmitted light is used), the wear regime of the mechanical system can be determined.

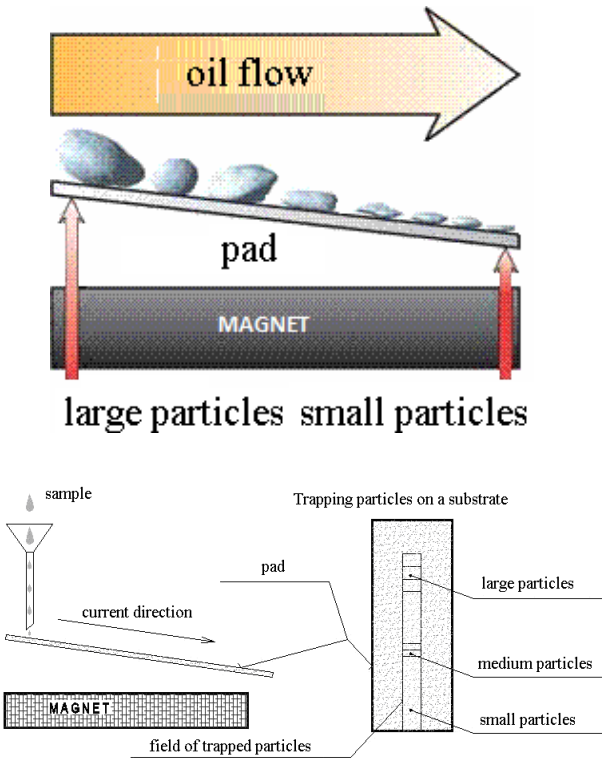

Fig. 3 Schematic of a ferrograph and the principle of ferrographic analysis

The operating conditions, in particular the efficiency of the air filter, the presence of water in the oil and the overall care of the technical staff for the equipment, shall be clearly indicated at the end of the sedimentation trace on the ferrogram. Image analysis can be used for quantitative evaluation of ferrograms. In Fig. 4 and Fig. 5 are particles isolated from oil filters.

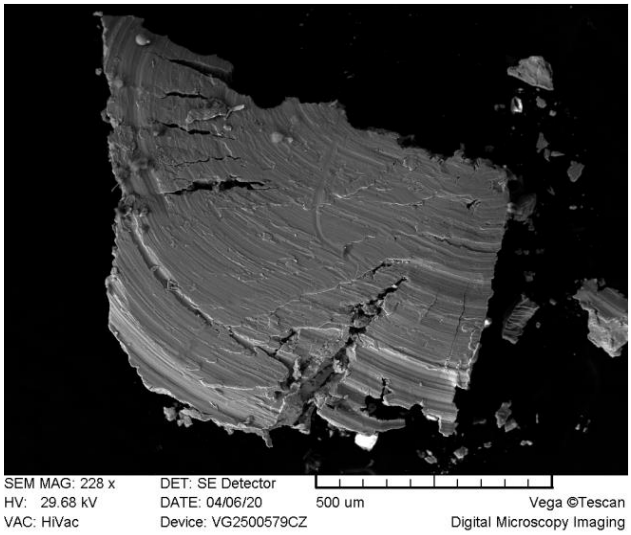

Fig. 4 Particles from oil filters

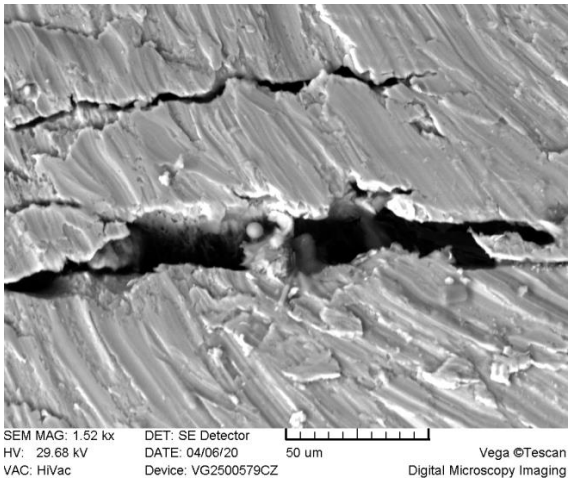

Fig. 5 Particles from oil filters

Fig. 4 shows laminar particles where traces of abrasive wear due to high pressures at the contact of the friction surfaces are visible and incipient cracks are visible in the edge portions. In Fig. 5 is a spheroid artifact typical of fatigue wear. The ball is formed by the slow growth of a fatigue crack extending into the oil-soaked surface [7].

3 Results and discussion

The maintenance program is usually based on vibration monitoring, selected operating parameters and tribodiagnostics, which allows you to assess the specific condition of the equipment in real time. It is important that maintenance only applies to those parts or machines that really need it. The fault can be detected at the stage of occurrence and thus prevent more extensive damage, there are no unexpected outages and at the same time no unnecessary work is performed. Tribodiagnostics is based on regular sampling of lubricants (oils) from monitored machines and their analysis. With the help of tribodiagnostic analysis, we can determine both the condition of the oil itself and especially the condition of the monitored machine. The lubricating oil serves as a medium containing wear particle of the lubricated parts of the monitored machine. By analyzing these particles, we obtain important information about the mode of wear and events in the machine. It is very important to monitor the machine systematically and continuously from the beginning of the operational deployment and to obtain trends in the content of particles in the oil, resp. other tribodiagnostic parameters in the oil, as this

information provides a reliable indication of changes in the wear regime and the actual technical condition. The second part of tribodiagnostics is the analysis of the oil itself, which we find out by changing its physico-chemical properties, as well as its pollution by foreign substances, e.g. water, mechanical pollution, chemical compounds. The basis of the success of tribodiagnostics is a correctly taken oil sample. The sample must be truly representative, ie. it must contain all substances in the proportion in which they occur in the lubrication system of the monitored machine. The optimal place for sampling is the return line, where the oil returns from the lubricated places to the oil tank. Some manufacturers already equip the machine (engine) with a sampling tap located just on the oil return line. Sampling must be performed while the machine is running, if possible, or shortly after it has stopped. Sampling containers (sample boxes) must be clean and dry. An important aspect of tribodiagnostics is the speed of response and the accuracy of the results. Regular samples should be analyzed quickly, based on the results of the diagnosis, the results are sent to the machine operator. Only the results of the analysis of the oil sample or the evaluation of the analysis with a recommendation for further action may be given in the relevant report. It depends on the system that suits the knowledge and experience of the workers.

4 Conclusion

This article briefly analyzes the crucial problems of friction and wear that occur during the operation of vehicles (especially vehicle combustion engine, transmissions, hydraulic systems, etc.), defined tribological unit as the smallest element where friction and wear take place. The tribological unit includes interactions of min. two friction surfaces, lubricant and environment. A separate part is devoted to the tribodiagnostic method of ferrography. This focuses on the detection of wear of oil-lubricated mechanical systems is based on the knowledge that the oil after a certain period of operation reflects the technical condition of the mechanical system and the operating conditions. There are still few such maintenance personnel who practically use and apply the current state of the art to identify the condition of the equipment based on the condition of the oil system. The introduction of new approaches to the care of means of production, technology, and processes enables the rational use of the results of analyzes for reliable and trouble-free operation. Proper treatment e.g. by filtering or adding the right additives will significantly affect the economy of operation. If the oil is still clean and properly maintained, it does not need to be changed. This will significantly reduce the environmental risk as well as increased environmental protection.

5 Acknowledgement

This work was also supported by the Research Agency of the Ministry of Education, Science, Research and Sport of the Slovak Republic under the contract (ITMS2014+) no. 313011W442-CEDITEK II.

References

[1] Deters, L. *Springer Handbook of Mechanical Engineering*, Part B. [s.1.]: [s.n.], Tribology, 2009. ISBN 978-80-540-491.

[2] Stodola, J.: *Diagnostika bojových a speciálních vozidel*. Vysokoškolská učebnice U- 3086: Univerzita obrany Brno, 2005. ISBN 80-7231-017-8.

[3] Macian, V., Tormos, B., Olmeda, P., Montoro, L.: *Analytical Approach to Wear Rate Determination for Internal Combustion Engine Condition Monitoring Based on Oil Analysis*. Tribology International 36 (2003), p. 771-776.

[4] Krtička, F.: *Obrazová analýza částic v provozních hmotách a konstrukčních materiálech pro dopravní prostředky*. Dopravní fakulta Jana Pernera. Univerzita Pardubice, 2007.

[5] Leugner, L.: *The Practical Handbook of Machinery Lubrication*. Maintenance Technology International, 2005.

[6] Michael A. Taylor.: *Quantitative Measures for Shape and Size of Particles*, Powder Technology, 124 (2001), p. 94–100.

[7] Totten, E., G.: *Handbook of Lubrication and Tribology*. Volume I. Taylor&Francis Group, New York, 2006, ISBN 0-8493-2095-X.

University Review, Vol. 15, Issue 1, p. 39-44, 2021.

UNIVERSITY REVIEW

COMPARISON AND ASSESSMENT OF THE CUZN30 BRASS STRUCTURE IN THE PRODUCTION OF THE 9X19 LUGER CARTRIDGE CASE

Miroslav Polášek[1*] – Matúš Danko[2]

[1, 2] Department of Mechatronics and Electronics, Faculty of Electrical Engineering and Information Technologies, University of Žilina, Univerzitná 8215/1, 010 26 Žilina

ARTICLE INFO…filled by the publisher

***Article history*:**
Received: 15.3.2021
Received in revised form: 23.4.2021
Accepted: 3.5.2021

Keywords:
metallography
cartridge case
CuZn30 brass
grain size
deep drawing
recrystallization
9x19 Luger

Abstract:

In the process of small-caliber ammunition production, the quality of the setting of the deep drawing technology of CuZn30 brass and its subsequent recrystallization is essential. The quality of the setting of this technological process is also very important for the final quality of the whole ammunition, as the cartridge case, or even the projectile, is produced by the technology of deep drawing. In deep drawing technology in cartridge case manufacturing, when CuZn30 brass already reaches the value required for recrystallization, the brass structure changes the grain size of the structure. And at the same time, makes it difficult to achieve a uniform grain size in the entire cartridge case cross-section after recrystallization or after some steps of the technological process.

1 Introduction

At present, which desires for the development of defense technologies, as well as the efficiency of ammunition production, the constant goal is to optimize production as much as possible with respect to the time and economy within the highest or required quality of the final product. In this work, I will compare and assess the structures in the semi-finished product for the production of cartridge cases in places, where the greatest transformation of the material is. Semi-finished products and inner products for the production of cartridge cases are from single-drawing technology of cartridge case production. This technology is older, it has been used since the beginning of ammunition manufacturing. It is less demanding on the stability of the input material, but it is less efficient for high production. Ideally, the metallographic structure of the cartridge case cross-section should be as regular as possible, without significant differences in the grain size of the structure, which could also ensure the multiple use of the cartridge case. Ensuring a uniform structure over the entire cross-section of the cartridge case is problematic and the differences in the structure of the material are according to different deformations in different parts of the material.

2 Description of the work methodology

2.1 Composition of the brass for the production of cartridge case

Cartridge case brass means brass intended for the manufacture of cartridge cases in the ammunition industry. The chemical composition of cartridge case brass is 70% Cu and 30% Zn. Cartridge case brass is binary brass. The newer designation of the cartridge case brass is CuZn30, the older designation that is still in use, is Ms70. In the past, CuZn28 brass (former designation Ms72) was also used to make cartridge cases. This brass has a higher content of copper. Copper is a more expensive raw material than zinc, so that´s why this type of brass has

[*] Corresponding author. Tel.: *0905 737 374*
E-mail address: polasek@stud.uniza.sk

mostly ceased to be used. Only some ammunition uses CuZn28 brass to make cartridge cases so far.

Table 1 Chemical composition of cartridge case brass according to DIN 17660 (wt.%)

Cu	69-71
Al. max.	0.02
Fe max.	0.05
Ni max.	0.2
Pb max.	0.05
Sn max.	0.05
other max.	0.1
Zn	rest

The integration of cartridge case brass into the Cu-Zn equilibrium binary diagram is observable in Fig. 1. The equilibrium binary diagram Cu-Zn consists of five simple peritectic diagrams.

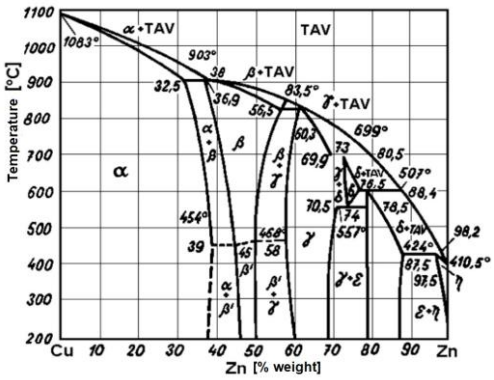

Fig. 1 Equilibrium binary diagram Cu-Zn [1]

In the case of cartridge case brass, the alpha phase is interesting, thus the phase rich in copper – more than 61-62% of copper in the alloy. Whereas the alpha phase is rich in copper, it also has a lattice like copper, a cubic lattice centered. The alpha phase is a solid solution of the substitution type, where some copper atoms have replaced zinc atoms.

2.2 Production procedure of 9x19 Luger cartridge case

Fig. 2 9x19 Luger cartridge case manufacturing process

Fig. 2 shows the sequential steps in a single-drawing (single-operation) technology for the production of a 9x19 Luger cartridge case from a semi-finished product cup (shown in Fig. 2 by the number 1). In this work, I will deal with the comparison of the structure in the cross-section of the semi-finished product after the second drawing (shown in Fig. 2 in Fig. 3). Further steps in production technology (steps 4-9 in Fig. 2) do not affect the change of material structure as much as steps 2,3. In step 5, a change in structure is visible when a primer hole is formed, but not as much as in steps 1,2,3.

2.3 Recrystallization annealing of brass

When forming or deforming a cartridge case brass, the grains in the microstructure elongate and break up. This creates their orientation. The orientation of the grains is in the direction of deformation. If the degree of deformation is large enough, the brass acquires a fibrous or fragmented structure, as seen in Fig. 3. Cartridge case brass acquires greater strength by forming, but the possibility of further forming is also exhausted. If we want to shape this material further, we need to include the recrystallization annealing operation among the forming.

Fig. 3 Structure of CuZn30 brass after deformation

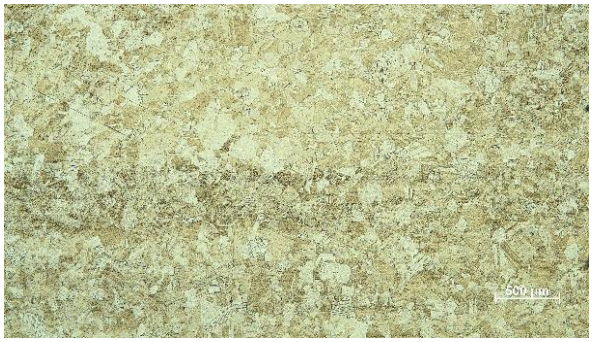

Fig. 4 Structure of CuZn30 brass after recrystallization

Recrystallization annealing removes the consequences of the previous cold forming (deformation strengthening), the malleable property of the material is restored Fig. 4. The conditions of recrystallization annealing are determined by the degree of transformation and the required properties of the annealed material. The standard annealing temperature for the production of CuZn30 cartridge cases is usually in the range from 500 to 650 °C, depending on the technology settings. In some manufacturing, they also use a different temperature range according to the degree of deformation of the material in the individual steps, and according to the time endurance at the temperature. The recommended grain size of the CuZn30 brass structure after recrystallization is in the range of 0.045-0.090 mm.

Hardness measurement and determination of the average grain size of CuZn30 brass after the second drawing in the production of a 9x19 Luger cartridge case

I will use a comparative method using the ČSN 42 0462 standard to assess the grain size. To assess the size of the deformation, I will use data from the work of Georg Vander Voort [7], the values of the deformation which are dependent on the measured hardness are in Table 2.

Table 2 Dependence on cold forming on CuZn30 hardness of George Vander Voort

Reduced CuZn30	Hardness
Without Reduced	57.9 ± 4.8 HV
Cold Reduced 15%	126 ± 11.3 HV
Cold Reduced 30%	159.8 ± 10.4 HV
Cold Reduced 40%	185.5 ± 6.2 HV
Cold Reduced 50%	194 ± 2.1 HV
Cold Reduced 60%	199.6 ± 5.2 HV
Cold Reduced 70%	231.9 ± 7.9 HV

Measurement and assessment were realized on the following five types of samples:

1. 4.5 grams cup for the production of a 9x19 Luger cartridge case
2. 4.5 grams cup after recrystallization
3. after the first drawing
4. after the first drawing and recrystallization
5. after the second drawing.

On these samples, I measured in places where the greatest deformation of the material is after deep forming in the technology of production of the 9x19 Luger cartridge case. In Fig. 5 are shown the locations on the cross-sections of the samples where the measurement was performed.

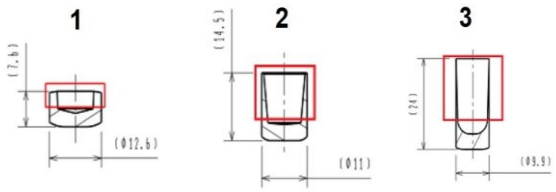

Fig. 5 Picture of samples for measuring with locations of the biggest transformation, number 1. Entry semi-finished product cup, number 2. After first drawing, number 3. After second drawing (from left to right)

3 Discussion of results

Recrystallization was performed on an entry semi-finished product cup and an after first drawing at a temperature of 520 °C in a continuous recrystallization furnace.

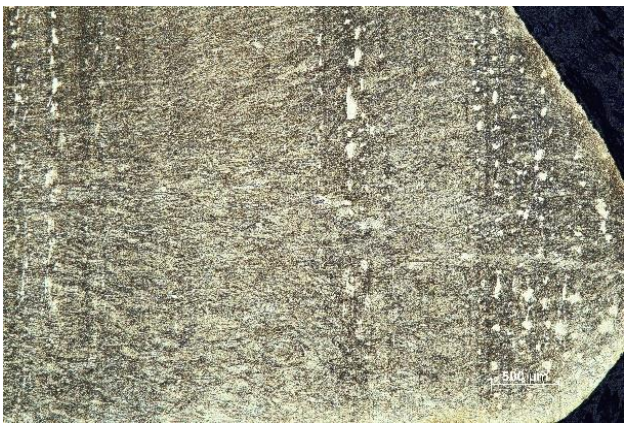

Fig. 6. Structure of entry semi-finished product cup

Fig. 7 Structure of entry semi-finished product cup after recrystallization

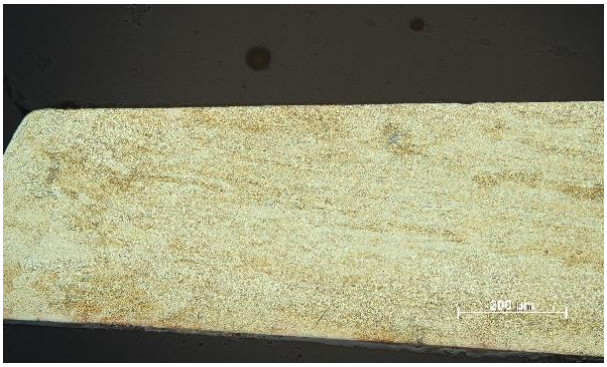

Fig. 8 Structure after first drawing

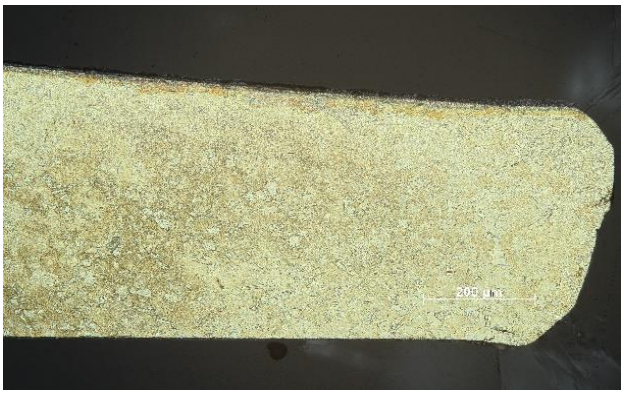

Fig. 9 Structure after first drawing and recrystallization

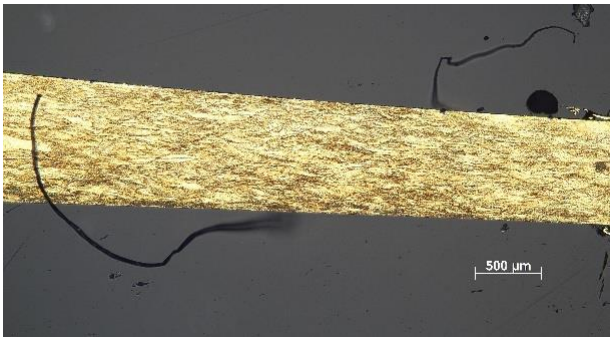

Fig. 10 Structure after second drawing

In Fig. 6, the structure of the CuZn30 brass is in place of the largest deformation on the cup as the semi-finished product of cartridge case. The cup is cut and drawn, so most of it has a narrowly shattered grain. In Fig. 7, there is a cup after recrystallization, so the structure of the CuZn30 brass can be seen in place of the largest transformation. In Fig. 8, there is the structure of the most deformed part after the first drawing, the structure is deformed and the grains are small and fragmented. In Fig. 9, there is the structure after the first drawing, but also after recrystallization, where we can see the renewed grains of the structure. In Fig. 10, the structure of the material is after the second drawing.

Table 3 Measured and calculated data at the most transformed locations during deep drawing and recrystallization

Place of the biggest transformation	Entry semi-finished cup	Entry semi-finished cup after recrystalization	After first drawing	After first drawing and recrystalization	After second drawing
	Hardness	Hardness	Hardness	Hardness	Hardness
Measurement 1	197 HV	96.8 HV	221 HV	91.2 HV	214 HV
Measurement 2	250 HV	98.9 HV	150 HV	69.3 HV	206 HV
Measurement 3	239 HV	91.8 HV	221 HV	76.1 HV	203 HV
Measurement 4	242 HV	96 HV	224 HV	-	-
Measurement 5	252 HV	-	213 HV	-	-
Average hardness	236 HV	95.88 HV	210 HV	78.87 HV	207.67 HV
Cold reduced	70%	less than 15%	less than 70%	less than 15%	less than 70%
Size of grain	-	0.088 mm	-	0.125 mm	-

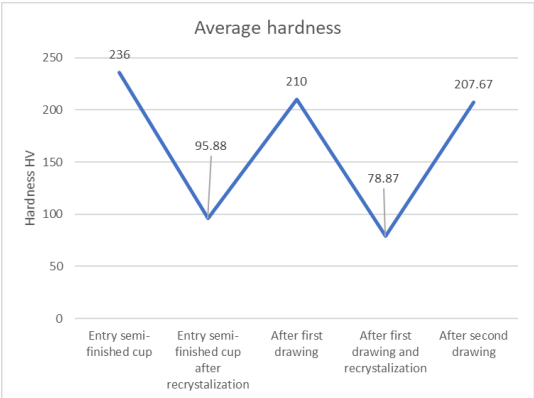

Fig. 11 Average hardness of the biggest transformation locations

From the measured and calculated data in Table 3 and in the graph (Fig. 11), it is clear how the structure of CuZn30 brass is fragmented after the drawing technology, the grain size is smaller or elongated. The hardness increases after this operation. The strength of brass also increases with increased hardness. Based on hardness, the percentage of cold reduced increases. After the recrystallization operation, the brass structure is restored, also grain growth and structure restoration can be seen. Of course, the hardness of the structure and its strength are smaller. Based on hardness, the percentage of

"cold reduced" decreases, so the restored structure of CuZn30 brass is ready for transformation again.
Entry semi-finished product cup is a semi-finished product made of CuZn30 material, which most of smaller ammunition buys as a basis for the production of a 9x19 Luger cartridge case. The structure of this product can be seen in Fig. 6. Larger ammunition is making these semi-finished products from sheet metal separately. This requires single-purpose technologies for cutting and deep drawing of this CuZn30 sheet metal. The standard weight of this semi-finished product is 4.5 g. After cutting and deep drawing, the entry semi-finished product cup has the exhausted possibility of structure for further forming. The structure has small dimensions or very stretched grains in the most deformed part. The average measured hardness is 236HV. This means that the rate of cold reduced is 70%. In order to further usage of this semi-finished product in the technological process of forming, the entry semi-finished product cup structure must be recrystallized.
Entry semi-finished product cup after recrystallization. The structure of this product can be seen in Fig. 7. The inner structure of the material was restored after recrystallization of the entry semi-finished product cup. The average hardness decreased from 236 HV to 95.88 HV in the place of largest deformation of the structure. This means that the cold reduced rate has been reduced from 70% below 15%. The measured value of the structure grain size is 0.088 mm. As shown in Table 4, this value is 0.0205 mm higher than the mean recommended value of the CuZn30 material after recrystallization, which is reported by Malov [5] in the publication Ammunition Manufacturing. This difference is a deviation of 30.37% from the ideal mean value after recrystallization. But it is still within the maximum recommended value after recrystallization, which is set at 0.090 mm.

Table 4 Grain size values after recrystallizations

	Entry semi-finished cup after recrystalization	After first drawing and recrystalization
Average hardness [HV]	95.88	78.87
Size of grain [mm]	0.088	0.125
Deviation from ideal value after recrystallization mean deviation 0.0675 mm	0.0205	0.0575
Deviation from ideal value after recrystallization mean deviation [%]	30.37	85.19
Deviation of the maximum recommended value after recrystallization mean deviation 0.090 mm	-0,002	0.035

After the first drawing, the inner structure of the material changed again in the place of the largest deformation. The inner structure and grain are elongated and shattered, as we can see in Fig. 8, also in the table of values 3. The fact that the structure changed resulted in an increase in hardness from an average value of 95.88 HV to a value of 210 HV.
This means that the cold reduced rate has increased from below 15% to value below 70%. This increased hardness means an increase in the strength value of the brass, as well as the exhaustion of the possibility of further reshaping without previous recrystallization of the structure.
We can see the structure after first drawing and recrystallization in Fig. 9. In comparison with the Fig. 8, the structure is restored. The restored grains of the structure are visible in the place of the greatest deformation after the previous forming. The average hardness of the material decreased from 210HV to 78.87 HV. This means that the cold reduced rate decreased from 70% below 15%. The measured value of the structure grain size is 0.125 mm. As shown in Table 4, this value is 0.0575 mm higher than the mean recommended value of CuZn30 after recrystallization, which is also reported by Malov [5] in publication Ammunition Manufacturing. This difference is a deviation of 85.19% from the ideal mean value after recrystallization. This value is 0.035 mm higher than the maximum recommended value after recrystallization, which is set at 0.090 mm.
After second drawing, the inner structure of the material changed again in the place of the greatest deformation. The inner structure and grain are elongated and shattered, as we can see in Fig. 10, also in the table of values 3. By changing the structure, it resulted in an increase in hardness from an average value of 78.87 HV to 207.67 HV. This means that the cold reduced rate increased from below 15% to value below 70%. This increased hardness means an increase in the strength value of the brass, as well as the exhaustion of the possibility of further bigger deformation.

3 Conclusion

According to the assumptions, the increase in hardness of the material is the highest in places where is the maximum value of deformation in the production of the 9x19 Luger cartridge case. Since the grains of the structure are stretching at first, the value of hardness increases as the structure changes

after deformation. Later, the grains break up, so the value of the structure grain size decreases. This causes the increase of the transformation degree of cold reduced. Gradually, the possibilities of further transformation of the material are exhausted if we do not include the recrystallization of the structure in the process. In our results we have maximum average values of hardness after forming from 207.67HV to 236 HV. Interesting thing is the lowest value of the average value after the second drawing, in which case after this operation until the end of production of the 9x19 Luger cartridge case, there are no other larger values of deformation. The other largest value of the deformation outside the production of the cup, the first and the second drawing, is in the calibration before turning. But this deformation is much smaller than in the first or second drawing, because this deformation is without changing the wall thickness. Practically, the hardness of the material does not change or just very slightly. The samples were from single-drawing technology, where is bigger area for slight changes in the quality of the input products stability, as I have already mentioned. This can also be seen in the resulting hardness after the second drawing, where the hardness is 207.67 HV. If we compare this with the results of hardness in the same area of the cartridge case (in the muzzle of the cartridge case, where the bullet is inserted, wall thickness approximately 0.3 mm) in multi-drawing technology, where hardnesses reach 230-250HV, there is still a reserve of transformation possibility in this part of the final cartridge case. This lower hardness can practically ensure a longer usage of the cartridge case for multiple reloading. Of course, multiple reloading is dependent on the size of the powder charge, the amount of crimping force required to pull the projectile out of the cartridge case, and the dimensional tolerance of the cartridge chamber from which the ammunition will be fired. From my experiences I will state entry semi-finished product cup after recrystallization, which I did let go through the entire production process of the 9x19 Luger cartridge case without recrystallization after the first drawing. The result was a standard cartridge case visually. This only served as visual test of the entire production line, without further testing of how this cartridge case would behave during firing. The omission of recrystallization after the first drawing could result in bursting of the cartridge case, which is very undesirable and sometimes dangerous element in shooting. During my measurement, after the first recrystallization of the entry semi-finished product cup, the size of grain structure was 0.088 mm, which is a very good value, even though it is only 0.002 mm below the maximum recommended value after recrystallization. During the second recrystallization, after the first drawing, the size of the structure was 0.125 mm, which is 0.035 mm above the recommended value after recrystallization, but it has no significant effect on the functionality of the technology or the final cartridge case. However, it is necessary to point out a possible problem. If we change the input material (for example within the standard range), recrystallization set up in this way, after the first drawing, could make a problem if this change in the input material accentuated such an extreme value. Therefore, it is good to have the whole technology set up universally and keep the values after recrystallization as close as possible to ideal value after recrystallization – 0.075 mm, which will ensure possible reserves in technology. For example, when changing within the standard or within other imperfect part of technological process.

References

[1] Polášek, M.: *Metalografické hodnotenie rakryštalizácie mosadze MS70 po tvárnení*, Fakulta špeciálnej techniky TU AD v Trenčíne, Trenčín, 2018. 65 s.

[2] Paur, V.: *Technológia tvárnenia*, ALFA, Bratislava, 1987. 227 s.

[3] Pernis, R.: *Teória a technológia výroby kalíškov*, Fakulta špeciálnej techniky TU AD v Trenčíne, Trenčín, 2009. 226 s.

[4] Martinec, Ľ., Šimkovič, M.: *Náuka o materiálech*, STU, Bratislava, 1997. 232 s.

[5] Malov, A. H.: *Výroba munície*, Moskva, 1947. 405 s.

[6] Voort, G. V.: *Deformation and Annealing of Cartridge Brass*, VAC AERO INTERNATIONAL INC., Canada, 2015. [online].

[7] Eckert, M., Krbata, M., Barenyi, I., Majerik, J., Dubec, A., Bokes, M.: *Effect of selected cooling and deformation parameters on the structure and properties of AISI 4340 steel*. Materials, Vol. 13 (2020), p.1-21.

[8] Zahalka, M., Raz, K.: *Completing and refining of the materiál library for forming simulations.* Annals of DAAAM and Procesings of the International DAAAM Symposium 30(1),(2019), p.384-389

University Review, Vol. 15, Issue 1, p. 45-50, 2021.

UNIVERSITY REVIEW

APPLICATION OF QUASI-STATIC NANOINDENTATION METHOD FOR THE RESEARCH OF MECHANICAL PROPERTIES MICROSTRUCTURAL COMPONENTS OF TOOL STEEL

Henrieta Chochlíková[1] - Jana Escherová[2]

[1] Department of Engineering Technologies and Materials, Faculty of Special Technology, Alexander Dubcek University of Trencin, Ku kyselke 469, Trencin Slovakia,

ARTICLE INFO

***Article history*:**
Received: 15.3.2021
Received in revised form: 23.4.2021
Accepted 3.5.2021

Keywords:
Young modulus,
Nanoindentation hardness,
Microstructural,
Steel 90MnCrV8.

Abstract:

The material 90MnCrV8 was used for the valuation of mechanical properties of microstructural components of tool steel. Tool steel has to satisfy high demands in industrial practice such as high strength, toughness, wear resistance, temperature stability and so on. Experimental measurements were performed on a Hysitron TI 950 Tridoindenter with Triboscan evaluation software. The Berkovich type was used as a test tip.
The quasi- static nanoindentation is used as a methodology of measurement. The methodology and evaluation of microanalysis of tested tool steel by light microscopy is described in chapter 2. Chapter 3 contains own measurements and evaluation of measured data of tested tool steel using the method of quasi- static nanoindentation. .

1 Introduction

Using quasi-static nanoindentation we can measure mechanical properties such as modulus and hardness of materials in different shapes, sizes and scales. Thanks to this method we can measure mechanical properties from the hardness materials to soft biomaterials in a couple minutes. Quasi- static nanoindentation is used in research in different industrial fields in order to find out of nanomechanical properties of thin layers in electronics and packaging materials, coatings of cutting tools, coatings for thermal barriers, visco- elastic properties of polymeres, microhardness in industrial quality and control, resistance against scratching and wear and many more. Nano- hardness H [GPa] isn´t the only value that comes from quasi- static nanoindentation. This method can be used also for measurement and evaluation of reduced Young modulus of elasticity E_r [GPa]. Nanoindentation techniques can also be used for the calculation of elastic modulus, deformation-curing exponent, fracture toughness (for example for brittle materials) and visco- elastic properties.

Fundamentally it is relatively simple method of researching local mechanical properties, which is based on the indentation of an object with known dimensions and mechanical properties with a certain force into the studied material with a penetration depth in the nanometer scale. Load and depth of indentation are recorded at each load increment, which ultimately provides a measure of modulus hardness as a function of depth below the surface. The loading part of indentation cycle can consist of the initial elastic contact following with plastic deformation or loading of tested material at higher loads. The maximal depth of indentation for specific

Corresponding author. Tel.: +421327400218
E-mail address: henrieta.chochlikova@tnuni.sk

loading together with inclination of indentation curve measured in tangent to the point considered at maximum load, leads to measuring the hardness and elastic modulus of sample material [1].

The main goal of quasi- static nanoindentation is to measure values of elastic modulus and nanohardness of the test material of the sample from the experimental values of the test tip of the load and penetration depth.

Nguyen et al. [6] aimed on measuring nanometric characteristics (microstructural characteristics and mechanical properties are investigated) of H13 material using scanning speed of 100 mm.s^{-1}. Measurements detected a relation between nanoindentational deformation and toughness. With an increase of speed of deformation (0,002 to 0,1 s^{-1}) the toughness is increased also in a range of 8,41 to 9,18 GPa. The work of these authors [8] presents a comparative study of several methods of nanoindentation which were applied on ferritic-martensitic steels of type T91 (9Cr-1Mo) and Eurofer 97 [7]. Measurements were realized with CSM method (Continuous Stiffness Measurement - CSM). Depth-controlled single cycle measurements atvarious indentation depths, force-controlled single cycle, force-controlled progressive multi-cycle measurements, ancontinuous stiffness measurements (CSM) using a Berkovich tip at room temperature have been combined to determine the indentation hardness and the elastic modulus, and to assess the robustness of the different methods in capturing the indentation size effects (ISE) of those steels [7]. Quasistatic methods for individual cycles with controlled depth and strength and progressive multicycle measurements show common accord, whereas continual measurements of toughness are depending on amplitude [8]. Studies [5] concerned with comparing curves *P-h* during maximal load, were used as a comparing curves *P-h* with results of exploring mechanical properties of microstructural parts of tool steel.

2 Material and methodology of measurement

2.1 Properties and microstructure of tool steel 90MnCrV8

Steel 19 312, 90MnCrV8 belongs to alloyed tool steels according to the STN standard. The most important alloying elements of these steels are Cr, Mo, V, and W. These elements are carbide- forming and they increase the hardness and stability of the carbide phase and reduce a decrease of hardness during tempering. They also increase resistance against wear in a large extent. As these alloying elements increase depth of hardening, it is possible to produce tools of bigger proportions. Besides, we can increase the toughness by adding Ni. Chemical composition of steel 90MnCrV8 is shown in table 1 [4]. Steel 90MnCrV8 is suitable for manufacturing cutting tools for non-metals (knives on paper), tools for cutting in cold conditions (different shaping dies), tools for pulling sheets, moderately stressed forms for pressing metalling and non- metalling powders, whose shape is more complicated, for processing plastics requiring good stability of dimensions after thermic processing, production of gauges [2],[3].

Table 1 Chemical composition of steel 90MnCrV8 [average wt. %] [4]

Chem. element	C	Mn	Si
Average wt. %	0,75-0,85	1,85-2,15	0,15-0,35
Chem. element	P	S	V
Average wt. %	Max 0,030	Max 0,035	0,10-0,20

Tested material 90MnCrV8 is steel with ferritic-pearlitic structure. The white areas represent ferritic grains, and the dark areas represent pearlitic grains, e.g. in Fig. 1.

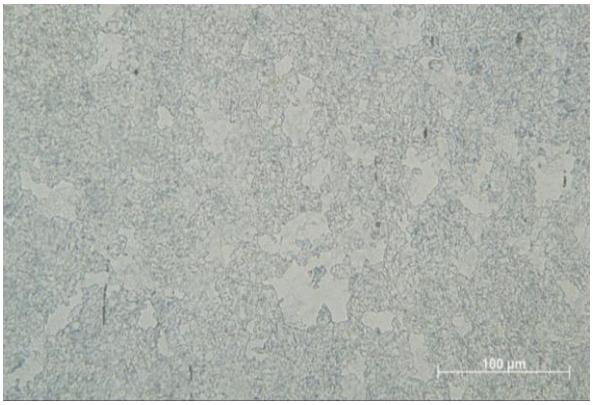

Fig. 1 Microstructure of testing steel 90MnCrV8

2.2 Methodology of measurement

Nanoindentation analysis was performed on a measuring device of the Hysitron TI 950 Tridoindenter with Triboscan evaluation software. The nanoindentation test was performed at room temperature with application of internal geometry the Berkovich in laboratory of mechanical tests CEDITEK on Faculty of special technology in Trenčín.

Quasi-static nanoindentation measurements were released on metallographic sample of tool steel 90MnCrV8 (equivalent 1.2842; STN 19 312). Measurement by the quasi-static nanoindentation method requires the indentation of test tip Berkovich geometry into the sample under specified load control or displacement. The displacement (*h*) is monitored as a function of the load (*P*) during the whole cycle of loading- unloading, where dependence *P-h* is known as nanoindentation curve. The area under curves of loading and unloading is then equivalent to energy of dispersion. In all the performed nanoindentation measurement, the load together with the displacement was recorded when the Berk test tip was pressed into the surface of the measured sample using standard *P-h* profiles. Parameters of tip are mentioned in table 2. The method of quasi-static nanoindentation was used on chosen spots of basic material of microstructural testing sample (Fig. 1). The area of research was specified using optic microscope as an inbuilt part of device. Subsequently was realized a so-called SPM scan of a selected area with dimensions 50x50 μm.

Table 2 Geometry of testing tip a its projection [1]

Testing tip	Projection surface	Top peak angle θ (deg)	Effective conic angle α (deg)	Intercept factor $^{a}\mathcal{E}$	Geometric correction factor β	Projection
Berkovich	$A = 3\sqrt{3}h_c^2 \tan^2\theta$	65,26°	70,3°	0,75	1,034	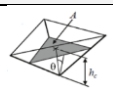

The selection of particular spots for realization of individual indents for chosen material were defined by mechanical form with selected number of indents on explored surface. The standard trapezoid with a maximum at 8000 μN and a total indentation endurance time *t = 2s* was used as a loading curve in the process of the performed experiment. Measured values of nanoindentation hardness *H* [GPa] and reduced Young modulus of elasticity E_r [GPa] were then evaluated in particular positions using Triboscan software.

The realization of measurement using loading cycle and the development of indent curve formation (on the left) is seen in the Fig. 2. Results of measurement were generated to xls table of hardness values *H* (GPa) and reduced Young modulus of elasticity E_r (GPa) (table 3).

After the termination of measurement *P-h* curves for particular indents are generated, e. g. in Fig 4.

3 Material Measurement of nanoindentation hardness *H* and reduced Young modulus of elasticity E_r on microstructural particles of steel 90MnCrV8.

Measurement were composed of six or seven indents on chosen spots in microstructural tested area (Boundary). Dimensions of measured areas were limited on 50x50 μm. In the research the standard trapezoid with maximum in 8000 μN and a total indentation endurance time *t* = 2s was used as a loading curve in the process of the performed experiment. A Hysitron Triboindenter TI950 was used as a test device.

The placement of indents of valued area of steel 90MnCrV8 sample on SPM scan are seen in the Fig. 3. Measured values of nanoindentation hardness *H* [GPa] and reduced Young modulus of elasticity E_r [GPa] are visible in table 3.

The shapes of the nanoindentation curves obtained from the indents on the SPM scan of the evaluated area of the test sample of 90MnCrV8 steel are shown in Fig. 3. There could be an overlap to the ferrite field during the evaluation of perlitic cementite. Therefore, lower values of nanohardness *H* [GPa] could be measured.

The summary of phases of observed tool steel and their nanohardness H and reduced Young elasticity modulus E_r is shown in table 4.

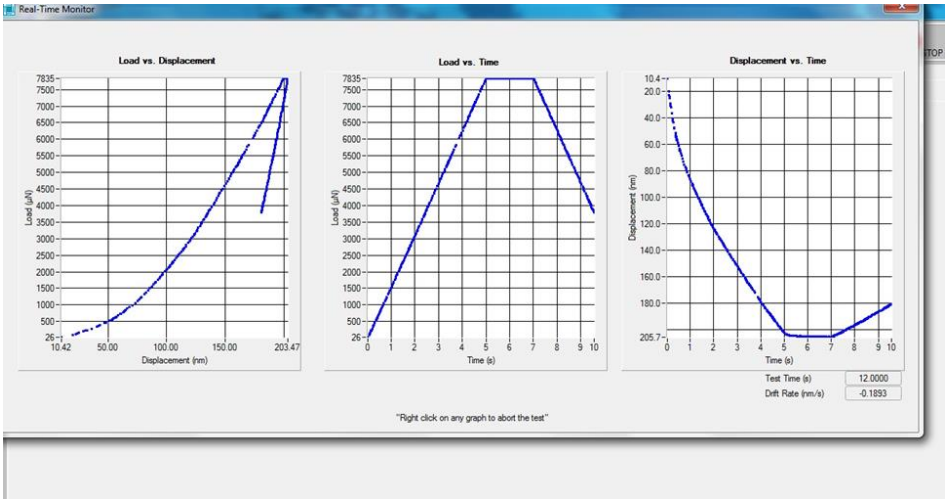

Fig. 2 The course of the measurement by the load cycle and the course of the curve formation.

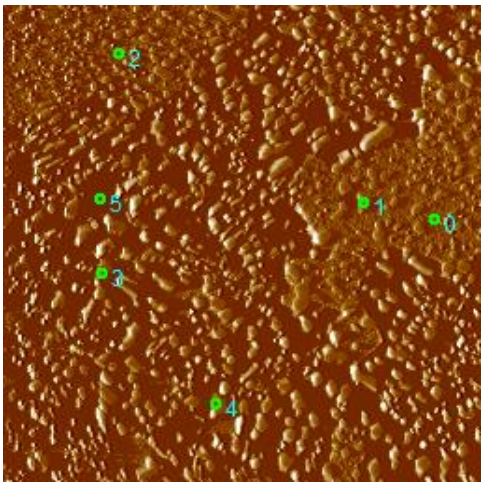

Fig. 3 Placement of indents on SPM scan steel 90MnCrV8

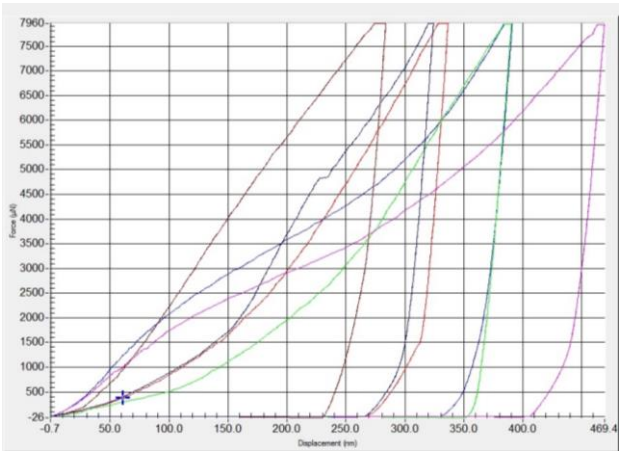

Fig. 4 Particular curves obtained from indents on SPM scan of steel 90MnCrV8.

Table 3 Local mechanical characteristics of steel 90MnCrV8 structure components.

Position	Nanohardness H [GPa]	Reduced modulus of elasticity E_r [GPa]	Phase (expected)
0	3,17	204,08	Ferrite
1	2,32	168,21	Ferrite
2	2,34	161,59	Ferrite
3	1,90	129,09	Perlite (Ferrite com.)
4	4,53	243,95	Perlite (cem. com.)
5	4,42	218,66	Perlite (cem. com.)

3.1 Calculation of Young modulus elasticity of the phase

Modulus of elasticity in overall talks about the ability of the material to resist elastic deformation under the influence of tension and is defined as a fraction of tension and deformation. From the analysis of indentation data, it is possible to obtain the modulus of elasticity from an angle of tangent the same way as using the determination of indentation toughness according to Oliver and Pharr [9] using the following relation (1).

The calculation of Young modulus of phase elasticity E_s for researched tool steel 90MnCrV8 was realized according to the equation 1.

$$E_s = (1 - \upsilon_s{}^2)/(\frac{1}{E_r} - \frac{1-\upsilon_i{}^2}{E_i}) \qquad (1)$$

where E_i is modulus of testing tip and υ_s and υ_i are Poisson constants for the sample and testing tip Berkovich. Values are E_i = 1141 GPa, υ_i = 0,07 and υ_s = 0,29.

Values of reduced Young modulus of elasticity E_r and Young modulus of phase elasticity E_s of tool steel 90MnCrV8 are written in table 5 and the comparision is shown in Fig. 5.

Tab. 4 Phases of steel and their nanohardness H [GPa] and reduced Young modulus of elasticity E_r [GPa]

Steel	Phase					
	Ferrite		Perlite (component of cementite)		Perlite (component of ferrite)	
	H	E_r	*H*	E_r	*H*	E_r
90MnCrV8	2,61	177,96	4,48	231,31	1,9	129,09

Tab. 5 Reduced Young modulus of elasticity E_r [GPa] and Young modulus of phase elasticity E_s [GPa].

Steel	Phase					
	Ferrite		Perlite (component of cementite)		Perlite (component of ferrite)	
	E_s	E_r	E_s	E_r	E_s	E_r
90MnCrV8	192,94	177,96	265,39	231,31	133,23	129,09

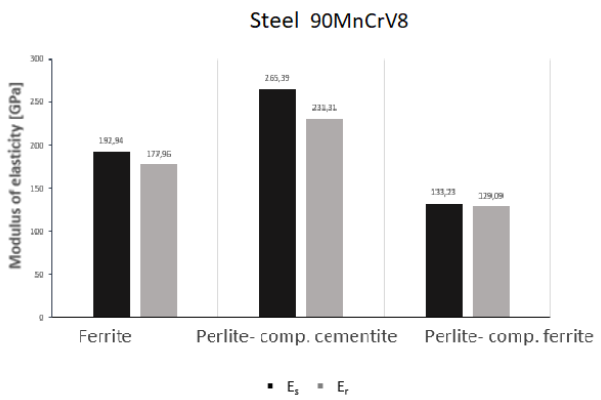

Fig. 5 Comparison of modules of elasticity phases of steel 90MnCrV8

4 Conclusion

The main goal of realized experiment was to test nanohardness of basic structural components ferrite and perlite of tool steel 90MnCrV8 using the method of quasi-static nanoindentation. The reason for choosing this particular kind of steel was the fact, that there are high demands on the material in industry, such as high strength, toughness, wear resistance, temperature stability and other mechanical qualities based on hardness.

The values of nanohardness of particular structural phases and reduced Young modulus of elasticity were detected using the testing device named Hysitron TI 950 Triboindenter, with Triboscan evaluation software. The Berkovich type was used as a test tip. Reduced modulus of elasticity was then used for the calculation of the modulus of elasticity of specific structural phase components according to the equation (1). Results of calculations are tabularly seen in the graph n. 1. From the mutual comparison it is visible that values of elasticity modulus in particular phases are higher by 4% up to 13% than their reduced elasticity modulus assuming the above-mentioned values of the Berkovich geometry test indentation tip used in the experimental process.

Using the experimental method of quasi-static nanoindentation and using the selection of test positions which correspond to particular phases, it is possible to determine mechanical characteristics of particular phases in explored areas on the nanolevel. This fact subsequently gives room for further re-

search of the basic material, for example by creating matrices of individual indents, where it is possible to determine the percentage of individual phases in the investigated microstructures.

5 Acknowledgement

This publication was created within the implementation of the project „Development and support of research and development activities of Center for Quality Testing and Diagnostics of Materials in the areas of specialization RIS3 SK", ITMS2014+:313011W442, supported from Operational program of Integrated Infrastructure and European Regional Development Fund.

References

[1] Fischer-Cripps, A.C.: *Nanoindentation* (3rd edition), Springer Science, 2013. New York, USA, 279 s. ISBN-13: 9781461429609.

[2] Martinec, Ľ, Šimkovič, M.: *Náuka o materiáloch,* 1. Vydanie STU Bratislava, 1997. 233 s. ISBN 80-227-1008-3.

[3] Ptáček, L. et al.: *Náuka o materiálu II.* 1. Vydání), CERM Brno, 2002, 392 s. ISBN 80-7204-248-3.
Mondolfo, L. F., Schmidt, T., Arribas, I., et al.: *Advanced photogrammetric for robust deformation and strain measurement*, Proceedings of the 2002 SEM Annual Conference, Milwaukee, Wisconsin USA, 2002, p. 1-6.

[4] Norma STN 41 9312 *Materiálový list ocele 19 312,* 90MnCrV8.

[5] Deng, G. Y. et al.: *Characterizing deformation behaviour of an oxodozed high speed steel: Effect of nanoindentation depth, friction and oxide scale porosity,* International Journal of Mechanical Sciences, Vol. 155, (2019), p. 267-285.

[6] Nguen, V. L. et al.: *Nano-mechanical behavior of H13 tool steel fabricated by a selective laser melting method,* Metallurgical and material transactions A: Physical metallurgy and materials science, Vol. 50, Issue 2, (2019), p. 523-528.

[7] M. Rieth et al.: EUROFER 97 Tensile, Charpy, creep and structural tests, FZKA 6911, 2003.

[8] Moreno, A. R., Hähner, P.: *Indentation size of ferritic/martensitic steels: A comparative experimental and modeling study,* Materials and Design, Vol. 145 (2018), p. 168 – 180.

[9] Pharr G. M., Oliver W. C., Brotzen F.R.: *On the generality of the relationship between contact stiffness, contact area, and elastic modulus during indentation,* J. Mater. Res. 7 (1992) 613-617.

HIGH TEMPERATURE DEFORMATION RESISTANCE OF BCT STEEL

Rudolf Pernis[1*] – Milan Škrobian[2]

[1]Farmet s.r.o., Robotnícka 4334, 017 01 Považská Bystrica, Slovakia
[2]INOVAL – Slovenská akadémia vied, Priemyselná 525, 965 01 Žiar nad Hronom, Slovakia

ARTICLE INFO

***Article history*:**
Received: 15.03.2021
Received in revised form: 23.4.2021
Accepted: 3.5.2021

Keywords:
high temperature deformation,
compression test
boron steel
peak stress
deformation curve

Abstract:

The knowledge of deformation resistance is needed for simulation of forming processes at higher and high temperatures. A static tensile test does not give an answer how deformation resistance depends on deformation rate. Deformation resistance was measured using dilatometer DIL805A/D equipped with hydraulic unit. This setting allows compression tests during high-temperature material forming. Material forming can be carried out under controlled conditions. Such conditions are deformation level, deformation temperature and deformation rate. Deformation rate can be set between 0.001 and 20 s^{-1}. Temperature can be kept from ambient temperature up to 1500 °C. BCT steel was used for experiments. Deformation resistance was measured for experimental matrix of 5 deformation temperatures by 5 deformation rates. The experimental results were described by a proposed mathematical model where deformation curve is a function of deformation. In addition, an equation is proposed for calculation of deformation resistance as a function of two variables: degree of deformation and temperature of deformation. Prediction of deformation curves was done using above equation for the temperatures of (850, 950, 1050, 1150) °C. A visualization of curves for various temperatures is shown in a paper.

1 Introduction

A dilatometer DIL805A/D [1] is designed mainly for measurement of phase transformations [2] and CCT diagrams [3, 4] (CCT – Continuous Cooling Transformation). It is equipped with hydraulic unit that allows compression deformation. A deformation mode allows forming of material under controlled conditions such as degree of deformation, deformation temperature and rate of deformation. A true compression stress is calculated from true deformation force and true sample cross-section. This relationship allows to construct true strain-true stress curves that are known as deformation curves [5, 6]. A curve deformation stress as a function of deformation is shown in Fig. 1. The Garofalo empirical equation [7, 8] is used to describe a high temperature deformation, which describes a strain rate in relation to a flow stress and an absolute temperature

* Corresponding author. Tel.: *00421-42-4 330 650*
E-mail address: pernis@seznam.cz

$$\acute{\varphi} = A \cdot \left[sinh\left(\alpha \cdot \sigma_p\right)\right]^n \cdot exp\left(-\frac{Q}{RT}\right) \quad (1)$$

where

$\acute{\varphi}$[s^{-1}] – strain rate
T [K] – absolute temperature
σ_p [MPa] – flow stress (peak stress)
Q [J.mol^{-1}] – activation energy of deformation
R [J.K^{-1}.mol^{-1}] – universal gas constant
n [–] – material constant
A [s^{-1}] – material constant
α [MPa^{-1}] – material constant

Calculation of constants Q, n, C and α in equation (1) using experimental data is described in details in [9]. Experimental data used are as follows: peak stress, peak deformation, deformation rate and temperature of deformation. However, equation (1) does not contain deformation variable φ. Therefore constants Q, n, C and α in equation (1) are expressed as polynomials containing variable φ.

$$Q = B_0 + B_1\varphi + B_2\varphi^2 + B_3\varphi^3 + \cdots + B_m\varphi^m \quad (2)$$

$$n = C_0 + C_1\varphi + C_2\varphi^2 + C_3\varphi^3 + \cdots + C_m\varphi^m \quad (3)$$

$$Ln\ A = D_0 + D_1\varphi + D_2\varphi^2 + D_3\varphi^3 + \cdots + D_m\varphi^m \quad (4)$$

$$\alpha = E_0 + E_1\varphi + E_2\varphi^2 + E_3\varphi^3 + \cdots + E_m\varphi^m \quad (5)$$

Degree of polynomial m in equations (2-5) takes values from 5 to 9. Value m=5 was chosen in [10]. In order to increase precision of approximation even higher degree of polynomial is often used, e.g. m=6 was used [11,12]. Even more, degree m=9 was used in [13] and 40 regression coefficients were calculated. Non-linear regression was needed to do so. Simpler empirical equation was used in this work that allows describe deformation curves while calculation of regression coefficients is easier.

2 Description of experiment

The measurements of deformation resistance were carried out using dilatometer DIL805A/D. The samples were in a form of cylinder with diameter of 5 mm and height of 10 mm. The temperatures of (800, 900, 1000, 1100, 1200) °C were used in the experiments. A deformation can be set in interval 0.05 up to 1.2. Deformation rate from 0.001 up to 20 s^{-1} can be used. The following values were chosen in experiments (0.001, 0.01, 0.1, 1, 10) s^{-1}. Steel with addition of boron knows as BCT steel was used for measurement of deformation resistance. This kind of steel is not standardized and belongs to group of special steels. Its chemical composition is shown in Table 1.

Table 1 Chemical composition of BCT steel (wt.%)

Element	Content
C	0.12
Mn	1.60
Si	0.45
P	0.013
Cr	0.04
V	0.002
Mo	0.02
Ni	0.07
Nb	0.04
Al	0.03
S	0.005
W	0.01
B	0.002
Fe	balance

A computer controlled equipment records deformation resistance of each test into individual file. Data are then exported for subsequent graphical and numerical treatment. An example of measured curves for deformation rate of 0.1 s^{-1} is shown in Fig. 1.

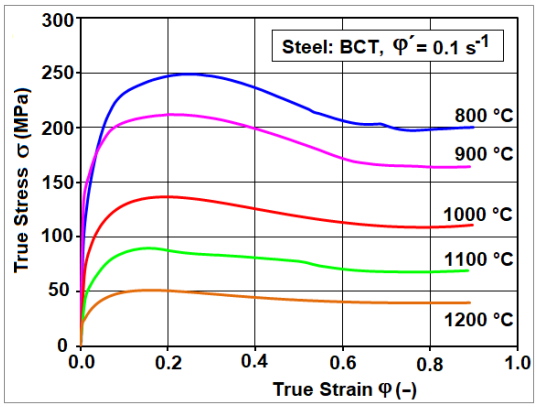

Fig. 1 Deformation resistance curves

3 Mathematical model of deformation curve

Mathematical model – equation describing deformation curve as function of deformation at constant deformation rate and deformation

temperature should fulfill the following requirements:

- passing through origin of coordinates, i.e. [0,0] point
- it has an extreme (maximum) at peak stress
- it has an inflexion point and continues to steady state without oscillations
- easy evaluation of regression coefficients that does not require use of non-linear regression

Deformation curve shown in Fig. 2 passes through origin of coordinate system following linear trend. Curve is subsequently growing to maximum at stress peak. It is lowering in third part due to a softening [14, 15] followed by steady state [16, 17].

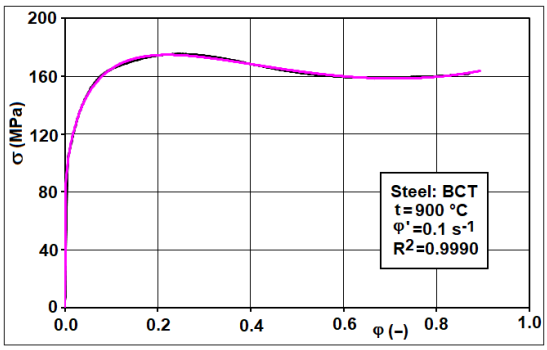

Fig. 2 Deformation curve

Deformation resistance as a function of deformation is recorded during hot compression test under controlled conditions, i.e. sample geometry, temperature and deformation rate [18, 19]. Based on an observed deformation curve the following equation is proposed

$$\sigma = \sigma_0 \varphi^{a_0} e^{F(\varphi)} \tag{6}$$

where

σ [MPa] – deformation resistance
σ_0 [MPa] – material constant
φ [–] – logarithmic deformation
a_0 [–] –constant
$F(\varphi)$ –appropriately selected function

The following polynomial equation is suitable as an *F*–function, i.e. function describing logarithmic deformation [20]

$$F(\varphi) = a_1\varphi^{-3} + a_2\varphi^{-2} + a_3\varphi^{-1} + a_4\varphi + \\ + a_5\varphi^2 + a_6\varphi^3 \tag{7}$$

Comparison of measured (black) and calculated (violet) curves is shown in Fig. 2. Regression coefficients were calculated using generalized linear regression. They are listed in Table 2. It should be noted that material constant σ_0 does not represent peak stress. Correlation coefficient R^2 has a value of 0.999.

Table 2 Regression coefficients for equation (6), unit σ_0 is (MPa)

Coefficient	Value
σ_0	3.526 257 E+02
a_0	2.741 264 E–01
a_1	-2.614 953 E–10
a_2	-8.274 522 E–07
a_3	1.027 312 E–03
a_4	-1.409 801 E+00
a_5	3.020 686 E–01
a_6	3.936 252 E–01

4 Mathematical model of deformation resistance for two variables

Equation (6) extended on variable of deformation temperature is used to describe deformation resistance depending on deformation and temperature [21]. Constant a_0 is replaced by an appropriate function of temperature *E(t)* and *F*–function is also extended to reflect temperature dependence. Thus equation (6) can be written as

$$\sigma = \sigma_0 \varphi^{E(t)} e^{F(\varphi,t)} \tag{8}$$

where

σ [MPa] – deformation resistance
σ_0 [MPa] – material constant
φ [–] – logarithmic deformation
t [°C] – deformation temperature
$E(t)$ – appropriately selected temperature function
$F(\varphi,t)$ – appropriately selected deformation and temperature function

As *E*–function an equation (9) is suitable

$$E(t) = a_0 + a_1 t + a_2 t^2 + a_3 t^3 \quad (9)$$

Dimensions of constants a_0, a_1, a_2 and a_3 are such as to keep function $E(t)$ dimensionless. Next, F–function is extended to reflect new variable – deformation temperature, as shown in equation (10) constants $ln\sigma_0$, a_1-a_3, b_1-b_{15} are shown in Table 3 in semi-logarithmic form. Resulting graph is shown in

$$F(\varphi, t) = b_1\varphi^{-3} + b_2\varphi^{-2} + b_3\varphi^{-1} + b_4\varphi + b_5\varphi^2 + b_6\varphi^3 + b_7 t + b_8 t^2 + b_9 t^3 + \\ +(b_{10}\varphi^{-3} + b_{11}\varphi^{-2} + b_{12}\varphi^{-1} + b_{13}\varphi + +b_{14}\varphi^2 + b_{15}\varphi^3)t^{-1} \quad (10)$$

Table 3 Regression coefficients for equation (8)

Coefficient	Value
$ln\ \sigma_0$	-3.753 950 E+02
a_0	3.275 665 E+03
a_1	-1.429 949 E+03
a_2	2.078 764 E+02
a_3	-1.006 274 E+01
b_1	6.009 430 E–10
b_2	-1.817 740 E–05
b_3	8.812 151 E–02
b_4	-9.254 156 E+01
b_5	1.264 784 E+02
b_6	-6.274 135 E+01
b_7	1.134 173 E+02
b_8	-8.792 280 E+00
b_9	5.240 818 E–02
b_{10}	-4.147 687 E–09
b_{11}	1.251 116 E–04
b_{12}	-6.124 560 E–01
b_{13}	6.267 982 E+02
b_{14}	-8.728 506 E+02
b_{15}	4.379 170 E+02

Dimensions of constants b_1 – b_{15} are such as to keep equation (10) dimensionless. Equations (8), (9) and (10) are used to visualize agreement between measured and calculated values of BCT steel for temperatures of (800, 900, 1000, 1100, 1200) °C at constant deformation rate of φ'=0.1 s^{-1}. Regression Fig. 3. Black curves are measured values of deformation resistance, the violet ones are calculated from equation (8). Prediction of deformation curves (blue in Fig. 3), i.e. their calculation from equation (10) was made for temperatures of (850, 950, 1050, 1150) °C. It was recognized during calculations that use of logarithmic temperature instead of direct temperature is more suitable leading to better agreement between observed and calculated values with increase of correlation coefficient.

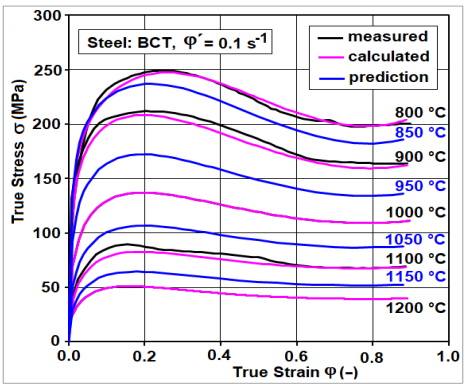

Fig. 3 Deformation resistance curves and their prediction

5 Discussion of results

Garofalo semi-empirical equation [7] was used long time to describe high-temperature deformation resistance. Its disadvantage is that it describes peak stress as a function of temperature and deformation rate [22, 23]. Various empirical equations were suggested in order to overcome this problem [24]. The constants in Garofalo equation were replaced by polynomial functions where variable is deformation. Number of regression constants in such case is from 24 up to 40 [10–13]. Mathematical model for calculation of deformation resistance for one variable deformation, equation (6) as well as for two variables – deformation, deformation temperature, equation (8) – is proposed. Using this model it is possible to calculated deformation curves for the temperatures that were not measured – see Fig. 3, blue curves.

6 Conclusion

A new mathematical model describing deformation curves allow calculate deformation resistance for two independent variables that are deformation and deformation temperature. Increase of precision of simulation of forming processes such as FEM (finite elements method) is possible by using this model. All proposed equations for calculation of deformation resistance are possible to be transformed into linear relationship via their logarithmic form. It allows use

of linear regression operations instead of complicated non-linear regression. Such approach makes it easier to treat experimental data. No specific software is needed – common software like Excel can be used to perform all calculation and graph drawing. Multi-linear regression, that is included in Excel, can be used or it can be programmed using Visual Basic that is part of MSO package.

7 Acknowledgement

Authors would like to express their thanks to prof. Ing. Tibor Kvačkaj, CSc. from Technical University of Košice who provided us with samples of BCT steel used in compression tests.

References

[1] DILATOMETRY, *TA Instruments*, Hüllhorst, Germany, 2013.

[2] Barényi, I., Krbaťa, M., Majerík, J., Mikušová, I.: *Effect of deformation parameters on microstructure evolution and properties of 33NiCrMoV15 steel*. IOP Conference Series: Materials Science and Engineering. 2020, 776, p. 1-7.

[3] Krbaťa, M., Majerík, J., Barényi, I., Eckert, M.: *Experimental determination of continuous cooling transformation diagram for high strength steel OCHN3MFA*. IOP Conference Series: Materials Science and Engineering. 2020, 776, p. 1-14.

[4] Eckert, M., Krbata, M., Barenyi, I., Majerik, J., Dubec, A., Bokes, M.: Materials, Vol. 13 (2020), 5585, p. 1–21.

[5] Mielnik, E. M.: *Metalworking Science and Engineering*, McGraw-Hill, New York, 1991.

[6] Pernis, R., Kasala, J., Bořuta J.: *High temperature plastic deformation of CuZn30 brass – calculation of the activation energy*, KOVOVE MATERIALY – METALLIC MATERIALS, Vol. 48 (2010), Issue 1, p 41-46.

[7] Garofalo, P.: Transaction of the Metallurgical Society of AIME, Vol. 227, April 1963, p. 351–355.

[8] Sellars, C. M., Tegart, W. J.: International Metallurgical Review, Vol. 17, (1972), p. 1–24.

[9] Pernis, R.: Acta Metallurgica Slovaca, Vol. 23, (2017), Issue 4, p. 319–329.

[10] Krbaťa, M., Eckert, M., Križan, D., Barényi, I., Mikušová I.: Metals. Vol. 9, (2019), Issue 10, p. 1-17.

[11] Quan, G., Pan, J., Wang, X.: Applied Sciences. Vol. 6, (2016), Issue 3.

[12] Wei, G., Peng, X., Hadadzadeh, A., Xie, W., Yang, Y., Wells, M. A.: Mechanics of Materials. 89 (2015), 241–253.

[13] Quan, G., Yu, C., Liu, Y., Xia, Y.: The Scientific World Journal, Vol. (2014), p. 12.

[14] Krbata, M.: *Influence of temperature deformation on peak stress steel 1.2379*. Proceedings of the International Scientific Conference EQUIPMENT AND TECHNIQUE OF LAND FORCES 2018. Liptovský Mikuláš: Academy of the A. F. of General M. R. Štefánik, 2018. p. 57-62, CD ROM.

[15] Drastík, F., Elfmark, J.: *Plastometers and formability of metals* (Plastometry a tvářitelnost kovů). Praha: SNTL, 1977. 392 p.

[16] Krbata, M., Mikuš, P.: *Deformation resistance of tool steel 19 573 when changing the deformation rate*. Proceedings of the International Scientific Conference EaTLF 2018. Liptovský Mikuláš: AAF gen. M. R. Štefánik. ISBN 978-80-8040-571-7. p. 88-93, CD ROM.

[17] Talbert, S. H., Avitzur, B.: *Elementary Mechanics of Plastic Flow in Metal Forming*. John Wiley & Sons, NY, 1996.

[18] Spigarelli, S., Cabibbo, N., Evangelista, E., Bidulská, J.: Journal of Materials Science, Vol. 38, (2003), Issue 1, p. 81–88.

[19] Kubina, T., Kliber, J., Kuncicka, L., Berkova, M., Horsinka, J., Boruta, J.: *Metalurgija*, Vol.52, (2013), p. 325–328.

[20] Pernis, R.: *Construction of a mathematical model of the deformation curve – I and II*. In: Vedecké práce a štúdie za rok 2017. Trenčín: TnUAD, FŠT, 2017. CD-ROM. ISBN 978-80-8075-798-4. p. 171-212.

[21] Pernis, R.: *Influence of temperature on peak stress* (Vplyv teploty na pikové napätie). In: Transfer 2017, Trenčín: TnUAD. 2017, 4 p., CD ROM. ISBN 978-80-8075-7787-8.

[22] Bidulská, J., Pokorný, I., Kvačkaj, T., Bidulský, R., Actis–Grande, M.: High Temperature Materials and Processes, Vol. 28, (2009), Issue 5, p 315–321.

[23] Kvačkaj, T., Kováčová, A., Kočiško, R.: Acta Physica Polonica A, Vol. 128, (2015), Issue 4, p. 689–692.

[24] Kvačkaj, T., Pokorný, I. Vlado, M.: Acta Metallurgica Slovaca, Vol. 6, (2000), Issue 3, p. 242–2.

University Review, Vol. 15, Issue 1, 56-62, 2021.

UNIVERSITY REVIEW

MATERIALS FOR INJECTION MOLDING MACHINES SCREWS FOR PROCESSING OF PLASTIC MATERIALS UP TO 30% OF GLASS FIBERS PRODUCED BY POWDER METALURGY

Juraj Majerský[1*] – Jozef Majerík[1] – Igor Barényi[1] – Henrieta Chochlíková[1]

[1]Department of Engineering Technologies and Materials, Faculty of Special Technology, Alexander Dubcek Univwersity of Trenčín, Ku kyselke 469, 911 06, Trencin, Slovakia

ARTICLE INFO

***Article history*:**
Received: 15.3.2021
Received in revised form: 23.4.2021
Accepted: 3.5.2021

Keywords:
mold
powder metallurgy
screws
glass fibers

Abstract:

In the article there are investigated materials, which are used for production of the injection molding machine´s screws used for processing of plastic materials with content of glass fibers up to 30%. These materials are produced by the powder metallurgy – by the HIP (Hot Isostatic Pressing). Structures of materials are analysed by optical microscope and compared with conventionally produced materials. Based on literature sources there are specified conditions of further processing of materials or rather conditions which are recommended for the test of these materials nitridation.

1 Introduction

During the 20th century man developed a new, cheap and easily workable material. Plastic. Plastic materials started expanding from the interwar period. Reason of its more often use was the fast development, price and properties. Step by step plastics started to push away wood, glass and later, the metal from some application fields. Intense evolution brought also its processing technology development. Widest processing technology is injection molding where melted plastic from plastification unit is injected into the mold under high pressure. Plastic solidifies in the mold and its dimensions are fixed partially. Final product is removed from the tool. Within the scope of development of plastics, its properties were elaborated. Toughness, rigidity, resistance against different substances or elasticity as the thermoplastic elastomers were in the focus of developers. Adjustment of the material content and various kinds of bindings had different influence on the injection molding screws – sticking on the screw, its corrosion up to abrasive wear by plastic material. By this reason producers of injection molding machines had to concentrate on the development of the screws – its geometry, but also the material of the screw. And therefore, step by step they got to some basic sorts of materials which are used for different groups of plastics. Basic differentiation of these materials is following:

1. Screws for using with plastic materials without glass fibers and fillers
2. Screws for using with plastic materials with fillers and glass fibers up to 30%
3. Screws for using with plastic materials with fillers and glass fibers up to 50%
4. Screws for using with special plastics (technical, transparent, etc.)

Most used category of the screws is those for using with plastic with glass fibers up to 30%. These screws are the most universal and shows usually best corrosion resistance. Most of plastic, if the higher toughness demanded, are used with the glass fibers up to 30%. Over this line there are used materials for special purposes and their representation in

[*] Corresponding author. Tel.: +421327400242
E-mail address: juraj.majersky@tnuni.sk

production is considerably lower. One of the reasons is the price of material used for their production, very expensive technological processes of machining, necessity of special tools using and etc.
Very interesting is category with 30% of glass fibers. Screws for most used diameters are produced by powder metallurgy. Among such materials there are powder metallurgy steels M390 and M398 Microclean© from Austrian company named Böhler.

Plastic material category / Screw diameter	Basic plastic materials without fillers and additives	Plastic materials with fillers and additives with glass fibers up to 30%	Plastic materials with fillers and additives with glass fibers up to 50%	Special applications: Chrome Nitride	Special applications: Titan Nitride
Screws up to diameter 65 mm	Nitriding steel, nitrided	Powder metallurgical steel, hardened and tempered	Full tungsten carbide armoring	Plastic mod steel, CrN-coated	Plastic mold steel - TiN coated
Screws over diameter 65	Quenched and tempered steel with flight armoring, nitrided	Quenched and tempered steel with flight armoring, nitrided	Full tungsten carbide armoring	Quenched and tempered steel with flight armoring and CrN coating	Quenched and tempered steel with flight armoring and TiN coating

Table 1 Materials for injection molding screws [1]

2 Experimental details

Powder metallurgy stainless steels M390 and M398 belong to categories of materials which properties supersede commonly produced steels. It is by the reason that HIP method is able to produce materials which are not possible to produce by standard approach otherwise during the cool down phase there would segregate single components. These powders steels are produced at approx. 06 - 0.8 * temperature of solidus [10] and high pressure, what allows the material to join into a compact pattern but it does not allow to change a position of single components. It is necessary to pay high attention at a thermal and thermo-chemical processing of these materials to avoid enormous growth of the grain and detracting of surface layer for the components which have important assignment (for example – during nitridation there comes a combination of Nitrogen and Chrome and creation of Chrome nitrides what decreases corrosion resistance of material.)

2.1 Böhler M390 Microclean© powder metalurgy steel and its properties

Material M390 has following composition and properties:
Steel composition:
1.90 % C, 0.70 % Si, 0.30 % Mn, 20% Cr, 1% Mo, 4% V, 0.60 % W.
Material properties:
Density at 20 °C – 7.54 kg/dm3
Thermal conductivity – 16.5 W/(m.K)
Thermal expansion between 20 °C and
20 °C - 100 °C - 10.4 x 10-6 m/(m.K)
20 °C - 200 °C - 10.7 x 10-6 m/(m.K)
20 °C - 300 °C - 11.0 x 10-6 m/(m.K)
20 °C - 400 °C - 11.2 x 10-6 m/(m.K)
20 °C - 500 °C - 11.6 x 10-6 m/(m.K)

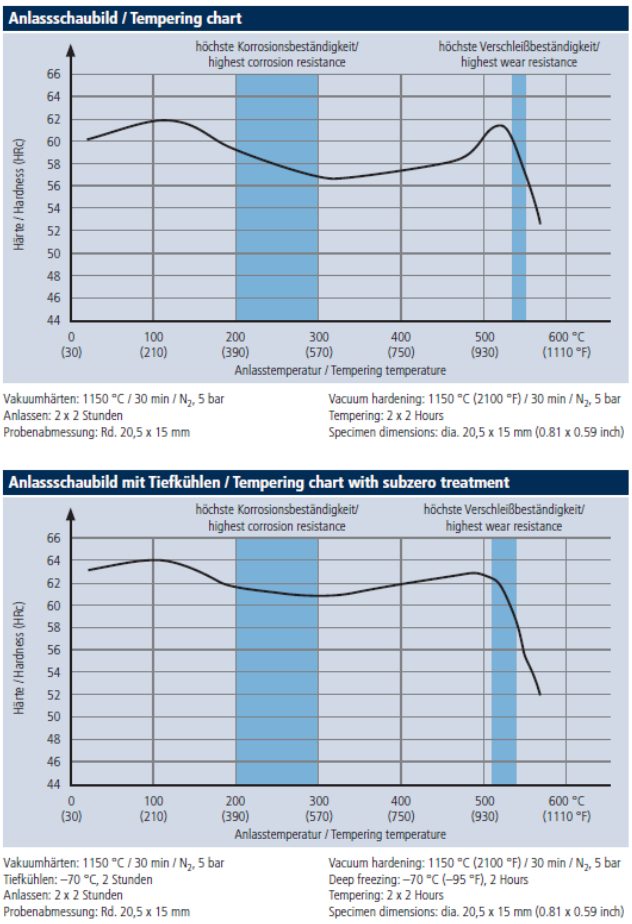

*Fig. 1 Tempering diagram –M390 steel – vacuum hardening at 1150 °C / 30 min/N2, 5 bar, tempering 2*2 hours, cross section of specimen: ø 20.5 * 15 mm [2]*

Material is delivered with 280 HB hardness.

Thermal processing:
Hardening is suitable at temperatures 1100 °C – 1180 °C. After through-heating of whole cross section, Holding time 20-30 minutes for hardening temperature 1100-1150 °C, 5-10 minutes at a hardening temperature 1180 °C. Cooling in the oil / N2. For tempering for highest corrosion resistance a sub-zero treatment for transformation of retained austenite, slow heating for tempering temperature – furnace time 1 hour for each 20 mm of material wall thickness, but minimum 2 hours at temperatures 200 – 300 °C is necessary. Producer recommends tempering of the material min. two times.
If it is necessary to have material tempered for achieving highest abrasion resistance the material must be cooled down below 0 °C for elimination of retained austenite and its transformation to martensite immediately after hardening. It is important also to take care of the shape of the tool after the hardening because there is a risk of the stress cracking. If the material is freezed the hardening at temperature 1150 °C and more is demanded. Slow heating is required for tempering – 1 hour for each 20 mm of material thickness but min. 2 hours. Tempering is recommended to realize min. 3 times and the third tempering is important for achieving complete transformation of retained austenite. Temperature is chosen 20 °C over secondary hardness [2].

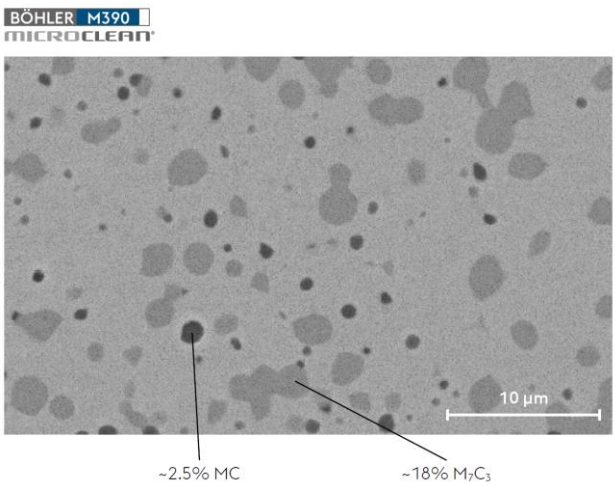

Fig. 2 M390 powder metallurgy steel (PMS)Microstructure [3]

2.2 Böhler M398 Microclean© powder metalurgy steel and its properties

Material M398 has following composition and properties:

Composition of the steel: 2.7% C, 0.5% Si, 0.5% Mn, 20% Cr, 1% Mo, 7.2% V, 0.7% W
Density at 20 °C – 7.46 kg/dm3
Thermal conductivity – 15.2 W/(m.K)
Thermal expansion between 20 °C and
20 °C - 100 °C - 10.4 x 10-6 m/(m.K)
20 °C - 200 °C - 10.6 x 10-6 m/(m.K)
20 °C - 300 °C - 10.9 x 10-6 m/(m.K)
20 °C - 400 °C - 11.2 x 10-6 m/(m.K)
20 °C - 500 °C - 11.5 x 10-6 m/(m.K)
Material is delivered with 330 HB hardness.
Thermal processing:
Hardening is suitable at temperatures 1120 °C – 1180 °C. After through-heating of whole cross section, Holding time 20-30 minutes at hardening temperature 1120-1150 °C, 5-10 minutes at hardening temperature 1180 °C. Cooling in the oil / N2.
During the tempering for achieving of maximum corrosion resistance sub-zero treatment for transformation of retained austenite, then slow heating to tempering temperature, furnace time 1 hour for each 20 mm of wall thickness but minimum 2 hours at temperatures 200 – 300 °C is necessary. Producer of material recommends to repeat tempering at least two times.

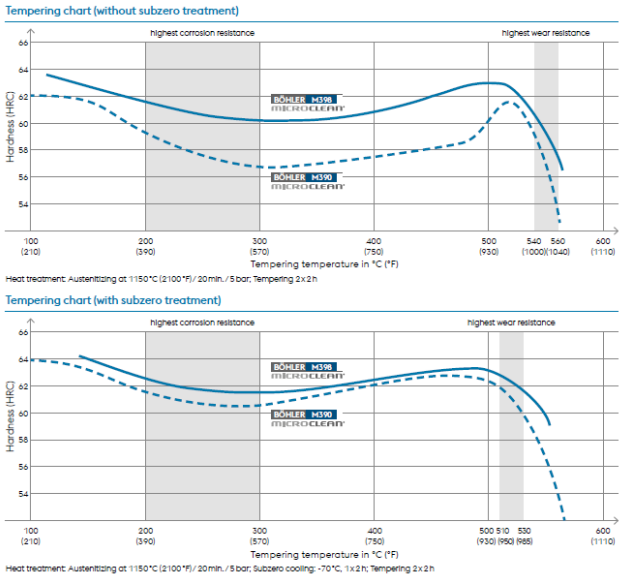

Fig. 3 Tempering diagram of M 398 steel [3]

Tempering for achieving of highest abrasion resistance also requires subzero treatment of material to eliminate retained austenite and its transformation to martensite immediately after hardening. It is necessary to consider the shape of the tool, because there is a risk of stress cracking. In case that material is freezed it is important hardening at tempera-

tures 1150 °C or more. For tempering slow heating is chosen to tempering temperature, holding time 1 hour for each 20 mm of wall thickness, but min. 2 hours. Tempering is recommended to repeat min 3 times and the third is necessary to achieving complete transformation of retained austenite. Temperature is chosen 20 °C over the max. secondary hardness [3].

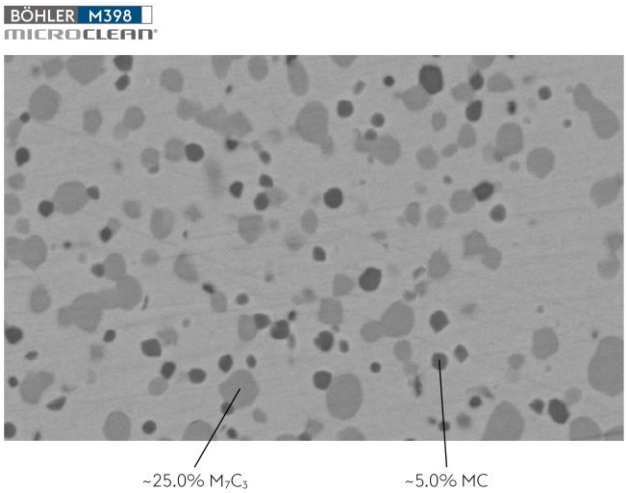

Fig. 4 M398 PMS Microstructure [3]

2.3 Optical microscopy

For analysis of materials was as first chosen optical microscopy. Samples were investigated by optical microscope NEOPHOT 32, linked with attached digital camera Canon from which the photos were transferred to connected computer.

Basic etching for highlighting of material structure was done by mixture of hydrogen nitrate (1-5 ml) and ethyl alcohol (95 ml), well known as a Nital. Samples were etched in Nital for 30 seconds. Then was washed by distilled water, alcohol and after that dried by hot air [9]. Due to excellent anticorrosion properties of materials the structure etched by Nital was nearly impossible to highlight the material structure.

On the surface (Fig.5) there was visible only mixture of darker and lighter grey blotches without any sharp differentiation. The deeper analysis of surface was not possible.

Due to these properties a mixture of acid and glycerine as an etcher had to be prepared:

10 ml HNO_3 + 20 ml HCl + 20 ml glycerine + 10 ml H_2O_2.

Samples were etched for 10 seconds, followed by washing with distilled water, alcohol and dried by hot air to remove the rest of liquids from the surface of sample.

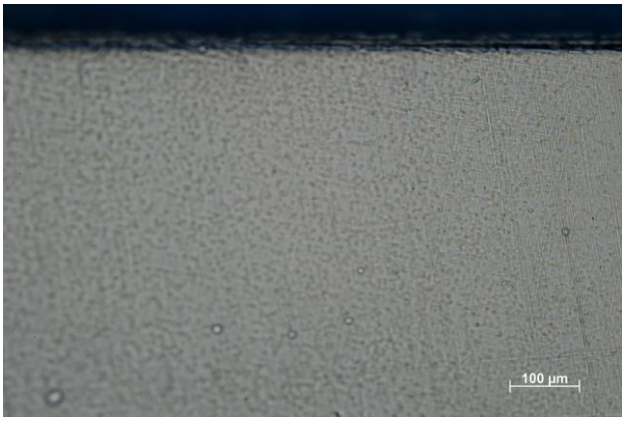

Fig. 5 Material M390 structure etched by Nital

New mixture helped to highlight the structure to state when it should be investigated under the optical microscope. Even the structure was visible, edges of structure was sharp, the analysis was problematic because of smooth material structure. Due to a structure smoothness the magnification 1000 x was chosen. On the sample of M390 (Fig. 6) we can see structure consisting of light and dark dots. The light dots seem as the base material, dark dots are in most probably way carbides of Chrome and other components. Deeper analysis from optical microscope photography is not possible.

On the sample of M398 (Fig. 7) there is visible similar structure as on M390 – dark and light dots. Even the material structure is alike there is visible difference especially in the range of dark dots. M398 has higher volume of dark dots what corresponds with its partially different composition, mostly represented by carbides of Chrome and other components based on higher Carbon content – 1.9% M390 / 2.7% M398.

Comparing the material structure from brochures (Fig. 2, Fig. 4) with material structures obtained by optical microscopy (Fig. 6, Fig. 7) shows that our assumption of the material structure of both materials are right, even that we are not able to look closer.

As a simple matching of structures of powder metallurgy materials and standard way produced material there is photography of grey cast iron structure (Fig. 8). With comparable magnification the structures are completely different in way of components formation visibility. While in PMS steels there are visible only light and dark dots, the formations of grey

cast iron components are clearly visible – basic material and formation of Carbon. This structure was added for better perception of the smoothness of

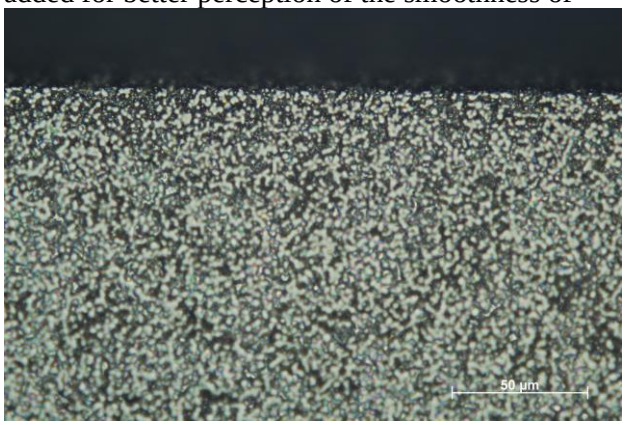

Fig. 7 Structure of Böhler M398 Microclean® material etched by glycerine mixture

Fig. 8 Structure of grey cast iron for comparing with the structure of M390 a M398

2.4 Wear and chemical resistance of M390 and M398 steels

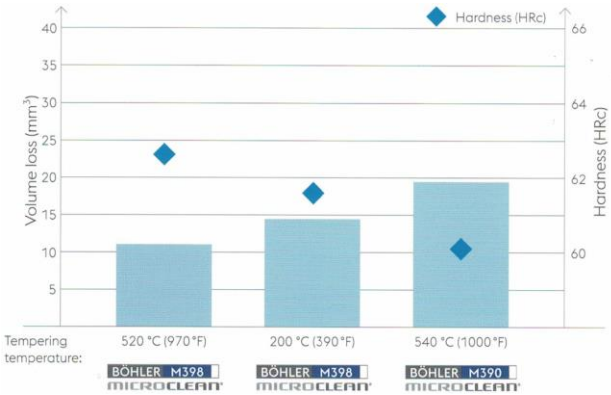

Fig. 9 Hardness and volume loss of M390 and M398 from the tests of material producer [3]

Both materials have much better anticorrosion and anti-abrasive properties in comparison with standard steels, which are the results of its process of production and content. In regard the M398 is a new material with development based on experiences with M390, its properties are in abrasive field increased so much that overcomes M390.

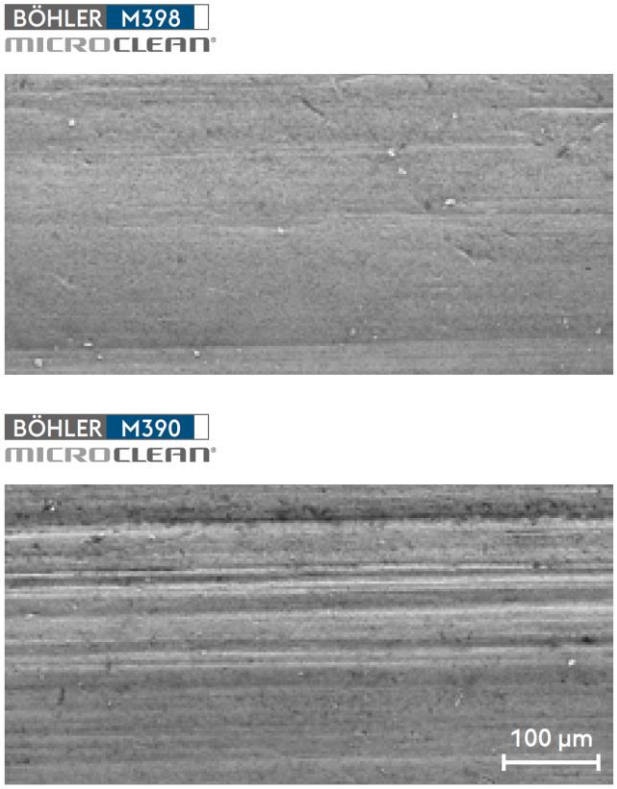

Fig. 10 Wear of materials M390 and M398 from the test at producer - company Böhler [3]

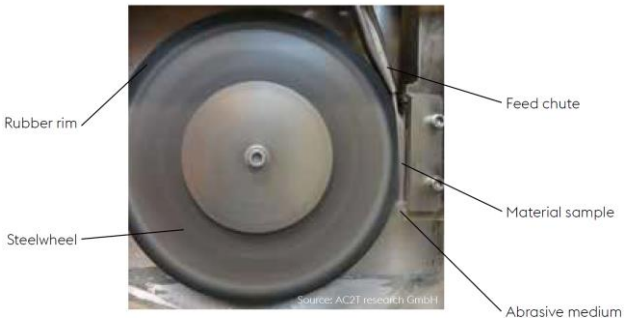

Fig. 11 Device for testing of abrasive wear: Test load 130 N, Sand grain size 100-400 µm, Feed rate 340 g/min, Sliding distance 4309 m [3]

From the producers data it is visible that M398 has much more better resistance against abrasive wear than M390, it is harder but has lower toughness.
Higher hardness and wear resistance should be anticipated from the samples appearance (Fig. 2 and Fig. 3). Higher value and densely placing of the carbides is clearly visible. According to Andreas Blutmager et al [5] carbides have influence on material resistance against wear by protecting basic ferrous matrix, which is washed away during the abrasive wear while carbides position stays nearly the same.

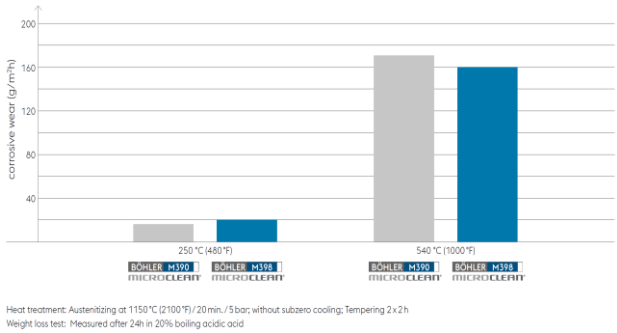

Fig. 12 Comparison of corrosion resistance of M390 and M398 steels [3]

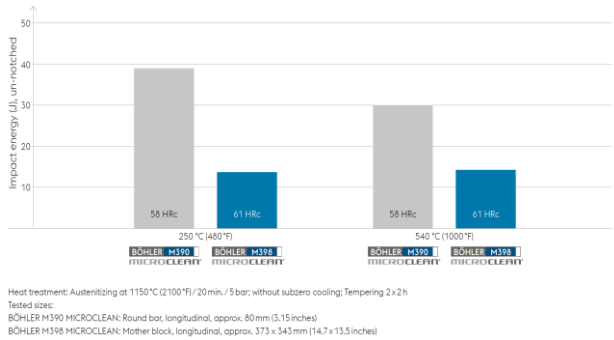

Fig. 13 Comparison of impact energy and hardness of materials M390 and M398 [3]

3 Results and discussion

From the production practice came a demand for simple and cheap material properties improvement for M390 steel – nitridation or some similar thermal or thermochemical treatment which would improve wear resistance while preserving or also improving the corrosion resistance. Nitridation of stainless steel with high Chromium content has some dangers. Three basics are following:

1. At anticorrosion steels with Chromium content comes to decreasing of the corrosion resistance by the influence of Chromium precipitation what causes depletion of surface layer for Chromium which decreases the corrosion resistance. [6]
2. The second risky case is high temperature during the thermal treatment. Within the effort of preserving the best material properties it is necessary to keep the nitridation temperature as low as possible (around 450 °C), what reduces the diffusion of the Nitrogen to surface layer. [7] [8]
3. Enormous grain growth during the long-term thermal treatment can cause mostly loss of mechanical, but also anticorrosion properties while the corrosion can grow between the grain borders.

As visible on the material surface (Fig. 6, Fig. 7), there is enormous number of Chrome carbides and other carbides, too, which can be during improper thermal / thermochemical treatment lost what should open the way for corrosion. Therefore the proper treatment have to be found.
From the main three reasons mentioned above there is necessary to search for technologies which are able to keep the demanded conditions and ensure sufficient diffusion of Nitrogen altogether with lowest segregation of Chromium and keep the grain growth under control.

4 Conclusions

In regard of lack of information about the corrosion of PMS steels and stainless steels in standard literature we had two main goals of this article. The first was to investigate the scientific databases and find the best possible sources, compare its results and find coherences between used methods and materials. In available literature, mainly at scientific articles in Scopus and Web of Science databases methods were found which should have important contribution for nitridation of M390 and M398 materials. It bargains for high density plasma nitridation which was tested on corrosion resistant steel by I. Braceras et al. [6]. This method achieved on the surface of corrosion resistant steel 1.4545 compact layer without cracks (commonly occur during the nitridation) able to resist corrosion influences better than basic surface.
Electrochemical nitridation, which properties presented in their works LV Jinlong et al. [7] According to authors it forms a passive compact layer that

helps to increase the corrosion resistance. This method uses lower temperatures as common nitridation what helps to decrease precipitation of anticorrosion components, especially of Chromium. Simple direct nitridation route at low temperatures, used by A. S. Hamdya et al. created outer layer with new type of nitride so called S-phase, characterized by high hardness and corrosion resistance. [8] Similar as formerly mentioned technologies the simple direct nitridation route has a work temperature at around 450 °C. If the temperature is increased to 600 °C corrosion resistance decreased. Very interesting should be a cooperation with company Rübig concerned in thermal treatment including nitridation. Their technology Plapol looks very attractive. It is necessary to investigate these methods deeper. The question is which technologies will be available during the research and also where the borders of technologies are shifted from the time of cited literal sources creation.

The second goal was to analyse samples of PMS steels M390 and M398 by the optical microscope. Even that the result is not sufficient and for more detailed view we have to use scanning electron microscope, we were able to contemplate the differences between these materials – mainly visual ratio of dark dots (carbides) and light dots (basic material) which show us difference between M390 and M398. As declared from producer the M398 contains more Carbon and Carbides and it is harder with higher wear resistance what is supported by visual observation of samples under the optical microscope. Analysis showed the very fine structure of both materials in comparison with standard materials as grey cast iron and others. Based on that it is visible and it is understandable that the PMS steels has much better physical properties than standard materials due to different kind of production which helps to prevent the lack of relatively big impurities or formation of material components.

We will continue in material investigation because we have to confirm or disprove the outputs from available literature sources which can bring us important findings.

5 Acknowledgement

Authors are grateful for the support of experimental works by project of Slovak Research and Development Agency under the contract No. APVV-15-0710.

References

[1] Wittmann Battenfeld: *Plasticizing systems, Wittmann Battenfeld 2019.* BPK0000037,

[2] Böhler: Katalóg produktov 2016 nástrojové a rýchlorezné ocele, *voestalpine Böhler Edelstahl GmbH & Co-KG 2016*.

[3] Böhler: M398 Microclean® Plastic mould steel *voestalpine Böhler Edelstahl GmbH & Co-KG. 2016. 10.2018*

[4] Böhler: M390 Microclean® Plastic mould steel *voestalpine Böhler Edelstahl GmbH & Co-KG. M390 DE – 07.2007 – 2.000 SPS*

[5] A. Blutmager et al: Abrasive/Erosive Wear on MMCs in Plastic Molds as a Function of Volumetric Flow Rates and Glass Fiber Distribution, *Polymer Engineering & Science published by Wiley Periodicals 2018*

[6] I. Braceras et al: Corrosion preserving high density plasma treatment of precipitation hardening stainless steel, *Surface and Coatings Technology 2018*

[7] Lv Jinlong, Liang Tongxiang, et. al: The effect of electrochemical nitridation on the corrosion resistance of the passive films formed on the 2205 duplex stainless steel, *Elsevier (2019)*

[8] Abdel Salam Hamdya, et. al: Corrosion behavior of nitride layer obtained on AISI 316L stainless steel via simple direct nitridation route at low temperature, *Elsevier (2011)*

[9] Radomila Konečná, Stanislava Fintová, Praktická metalografia, *Žilinská Univerzita (2010)*

[10] Ján Moravec, Elena Kantoríková, Peter Fabian, Prášková metalurgia, *Žilinská Univerzita (2020)*

University Review, Vol. 15, Issue 1, p. 63-69, 2021.

UNIVERSITY REVIEW

COMPARISON DIFFERENT TYPES OF MATERIALS FOR 3D PRINTING FROM DIMENSIONAL RESPECT

Maroš Eckert[1*]

[1]Design and Special Technology Department, Faculty of Special Technology, Alexander Dubcek University of Trencin, Ku kyselke 469, 911 06 Trencin

ARTICLE INFO

***Article history*:**
Received: 15.3.2021
Received in revised form: 23.4.2021
Accepted:3.5.2021

Keywords:
Additive technology
3D printing
Filament
ABS
PLA

Abstract:

The aim of the work was to compare currently available and expanded materials for 3D printers using FFF technology. This technology is currently one of the most widespread additive technologies and therefore great attention is paid to the material for this type of 3D printing. The materials used in the experiments were PLA, ABS, PET-G, NYLON and a flexible material with the trade name FLEX. The experimental part consisted of printing test samples from each of these materials. The test sample had randomly selected geometric elements, which were then measured with a caliper and averaged values from 3 identical samples. The results show that a test sample was printed from all the set materials. The best results of accuracy and surface quality were achieved by ABS and PLA materials. In the case of ABS, there was a slight problem with thermal deflection. PET-G material also achieved very good accuracy results, but it required tuning of process parameters. NYLON and FLEX materials are problematic materials for 3D printing, which was also confirmed in tests. Samples from these materials did not achieve the required accuracy and the surface quality was very low. By optimizing the printing process and the input CAD model, some errors could be eliminated, but the print quality would still not reach the value of standard materials.

1 Introduction

3D printing is the process of producing three-dimensional solid objects from a digital file. The creation of a 3D object is achieved by the method of layering the material. The layering process indicates that there is a slow addition of material layer by layer until the product is formed. Each layer is visible on the manufactured part until the final machining (different types of finishing for different types of materials. 3D printing is the exact opposite of machining by drilling or milling using a finished piece of material. This manufacturing process allows complex shapes to be produced using less material than conventional machining methods [1].

Constant developments in this area led to development of alternate print technologies such as fused filament fabrication (FFF – also known as Fused

* Corresponding author. Tel.: +421 32 7400 246
E-mail address: maros.eckert@tnuni.sk

Deposition Modeling FDM), digital laser printing (DLP), selective laser sintering (SLS), material jetting, selective laser melting (SLS), and Laminated Object Manufacturing (LOM) [2]. Today, with such large variety of available 3D print technologies, researchers have applied the technology to printing custom labware, environmental studies, tissue engineering, biological sensing, microfluidics, lab-on-a-chip devices, medicine, and electrochemical devices [3]. 3D printing has gained special attention from analytical chemists due to advantages like low fabrication cost, time efficiency, and flexibility to modify surfaces of materials. Additive manufacturing allows users to produce complex 3D structures with precision.

Fig. 1 outlines the steps associated with producing an actual 3D printed object. First, a computer aided design (CAD) software is used for designing a virtual 3D structure in silico. The CAD software also provides an idea of expected structural integrity of the finished product. The next step is the conversion of CAD file to STL (Standard Tessellation File) format, the basic idea behind tessellation is to covert the 2D outer surface of constructed 3D model into tiny triangles known as "facets" which are responsible in describing the surface geometry of object without any representation of texture, color or any other attributes associated with the model. Next step is to transfer the STL file to the computer which is connected to the 3D printer before the actual building of the object takes place on the build stage. Time required and spatial resolution for building can vary significantly depending on the 3D printer under use. After completion of the building, now the object is ready to remove off the printing bed. Depending upon the requirements of the final product, the final step, postprocessing can vary and involves steps like painting, sanding, gluing etc. [4].

3D printing has already become the most prevalent manufacturing technology in the case of prosthetics (e.g. bone and cartilage replacements), dental implants and hearing aids [5,6,7,8]. In other industries, e.g. in the aerospace and automotive sectors, a growing number of major players have adopted 3D printing beyond prototyping to directly manufacture end-use parts and products—Airbus, Ford, General Electric are just a few of many companies that make a significant use of 3D printing technologies [9].

2 Material and Methods

Experimental measurements were based on a comparison of the achieved accuracies and tolerances using the most common materials for FFF printing technology. FFF is an additive manufacturing process that belongs to the material extrusion family. In FFF, an object is built by selectively depositing melted material in a pre-determined path layer-by-layer. The materials used are thermoplastic polymers and come in a filament form. FFF is the most widely used 3D Printing technology: it represents the largest installed base of 3D printers globally and is often the first technology people are exposed to. In this article, the basic principles and the key aspects of the technology are presented. The materials used in the experiment were ABS, PLA, PET-G, NYLON and a flexible material with the trade name FLEX.

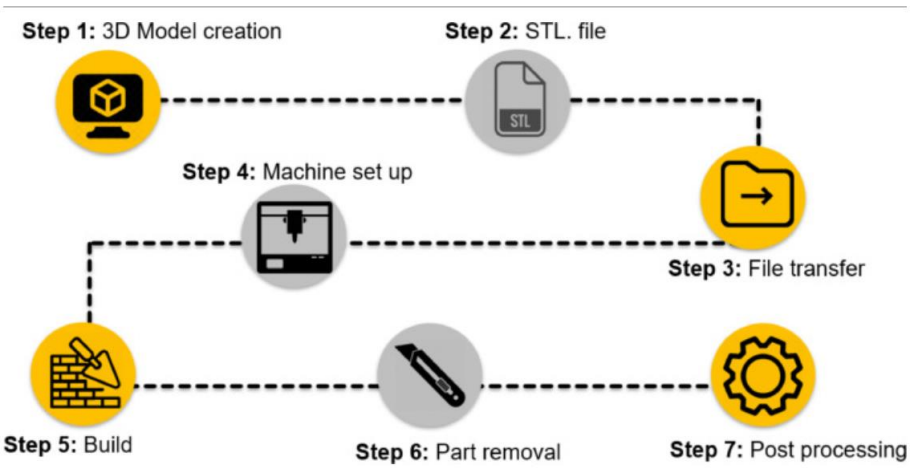

Fig. 1 Steps involved in 3D printing of an object [4]

ABS - Acrylonitrile butadiene styrene is a material based on oil thermoplastic, which is commonly found in timing pipe systems, automotive linings, protective work equipment or toys (Lego). ABS-made components have better strength, flexibility and durability over components made of PLA. ABS printing is more expensive and demanding (it produces unpleasant fumes when heated plastic) [10].

PLA - Polyactic Acid for short PLA is a biodegradable thermoplastic made from renewable sources such as corn starch or sugar cane. In addition to 3D printing, this material is also used for implants in the hospital sector, food packaging but also disposable tableware. The biggest advantage of PLA is that this material is very easy to work with when printing. Compared to ABS material, it works at lower melting temperatures (Tab. 1). PLA is the most widely used material used in 3D printing, not because it would be the best material, but because printing with it is easy. It is used wherever mechanical properties, strength, endurance or wear are not required. This material should not be used anywhere where there is a possibility of breakage, bending, high temperatures or direct UV radiation [10].

PETG - Polyethylene tetraflate glycol is a thermoplastic that is characterized by a particularly high percentage of transparency and a low amount of viscosity. No special accessories are required for printing, printing takes place with parameters similar to PLA [10].

Nylon - nylon fibre is one of the polyamides (PA) - linear polymers with regular amide bonds. Nylon is the first synthetic fibre made exclusively of carbon, water and air. The filament tends to be highly deformed, but the products excel in high strength, resistance and very high resistance to chemicals. Nylon is suitable for printing gears or screws [11,12].

FLEX - Flexible filament has a number of functions, making it an excellent choice for a wide range of applications. The material is resistant to abrasion, oil-based substances, chemicals and wear, making it ideal for use in the automotive industry. Extruded parts made of this material are resistant to low temperatures without becoming a brittle material. The printed products are not subject to severe deformation and almost always return to their original shape. The disadvantage of the flexible filament is that the material shrinks during printing and the printed part peels off from the printing substrate in several layers. To avoid this problem, it is necessary to improve the adhesion by adding a 10 mm single-layer bead around the printed part, which ensures heat dissipation over a larger area [13].

Printing took place on a 3D printer PRUSA I3 MK3 using FFF technology. The print parameters were the same for all materials. The diameter of the Tyrolean was 0.4 mm, the print speed was 200 mm/s and the filling was a rectangular pattern with a density of 80 %.

Tab. 1 Printing parameter and properties of the most used materials for 3D printing

	PLA	**ABS**
Extruder temperature	180-230 °C	210-250 °C
Bed temperature	20-60 °C	80-110 °C
Bed	optional	required
Enclosure	optional	recommended
Adhesion of the first layer	moderately difficult	moderately difficult
Vapors	Almost none	more and intensely
Moisture absorption	yes	yes

The evaluation of the accuracy and quality of the component created for the individual materials was evaluated by measuring the selected dimensional parameters and optical evaluation of the surface quality. Each test piece of a given material was printed 3 times. Using a caliper, 3 the selected dimensions were measured, and average value and standard deviation were calculated. Three identical measurements were performed for each measured parameter. From the average data thus obtained, graphical dependencies were created that show the actual dimension from the ideal. The dimensions that were evaluated were an inner diameter of Ø10 mm, an outer diameter of Ø6 mm, an element height on the part of 6 mm and an edge in the X-axis direction of the part of 20 mm.

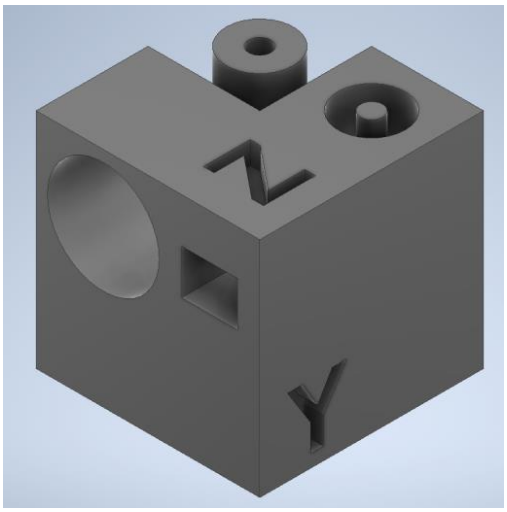

Fig. 2 Model of test specimens

3 Results and Discussion

Test components made of PLA material (Fig. 3) achieved very good results in dimensional stability and accuracy. There were also no significant optical and surface defects on the components. Minor errors occurred on the letters X and Z due to insufficient air access from the fan. The last damage remains the reduced space of the hole in the cylinder on the test cube, which was created due to the thickness of the printing layer.

The parts extruded from the ABS material were also free of significant damage or inaccuracies, but the first cube deformed the first layers, all three damaged the letter X, and the internal holes in the samples narrowed due to the thermal extensibility of the material. This material is a modified version of the most used plastic in the world PET. It was formed by adding G-modified glycol, which is added to the material composition during polymerization. The result is a stronger fiber, less brittle, but very difficult to print. After requesting the process parameters, the printing of the components went without major problems. The surface and dimensions of the components were at a very good level comparable to PLA and ABS materials.

NYLON is one of the strongest filament materials for FFF printers. Nylon is a synthetic polymer based on polyamides. It is durable, strong, flexible and a bit flexible. Nylon is a hygroscopic material and must be stored in a dry place and dried before each print. Printing this material is very demanding, as evidenced by our results. Samples of this material had many surface defects and damage, as well as dimensional accuracy was very poor.

Flexible material FLEX is suitable for printing seals and components with the need for high material flexibility. When printing, we used a single-layer edge around the sample to ensure adhesion, as the flexible material tended to shrink. Some samples were visually damaged, but the biggest problem with printing from this material is smaller holes and holes, which was also shown in the resulting values. Also, the surface of samples showed significant imperfections (Fig. 4).

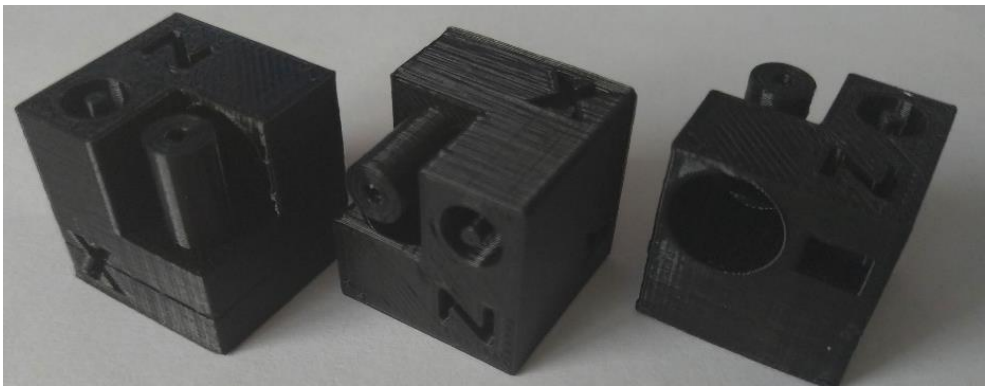

Fig. 3 Test specimens made of PLA material

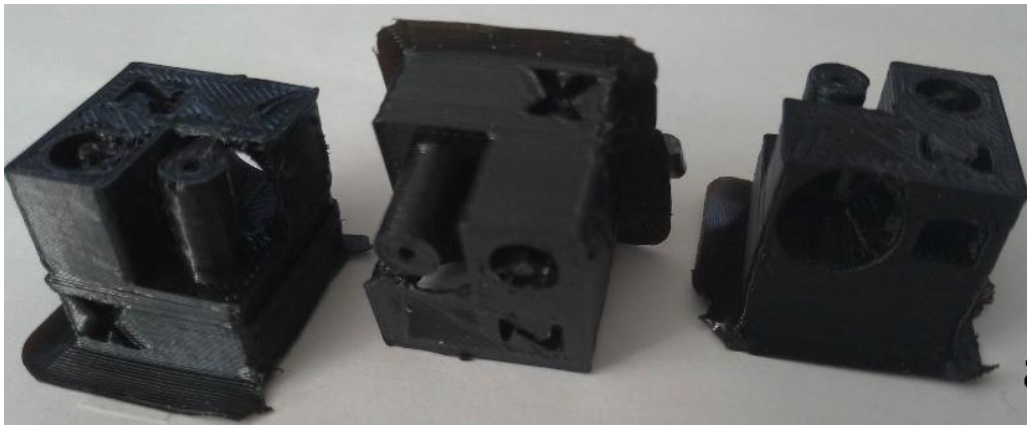

Fig. 4 Test specimens made of FLEX material

The measured and calculated average values of the actual dimensions are listed in Tab. 2. The average values of the measured elements and their standard deviation are also given there. A graphical representation of the results together with the deviations in the form of error bars and an indication of the ideal value of the measured parameters is shown in Fig. 5. As the graph shows in terms of accuracy, the standard ABS and PLA materials are best used. The deviations measured for these materials were within the general tolerances of ISO 2768-m.

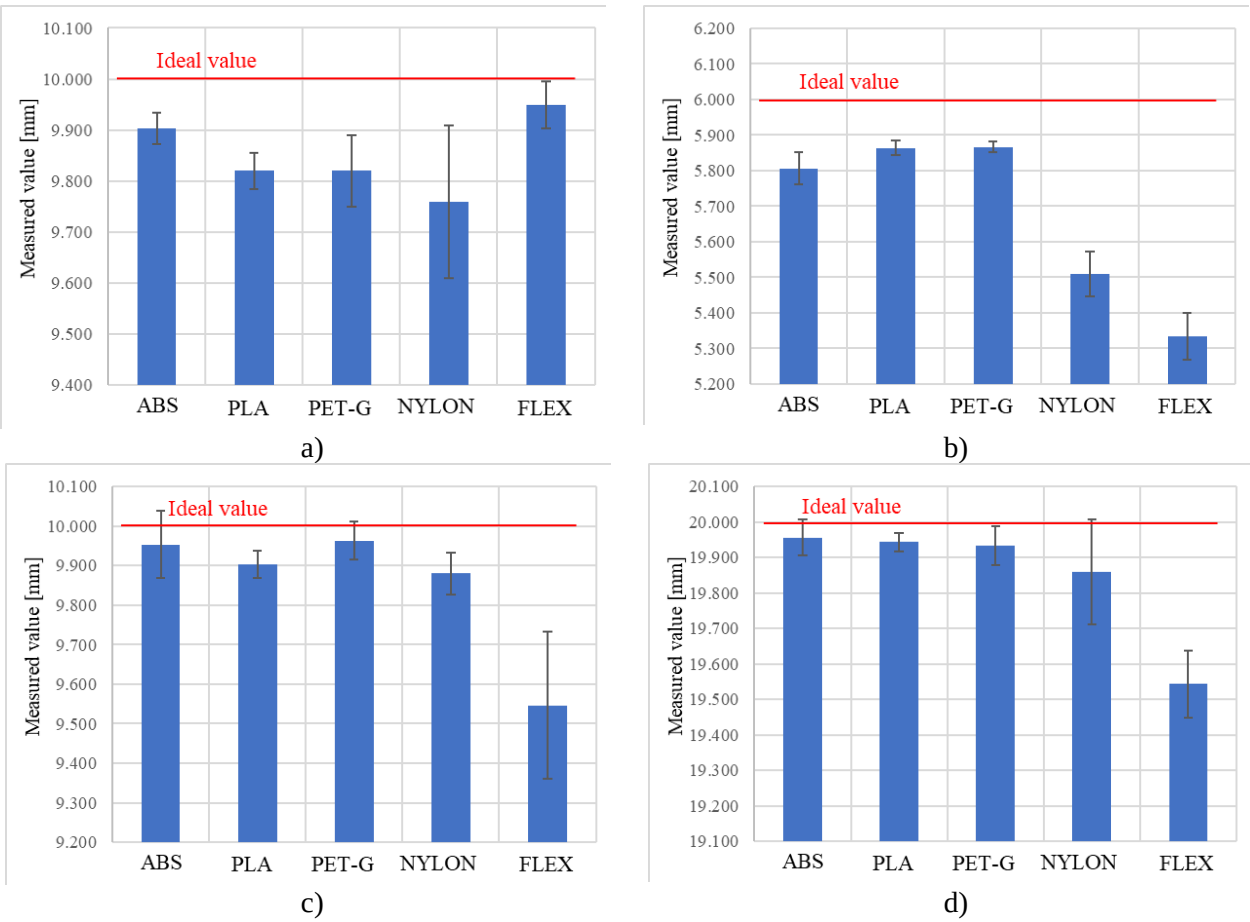

Fig. 5 a) Obtained actual values of inner diameter Ø10 mm, b) Obtained actual values of outer diameter Ø6 mm, c) Obtained actual values of element height 10 mm, d) Obtained values of part edge length 20 mm in X direction

Tab. 2 Measured and calculated values of geometric dimensions of printed samples

		ABS	PLA	PET-G	NYLON	FLEX
Diameter Ø 10 mm	Sample 1 [mm]	9.91	9.86	9.9	9.59	9.94
	Sample 2 [mm]	9.93	9.79	9.78	9.87	10
	Sample 3 [mm]	9.87	9.81	9.78	9.82	9.91
	Average value [mm]	9.903	9.820	9.820	9.760	9.950
	Standard deviation [mm]	0.031	0.036	0.069	0.149	0.046
Diameter Ø 6 mm	Sample 4 [mm]	5.81	5.87	5.85	5.49	5.35
	Sample 5 [mm]	5.76	5.84	5.87	5.46	5.39
	Sample 6 [mm]	5.85	5.88	5.88	5.58	5.26
	Average value [mm]	5.807	5.863	5.867	5.510	5.333
	Standard deviation [mm]	0.045	0.021	0.015	0.062	0.067
Height 10 mm	Sample 7 [mm]	9.89	9.94	9.91	9.92	9.76
	Sample 8 [mm]	9.92	9.9	10	9.82	9.46
	Sample 9 [mm]	10.05	9.87	9.98	9.9	9.42
	Average value [mm]	9.953	9.903	9.963	9.880	9.547
	Standard deviation [mm]	0.085	0.035	0.047	0.053	0.186
Length 20 mm	Sample 10 [mm]	19.97	19.94	19.88	19.95	19.51
	Sample 11 [mm]	19.9	19.92	19.93	19.94	19.65
	Sample 12 [mm]	20	19.97	19.99	19.69	19.47
	Average value [mm]	19.957	19.943	19.933	19.860	19.543
	Standard deviation [mm]	0.051	0.025	0.055	0.147	0.095

The surprise is the PET-G material, which also reached all dimensions within a given tolerance. NYLON material no longer reached the given tolerance in most of the examined dimensions. The worst result was the FLEX material, whose deviations were in some cases up to 0.7 mm.

4 Conclusion

The aim of the work was to compare currently available and expanded materials for 3D printers using FFF technology. This technology is currently one of the most widespread additive technologies and therefore great attention is paid to the material for this type of 3D printing. From the achieved results of this work, it can be stated that all selected materials, i.e. ABS, PLA, PET-G, NYLON and FLEX were able to print the test part. In the case of ABS, PLA and PET-G, there was no significant printing problem, and the process parameter was based on software or manufacturer's recommendations. The accuracy achieved with these materials met the ISO 2768-m standard. However, there were significant problems with NYLON and FLEX printing. In the case of NYLON material, it could also be caused by air humidity, which affected the print. This type of material should be placed in a hermetically sealed container during printing and only the part of the filament associated with the extruder should be exposed to atmospheric moisture. FLEX is a very difficult to print flexible material, where achieving accurate dimensions often depends on a trial-and-error method, and it is always necessary to adjust the geometry of the model and add or remove material for each geometric element to achieve the final dimension within the required tolerance.

Acknowledgement

This work was supported by the Research Agency of the Ministry of Education, Science, Research and Sport of the Slovak Republic under the contract 001TnUAD-4/2020.

References

[1] J. Larson: 3D Printing Designs. Packt Publishing. 2016, ISBN 978-1785884320.
[2] B. Gross, S.Y. Lockwood, D.M. Spence: Recent Advantages in Analytical Chemistry by 3D Printing. Anal. Chem., 2016, 89, 57-70.
[3] A. Ambrosi, M. Pumera: 3D Printing Technologies for Electrochemical Applications. Chem. Soc. Rev., 2016, 45, 2740-2755.
[4] H. Agrawaal, J.E. Thompson: Additive Manufacturing (3D Printing) for Analytical Chemistry. Talanta Open, 2021, 100036.
[5] S. Davies: 3D Printing is new face of medicine. Financial Times, 2013.
[6] I.J. Petrick, T.W. Simpson: 3D Printing disrupts manufacturing: how economics of one create new rules of competition. Research-Technology Management, 2013, 56, 12-16.
[7] C.G. Sandstrom: The non-disruptive emergence of an ecosystem for 3D printing– insights from the hearing aid industry's transition 1989–2008. Technol. Forecast. Soc. Change, 2016, 102, 160-168.
[8] T. Wohlers: Wohlers Report 2020: 3D Printing and Additive Manufacturing Global State of the Industry. Technical report, Wohlers Associates, 2020, ISBN 978-0991333264.
[9] T. Rayna, L. Striukova: Assessing the effect of 3D printing technologies on entrepreneurship: An exploratory study. Technological Forecasting and Social Change. 2021, 164, 120483.
[10] MATERIALPRO3D, Rozdiely materiálov vhodných pre 3D tlač (In Slovak). 2018, [online]. [cit. 7.2.2021] Available: https://www.materialpro3d.cz/blog/ rozdily-abs-pla-petg /.
[11] FILAMENTWORD, Nylon filament. 2020. [online] [cit. 7.2.2021] Available: https://www.filamentworld.de/produkt-kategorie/special-filament/nylon-filament/.
[12] 3DPRINTING, Nylon. 2020 [online]. [cit. 7.2.2021] Avalaible: https://3dprinting.com/filament/3d-print-nylon-filament-tips/.
[13] PROFI-FILAMENTS, Flexibilný filament. 2020 [online]. [cit 8.2.2021] Available: https://www.profi-filaments.sk/p/189/fiberflex-300-black-1-75mm-f-1kg .